APPENDIX 1: Morphology and Dynamics of the Straits Examined in This Study

by Robert W. Dalrymple, P.Geo.

This appendix, which accompanies the paper entitled "*A Review of the Morphology, Physical Processes and Deposits of Modern Straits*" by Robert W. Dalrymple, which appears in Geological Society London Special Publication 523 "*Straits and Seaways: Controls, Processes and Implications in Modern and Ancient Systems*", contains a summary of the information obtained from the literature review concerning each of the 33 straits examined in this study. For each strait, the following information is provided:

- A Google Earth © image of the strait, with bathymetric contours superimposed, plus arrows showing the general current-flow directions extracted from the literature;
- The dimensions (length, width and depth) of the strait;
- A description of the strait, including information on its geologic origin, hydrodynamics and nature of the sediments; and
- A list with full citations of the literature consulted about that strait.

In the following set of images showing the morphology of the 33 straits examined in this study, the plan shape of the straits is illustrated using Google Earth © images; the yellow outline shows the shoreline as indicated by Google Earth ©. Credit for the source of each image is provided in the individual captions. The bathymetry of each strait, which is shown using white lines, has been derived mainly from location maps in published papers; those sources are acknowledged in the captions. Arrows of various weights and colours have been superimposed to illustrate the main currents that flow through each strait, emphasizing particularly the 'permanent' or prevailing currents which are not always the most energetic water movements that are commonly 'episodic' (i.e., tidal or meteorological) currents. The flow directions are highly simplified and are derived from a reading of the relevant literature; the most important source(s) are cited in the caption. The names of the straits are preceded by a number from 1 to 33. This number corresponds with the number used in the global map in Fig. 2 in the main paper that shows where each strait is located. An abbreviated summary of the information provided here is presented in Table 1 in the main paper.

Note that this Appendix has not been formally copy-edited. Although care has been taken to ensure the accuracy of all summaries and references, errors and typographical issues may still exist. I apologize for any errors that might remain.

List of Straits Studied

Each of the following names of straits is hyperlinked to the corresponding description. At the end of each section (following the list of references), there is a hyperlink that returns to this location.

3- Georgia Strait
4- Strait of Juan de Fuca
5- The Golden Gate, San Francisco Bay
6- Strait of Magellan
7- Florida Straits
8- Long Island Sound–East River
9- Minas Passage and Minas Channel
10- Northumberland Strait
11- Straits of Mackinac
12- Hudson Strait
13- Kattegat and Skagerrak
14- Menai Strait
15- English Channel and Strait of Dover
16- Strait of Gibraltar
17- Messina Strait
18- Dardanelles and Bosphorus
19- Strait of Hormuz
20- Bab el Mandeb
21- Mozambique Channel
22- Palk Strait
23- Malacca Strait–Singapore Strait
24- Lombok Strait
25- Makassar Strait
26- Vitiaz Strait
27- Torres Strait
28- Bass Strait
29- Cook Strait
30- Tarama Strait
31- Tokara Strait
32- Osumi Channel
33- Bungo Channel–Hayasui Strait

Abbreviations for the suppliers of data for the Google Earth © images

- CA OPC—California Ocean Protection Council
- CNES—Centre national d'études spatiales
- CSUMB SFLM—California State University Monterey Bay Sea Floor Mapping Lab
- GEBCO—General Bathymetric Chart of the Oceans
- IBCAO—International Bathymetric Chart of the Arctic Ocean
- INEGI-- Instituto Nacional de Estadística y Geografía
- LDEO –Lamont-Doherty Earth Observatory
- NGA—National Geospatial-Intelligence Agency
- NOAA—National Oceanographic and Atmospheric Administration

- NSF—National Science Foundation
- SIO—Scripps Institute of Oceanography
- U.S. or US—United States

1—BERING STRAIT

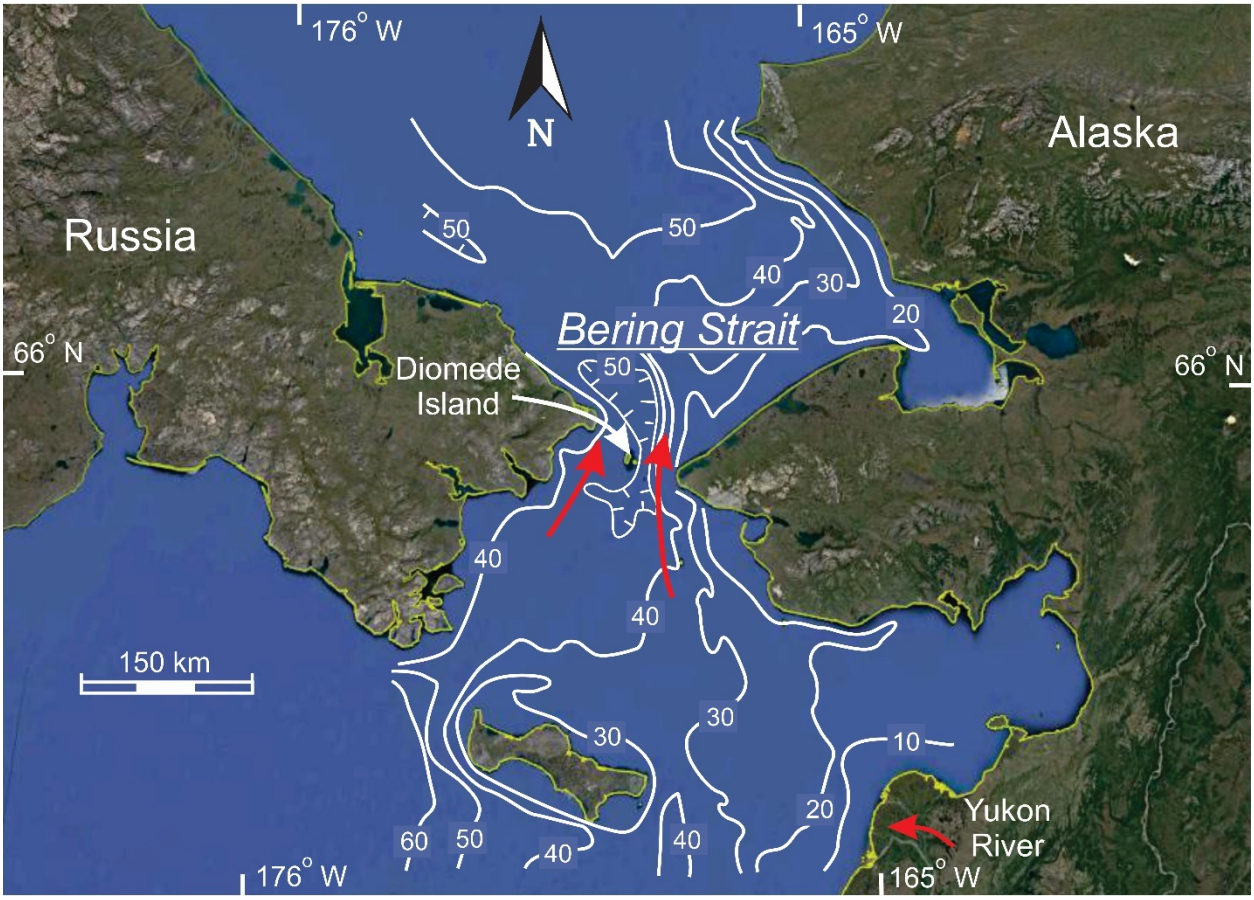

Fig. A1. <u>Bering Strait</u>*: Bathymetry after Roach* et al. *(1995, fig. 1; © American Geophysical Union). Depths in metres. Satellite image from Google Earth ©. (Data: SIO, NOAA, U.S. Navy, NGA, GEBCO. Image: Landsat/Copernicus). Diomede Island is the small island in the centre of the strait at its narrowest point. The southward-branching central depression to the immediately east of Diomede Island might have originated as a fluvial valley during lowstand. The dominant flow is to the north, into the Arctic Ocean. The Coriolis effect makes the current stronger on the Alaskan side (Aagaard* et al. *1985; Roach* et al. *1995; Woodgate & Aagaard 2005), where the Alaskan Coastal Current is strong enough to generate dunes (Field* et al. *1981) at depths below the wave-dominated shoreface. Tidal currents are of moderate strength (Mofjeld 1986; Foreman* et al. *2006a).*

Length

The land on either side consists of pointed headlands, so the narrowest part is very short, with rapid flaring to both the north and south. The main constriction is only ~40 km long.

Width

83 km total from Alaska to Russia, but there are two islands in the middle that subdivide the strait into two approximately equal parts: western part--36 km; eastern part--36 km.

Depth

Depths are generally less than 50 m. The deepest bathymetric contour on the Roach *et al*. (1995) map is 40 m. There does not appear to be any deep channel, the presence of which is suggested in Google Earth © by the labelling of a 'Bering Strait Valley' immediately to the east of the Diomede Island in the middle of the Strait. This is said to be a relict fluvial valley. Specific mention is made of a southerly-directed valley, but there might also have been one flowing to the north?

Description

The Strait is apparently a graben that opened at the end of the Miocene, with relict terrestrial valleys. This extension is related to the south-westward extrusion of western Alaska in response to northward subduction along the southern side of Alaska and the accretion of small continental blocks. The northward water flow is caused by a 'pressure head difference' (i.e., to a water-surface slope) from the Pacific to the Arctic, that might be due to regional winds, OR to a 'steric effect'-- the Pacific is less dense due to lower salinity and warmer water--than the Artic, so the Arctic is lower than the Pacific by ~0.5 m. Temporal variability in the strength of the current is strongly correlated with winds. The Alaskan Coastal Current (ACC) along the Alaskan coast is the fastest part of the northward flow, generating a cross-strait asymmetry in flow strength as a result of the strong influence of the Coriolis effect at such high latitudes. On the open shelf, north-directed current speeds are typically 3 cm s^{-1} and locally reach 10 cm s^{-1}. Current speeds in the ACC reach a maximum of 170 cm s^{-1}, 9 m above the bed. This current is ~10 km wide and 40 m deep. This current is up to 1 m s^{-1} faster than flow outside the current. The mean northward flow is 20-50 cm s^{-1} in spring and summer, 5-15 cm s^{-1} slower in fall and winter, and flow can be reversed by strong northerly winds, with the strongest southerly flow along the Russian coast (due to Coriolis effect, presumably). Most of the sediment surface appears to be covered with sandy sediment, although these samples were from the seas at either end, not the Strait *sensu stricto*. Bedrock outcrops are widespread in the northern Strait. Up to 40% of the Yukon River's load bypasses its delta and is carried northward through Bering Strait. Dunes are present on the transgressive sandy lag immediately southeast of Bering Strait, in water 10-20 m deep. They are mainly localized to areas of sand accumulation in ridges. The tidal energy flux through Bering Strait is 'very small' (shown as zero in their table; Forman *et al.* 2006). Tidal currents are weak, and 2/3 of the current energy is attributed to wind forcing.

References

Aagaard, K., Roach, A.T. and Schumacher, J.D. 1985. On the wind-driven variability of the flow through Bering Strait. *Journal of Geophysical Research*, **90**, 7213– 7221.

Aagaard, K., Weingartner, T.J., Danielson, S.L., Woodgate, R.A., Johnson, G.C. and Whitledge, T.E. 2006. Some controls on flow and salinity in Bering Strait. *Journal of Geophysical Research*, **33**, L19602, https://doi: 10.1029/2006GL026612

Asahara, Y., Takeuchi, F., Nagashima, K., Harada, N., Yamamoto, K., Oguri, K. and Tadai, O. 2012. Provenance of terrigenous detritus of the surface sediments in the Bering and Chukchi Seas as derived from Sr and Nd isotopes: Implications for recent climate change in the Arctic regions. *Deep-Sea Research II*, **61-64**, 155-171.

Dixon, J.E. and Monteleone, K. 2014. Gateway to the Americas: Underwater archeological survey in Beringia and the North Pacific. *In*: *Prehistoric Archaeology on the Continental Shelf: A Global Review*, Evans, A.M., Flatman, J. and Flemming, N. (eds), Springer Science+Business Media, New York, 95-114.

Field, M.E., Nelson, C.H., Cacchione, D.A. and Drake, D.E. 1981. Sand waves on an epicontinental shelf: northern Bering Sea. *Marine Geology*, **42**, 233-258.

Foreman, M.G.G., Cummins, P.F. Cherniawsky, J.Y. and Stabeno, P. 2006a. Tidal energy in the Bering Strait. *Journal of Marine Research*, **64**, 797-818.

Gladenkov, A.Yu., Oleinik, A.E., Marincovish, L., Jr. and Barinov, K.B. 2002. A refined age for the earliest opening of Bering Strait. *Palaeogeography, Palaeoclimatology, Palaeoecology*, **183**, 321-328.

Mackey, K.G., Fujita, K., Gunbina, L.V., Kovalev, V.N., Imaev, V.S., Koz'min, B.M. and Imaeva, L.P. 1997. Seismicity of the Bering Strait region: Evidence for a Bering block. *Geology*, **25**, 979-982.

Mofjeld, H.O. 1982. *Recent Observations of Tides and Tidal Currents from the Northeastern Bering Sea Shelf*. NOAA Technical Memorandum ERL PMEL-57, 36 p.

Mofjeld, H.O. 1986. Observed tides on the northeastern Bering Sea shelf. *Journal of Geophysical Research*, **91**, C2, 2593-2606.

Pearson, C.A., Mofjeld, H.O. and Tripp, R.B. 1981. Tides of the eastern Bering Sea shelf. *In*: *The Eastern Bering Sea Shelf: Oceanography and Resources*, Volume 1, Hood, D.W. and Calder, J.A. (eds), United States Department of Commerce, 111-130.

Roach, A.T., Aagaard, K., Pease, C.H., Salo, S.A., Weingartner, T., Pavlov, V. and Kulakov, M. 1995. Direct measurements of transport and water properties through the Bering Strait. *Journal of Geophysical Research*, **100**, C9, 18,443-18,457.

Svitoch, A.A. and Taldenkova, E.E. 1994. Recent history of the Bering Strait. *Oceanology*, **34**, 400-404.

Woodgate, R.A. and Aagaard, K. 2005. Revising the Bering Strait freshwater flux into the Arctic Ocean. *Geophysical Research Letters*, **32**, L02602, https://doi:101029/2004GL021747

Return to List of Straits

2—JOHNSTONE STRAIT–QUEEN CHARLOTTE SOUND

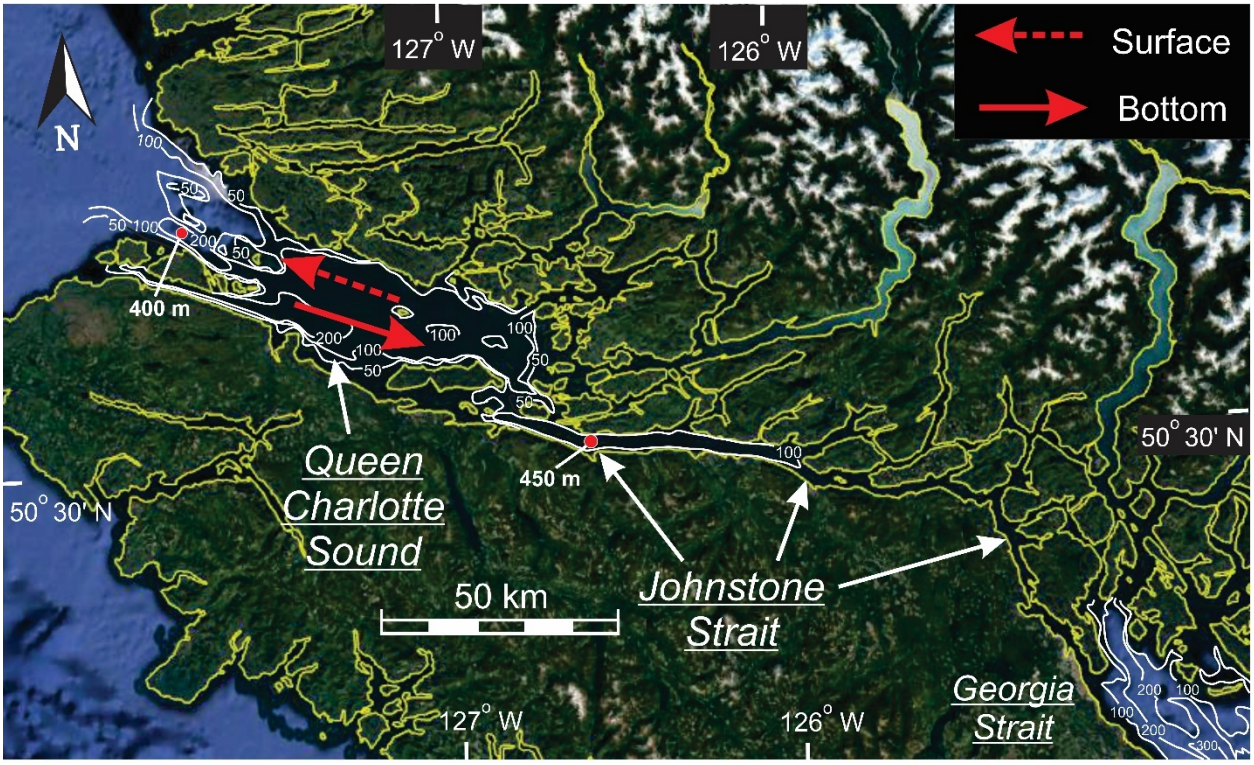

Fig. A2. *Johnstone Strait–Queen Charlotte Sound: Bathymetry of Queen Charlotte Sound and Johnstone Strait from Foreman* et al. *(2006, fig. 2; reproduced with permission of the Canadian Meteorological and Oceanographic Society); bathymetry of Georgia Strait (bottom right-hand corner) from Foreman* et al. *(1995; © American Geophysical Union). Depths in metres. Satellite image from Google Earth ©. (Data: SIO, NOAA, U.S. Navy, NGA, GEBCO. Image: Landsat/Copernicus). There are isolated, glacially scoured depressions with maximum depths that are > 400 m below sea level. Johnstone Strait and Queen Charlotte Sound experience estuarine circulation, with north-westward flow of the surface water, and inward (south-eastward) flow of the bottom water (Thomson 1976, 1977; Khangaonkar et al. 2017), driven by the discharge of the Fraser River into Georgia Strait. Tidal currents each 7.7 m* s^{-1} *in narrow sections of Johnstone Strait (Sutherland* et al. *2007), because tidal heights are nearly perfectly out of phase between Queen Charlotte Sound and Georgia Strait.*

Length

Johnstone Strait: ~160 km from Georgia Strait to Queen Charlotte Sound; more or less straight, but with jogs. Queens Charlotte Strait: ~90 km.

Width

Johnstone Strait: 3-3.5 km in its wider western section; 1.75-2.5 km wide in its narrower, more sinuous southeastern part; the narrowest point is only ~1.1 km wide. Seymour Narrows: minimum width 0.8 km. Cordero Channel: minimum width 0.5 km. Queen Charlotte Sound: 24 km at its widest; its mouth is blocked by a series of islands in a chain that is ~E-W; it narrows fairly rapidly at its southeastern end.

Depth

Queen Charlotte Sound: much of the area is 100-200 m deep, but there are two elongate areas along the southern shore that are up to 400 m deep locally. Johnstone Strait: maximum depth 450 m at the western end; commonly 200-300 m deep in the middle section; the eastern part is ~ 100 m deep, with some sills only 50 m deep. Seymour Narrows and Cordero Channel: minimum depth 50 m.

Description

Queen Charlotte Sound and Johnstone Strait occupy the northern part of the Georgia Depression. Structurally, it is a forearc basin, and also lies along the suture between the Insular and Coastal Mountains structural terranes. The entire area was glaciated, leading to the formation of glacially over-deepened straits and fjords. During the glacial maximum, the ice flow was to the W-SW, but during deglaciation, there may have been valley glaciers in the channels, flowing to the S or NW: Blaise *et al.* (1990) show an ice divide near the southern end of Johnstone Strait, with flow in both directions along the lowland valley. Deglaciation may have started as early as 13,630 yr BP. Maximum sea level was slightly above +90 m relative to modern sea level. There is significant estuarine flow in Johnstone Strait: northward in the surface layer; southward in the basal layer. The pycnocline at the study site was at a depth of ~120 m. Mean tidal range at the northwestern end of Johnstone Strait is 2.5 m, decreasing south-eastward (inward) to 1.8 m about half way along the Strait. The tide in Johnstone Strait is the result of a landward-propagating surface barotropic M_2 tide and a seaward-propagating internal baroclinic M_2 tide. The entire system is highly dissipative and numerical models of the tide require a larger-than-normal friction to reproduce the form drag of islands, and of the complex morphology and bathymetry. The tidal flux through Johnstone Strait is 1/15th that through Juan de Fuca Strait. The K_1 tide increases northward through Strait of Georgia, and southward through Queen Charlotte Strait (but less than in Strait of Georgia). The tidal phase lag between northern Strait of Georgia and Queen Charlotte Strait is ~180^o. Tidal currents in the wider western part average 0.5-1.5 m s^{-1}. Current speeds in Johnstone Strait reach 7.7 m s^{-1}. Maximum speeds in Gillard Passage and Arran Rapids (Cordero Channel) are 5.7 m s^{-1} and 6.7 m s^{-1}, respectively. Cordero Channel has a larger flux than Discovery Passage. The flux into Georgia Strait is 1/6-1/3 of that through Haro Strait. Overall, in Johnstone Strait salinities increase northwestward toward Queen Charlotte Sound. Despite the narrowness of the channel, there is thought to be a measurable Coriolis effect, although the cross-channel slope could be due to sinuosity. There is also a baroclinic tidal component caused by interaction of the barotropic tide with shallow sills. There appears to be slumping on the channel margins. Oxygen levels are high through the entire depth due to strong tidal mixing. Throughout the entire area (including Queen Charlotte Sound), salinities are equal to or less than 30 ppt in the spring. Long-term flows are seaward everywhere in the surface layer because of river input, especially by the Fraser River. At 80 m depth, all of the narrow channels still have seaward flow, but the deeper central part of Queen Charlotte Sound has weak landward flow, implying that the surface layer thins in a seaward direction.

References

Barrie, J.V. and Conway, K.W. 2002. Contrasting glacial sedimentation processes and sea-level changes in two adjacent basins on the Pacific margin of Canada. *Geological Society, London, Special Publications*, **203**, 181–194, https://doi.org/10.1144/GSL.SP.2002.203.01.10

Blaise, B., Clague, J.J. and Mathewes, R.W. 1990. Time of maximum Late Wisconsin glaciation, west coast of Canada. *Quaternary Research*, **34**, 282-295.

England, T.D.J. and Bustin, R.M. 1998. Architecture of the Georgia Basin southwestern British Columbia. *Bulletin of Canadian Petroleum Geology*, **46**, 288-320.

Foreman, M.G.G., Stucchi, D.J., Zhang, Y. and Baptiste, A.M. 2006b. Estuarine and tidal currents in the Broughton Archipelago. Atmosphere-Ocean, **44**, 47-63.

Khangaonkar, T., Long, W. and Xu, W. 2017. Assessment of circulation and inter-basin transport in the Salish Sea including Johnstone Strait and Discovery Islands pathways. *Ocean Modelling*, **109**, 11-32.

Sutherland, G., Foreman, M. and Garrett, C. 2007. Tidal current energy assessment for Johnstone Strait, Vancouver Island. *Proceedings of the Institute of Mechanical Engineering*, 221, Part A: J. Power and Energy, Special Issue Paper 147, 147-157.

Thomson, R.E. 1976. Tidal currents and estuarine-type circulation in Johnstone Strait, British Columbia. *Journal of the Fisheries Research Board of Canada*, **33**, 2242-2264.

Thomson, R.E. 1977. Currents in Johnstone Strait, British Columbia: Supplemental data on the Vancouver Island side. *Journal of the Fisheries Research Board of Canada*, 34, 697-703.

Return to List of Straits

3—GEORGIA STAIT

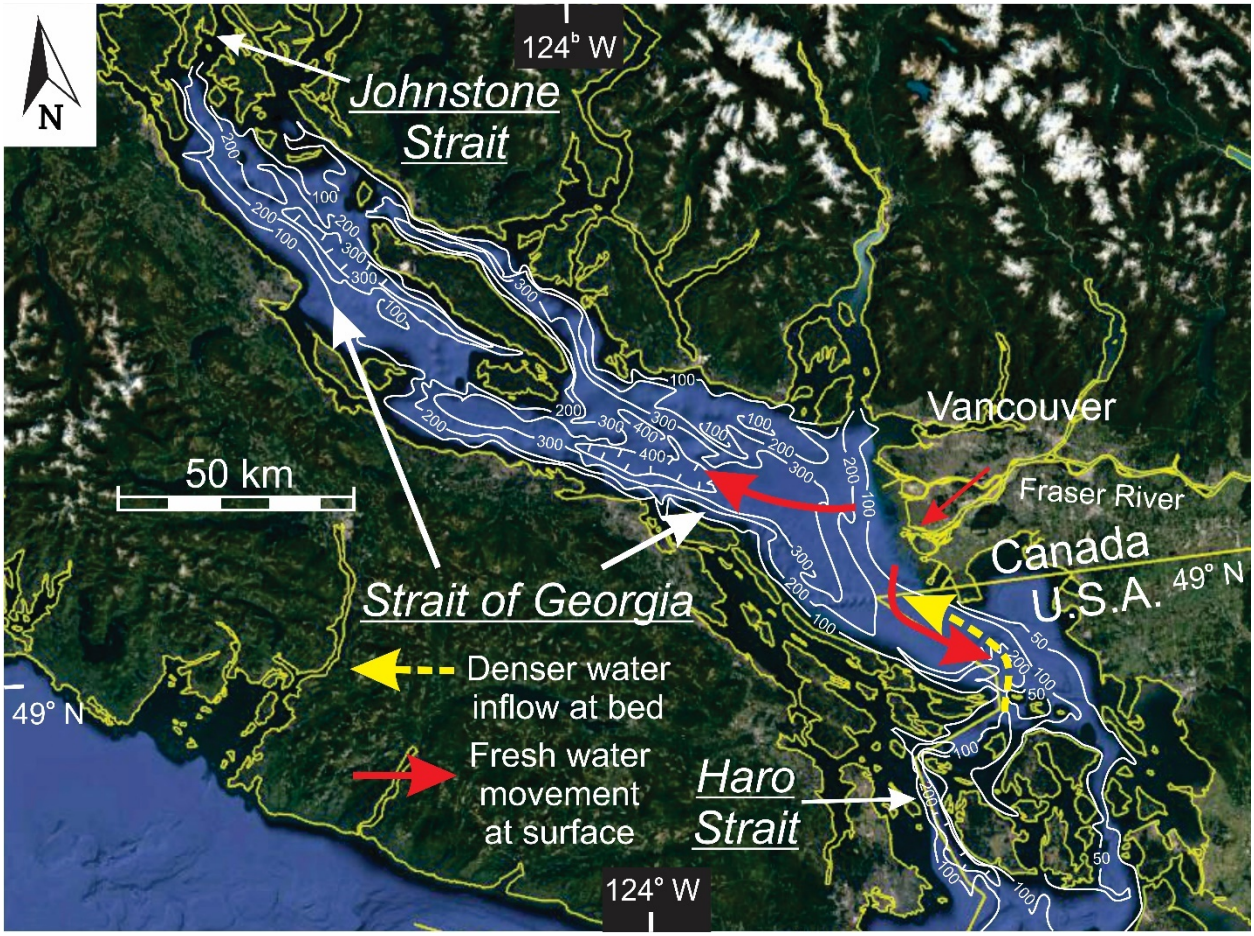

Fig. A3. *Georgia Strait: Bathymetry from Foreman* et al. *(1995, fig. 1; © American Geophysical Union). Depths in metres. Satellite image from Google Earth ©. (Data: SIO, NOAA, U.S. Navy, NGA, GEBCO. Image: Landsat/Copernicus). The basin is deep because of structural motion, but was accentuated by glacial scour. It is flanked at its ends by two constrictions, Haro Strait in the south, and Johnstone Strait in the north. Water movement in Georgia Strait is controlled by the discharge of fresh water by the Fraser River at Vancouver (LeBlond 1983), with divergent surface flow, driving estuarine circulation in both Johnstone Strait–Queen Charlotte Sound to the northwest (Thomson 1976, 1977; Khangaonkar* et al. *2017), and in the Strait of Juan de Fuca to the southwest (Ott & Garrett 1998; Masson & Cummins 2004), the later dominating over the former in the regional circulation because of the more constricted channel network to the northwest. Denser water enters Georgia Strait from the south seasonally (Masson 2002, 2006).*

Length

225 km from the San Juan Islands that define Haro Strait in the south to Discovery Passage at the entrance to Johnstone Strait in the north.

Width

The southern half averages 28 km wide, ranging from 17.5-35 km. The northern half is 12.5-17.5 km wide, with a funnel-shaped narrowing into the small passages at the northern end (Discovery Passage, etc.).

Depth

Maximum depth 420 m in the deep, central basin, north of the mouth of the Fraser River.

Description

Georgia Strait occupies the southern part of the Georgia Depression. Structurally, it is a forearc basin, and also lies along the suture between the Insular and Coastal Mountains geological terranes. There was initially rapid subsidence, followed by an episode of thrust faulting, shortening and shallowing, followed by renewed subsidence recently. There may also be some right-lateral strike-slip motion. Glaciation reached its maximum extent ~14,000 yr BP, followed by rapid deglaciation so it was ice-free by ~ 11,300 yr BP. There is a thick (~ 50 m) till succession, overlain by ice-proximal glaciomarine deposits and then by a thin succession of ice-distal glaciomarine sediments. In northern Georgia Strait, initial submergence immediately after deglaciation was up to 197 m above modern sea level, then sea level fell to its present level. There was no lowstand as occurred in the southern Strait. Most tidal energy enters from the south, because the northern channels are so small and tortuous. The tidal range increases northward from the Strait of Juan de Fuca into the northern part of Strait of Georgia. The islands near the southern end of the Strait of Georgia and between there and Queen Charlotte Sound to the north (Johnstone Strait and Discovery Passage) are the major locations of tidal energy dissipation. The tidal wave enters from both the south (Juan de Fuca Strait) and north (Queen Charlotte Sound). The Strait of Georgia overall becomes less saline to the north, although salinities are only 30-31 ppt at their lowest. The water at the bottom of the deep basin has a low oxygen content (2.5-3.5 ml l^{-1}; surface water has > 5.5 ml l^{-1}). Water entering from Johnstone Strait is significant in the northern part of Georgia Strait, but, like the water coming in through Haro Strait in the south, spreads at an intermediate depth due to mixing of sea water and fresh water. At the Fraser River mouth, tides average 3.2 m. All of the sediment supplied by the Fraser River is retained in the Georgia Basin. There is a flood-tide dominance across the delta front (flood: 1.2 m s^{-1}; ebb 0.5 m s^{-1}), such that most of the outflow goes to the north, despite the tendency of the hypopycnal river plume to turn south because of the winds. The flood tidal currents locally generate dunes in shallow water. This causes the delta to be somewhat asymmetric. The delta has prograded 5.4 km in the last 2250 years. The northerly flow on the east side of the Basin is balanced by a southerly flow on the west side. In the channels, including Haro Strait, through the San Juan Islands, tidal speeds reach 5 m s^{-1}. The bottom topography of the southern half of the Georgia Basin is smooth due to deposition of sediment from the Fraser delta, whereas the northern half has a rugged topography, with relief of ~400 m, implying little or no recent sediment accumulation, and perhaps more active tectonic movements. In the southern part, sediment generally becomes finer to the north, from sandy deposits near the San Juan islands, to clays in the area near the narrowing at the northern end of the main basin. Shallow areas are coarser and have little accumulation. Sedimentation rates are highest directly off and immediately to the north of the Fraser delta. Sediment deposition is by direct settling, and by turbidity currents (confined and unconfined) and mass failures from the Fraser delta. There are up-slope migrating sediment waves off the main river mouth.

Elsewhere, sedimentation is slow. There is little or no sedimentary signal of the presence of Vancouver Island. Much sediment is trapped in fjords on both shores. Even in deep water, there can be current winnowing, generating sandy lags. This also raises the possibility that sediment drifts are present but not yet reported. There is an 'estuarine' turbidity maximum in the Haro Strait area because of the intense tidal currents that mix the water and resuspend particles. There is abundant (biogenic) gas in the sediments of the Fraser delta. The fresh-water plume is 2-10 m thick and best developed when the river discharge is highest.

References

Ayranci, K. and Dashtgard, S.E. 2016. Asymmetrical delta below wave base: Insights from the Fraser river Delta, Canada. *Sedimentology*, **3**, 761-779.

Barrie, J.V. and Conway, K.W. 2002. Contrasting glacial sedimentation processes and sea-level changes in two adjacent basins on the Pacific margin of Canada. *Geological Society, London, Special Publications*, **203**, 181–194, https://doi.org/10.1144/GSL.SP.2002.203.01.10AAraard

Bornhold, B.D. and Barrie, J.V. 1991. Surficial sediments on the western Canadian continental shelf. *Continental Shelf Research*, **11**, 685-699.

Burd, B.J., Barnes, P.A.G., Wright, C.A. and Thomson, R.E. 2008. A review of subtidal benthic habitats an invertebrate biota of the Strait of Georgia, British Columbia. Marine Environmental Research, **66**, https://doi.10.1016/j.marenvres.2008.09.004

England, T.D.J. and Bustin, R.M. 1998. Architecture of the Georgia Basin southwestern British Columbia. *Bulletin of Canadian Petroleum Geology*, **46**, 288-320.

Fedje, D., McLaren, D., James, T.S., Mackie, Q., Smith, N.F., Southon, J.R. and Mackie, A. 2017. A revised sea level history for the northern Strait of Georgia, British Columbia, Canada. *Quaternary Science Reviews*, **102**, 300-316.

Hart, B.S. 1993. Large-scale in situ rotational failure on a low-angle delta slope: The Foreslope Hills, Fraser Delta, British Columbia, Canada. *Geo-Marine Letters*, **13**, 219-226.

Hill, P.R., Conway, K., Lintern, G., Meulé, S., Picard, K. and Barrier, J.V. 2008. Sedimentary processes and sediment dispersal in the southern Strait of Georgia, BC, Canada. *Marine Environmental Research*, **66**, https://doi:10.1016/j.marenvres.2008.09.033

Johannessen, S.C., Macdonald, R.W. and Paton, D.W. 2003. A sediment and organic carbon budget for the greater Strait of Georgia. *Estuarine, Coastal and Shelf Science*, **56**, 845-860.

Johnannessen, S.C., Masson, D. and Macdonald, R.W. 2006. Distribution and cycling of suspended particles inferred from transmissivity in the Strait of Georgia, Haro Strait and Juan de Fuca Strait. *Atmosphere-Ocean*, **44**, 17-27.

Khangaonkar, T., Long, W. and Xu, W. 2017. Assessment of circulation and inter-basin transport in the Salish Sea including Johnstone Strait and Discovery Islands pathways. *Ocean Modelling*, **109**, 11-32.

LeBlond, P.H. 1983. The Strait of Georgia: functional anatomy of a coastal sea. *Journal of Fisheries and Aquatic Science*, **40**, 1033-1063.

Lintern, D.G., Hill, P.R. and Stacey, C. 2016. Powerful unconfined turbidity current captured by cabled observatory on the Fraser River delta slope, British Columbia, Canada. *Sedimentology*, **63**, 1041-1064.

Masson, D. 2002. Deep water renewal in the Strait of Georgia. *Estuarine, Coastal and Shelf Science*, **54**, 115-126.

Masson, D. 2006. Seasonal water mass analysis for the Straits of Juan de Fuca and Georgia. *Atmosphere-Ocean*, **44**, 1-15.

Masson, D. and Cummins, P.F. 2004. Observations and modeling of seasonal variability in the Straits of Georgia and Juan de Fuca. *Journal of Marine Research*, **62**, 491-516.

McKenna, G.T., Luternauer, J.L. and Kostaschuk, R.A. 1991. Large-scale mass-wasting events on the Fraser River delta front near Sand Heads, British Columbia. *Canadian Geotechnical Journal*, **29**, 151-156.

Pharo, C.H. and Barnes, W.C. 1976. Distribution of surficial sediment of the central and southern Strait of Georgia, British Columbia. *Canadian Journal of Earth Sciences*, **13**, 674-696.

Sutherland, G., Garrett, C. and Foreman, M. 2005, Tidal resonance in Juan de Fuca Strait and the Strait of Georgia. *Journal of Physical Oceanography*, **35**, 1279-1286.

Return to List of Straits

4—STRAIT OF JUAN DE FUCA

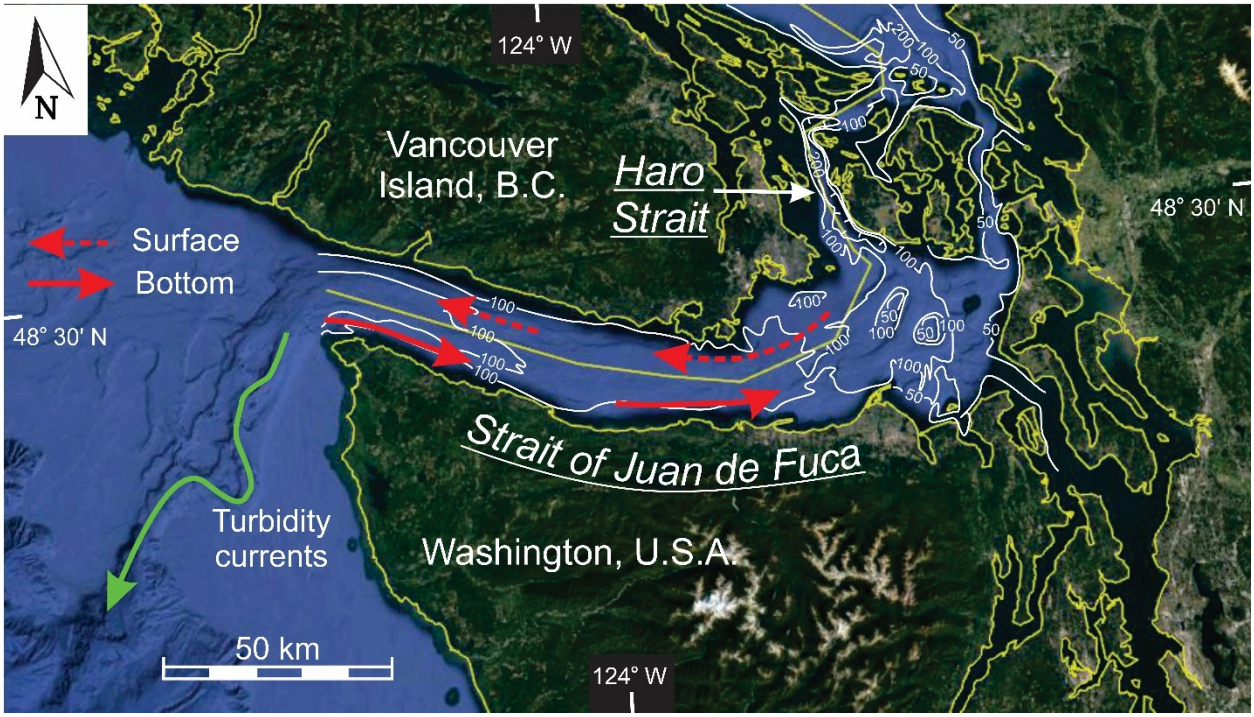

Fig. A4. *Strait of Juan de Fuca: Bathymetry from Foreman* et al. *(1995, fig. 1; © American Geophysical Union). Depths in metres. Satellite image from Google Earth ©. (Data: SIO, NOAA, U.S. Navy, NGA, GEBCO, LDEO-Columbia, NSF. Image: Landsat/Copernicus). The basin has a structural origin, but was accentuated by glacial scour; it is essentially a fjord, created by one of the major glaciers that flowed outwards from an ice divide in southern British Columbia. This map overlaps with the map for Georgia Strait to the north. Flow in the Strait of Juan de Fuca is dominated by tidal currents (Foreman* et al. *1995; Sutherland* et al. *2005), but there is a background estuarine circulation that is driven by discharge from the Fraser River in the Strait of Georgia (Ott & Garrett 1998; Masson & Cummins 2004; Masson 2006; Thomson* et al. *2007). Because of the Coriolis effect, the incoming flow is mainly on the southern side, whereas the surficial, outgoing flow is on the northern side. A turbidity-current canyon originates as the mouth of the Strait; it was presumably active when the glacial terminus was at this location during the last glacial maximum (Hewitt & Mosher 2001; Mosher & Hewitt 2004).*

Length

~140 km long, from its western entrance at Cape Flattery, Washington, to the entrance of the small channel, Haro Strait, on the west side of the San Juan Islands. The Strait trends ESE-WNW, but bends sharply to the north at its eastern end.

Width

Approximately parallel sided. Widest point is 22 km in the parallel-sided part, expanding to > 40 km at entrance to Puget Sound. Narrowest point, 14 km, south of Victoria. Narrows abruptly as it passes mainly to the west of the San Juan Islands (= Haro Strait).

Depth

Glacially scoured deep channel in the axis of the strait continues directly westward into a submarine canyon at ~ -150 m. The axis of the Strait deepens to the west, from ~50 m on bank crests near the mouth of Puget Sound, to >200 m deep at the west end. Between the banks that lie just west of the San Juan Islands, the channels reach ~150 m deep. The Strait is broadly U-shaped in section, especially in the eastern part.

Description

The Strait is localized by tectonic features, but has been repeatedly occupied and scoured by glaciers (4 regional-scale glaciations). The faulting appears to be mainly normal and/or reverse, suggesting the Strait is a graben that might have been partially inverted. Some faults in the eastern Strait have been active in the Holocene, with transpressive motion with northward-directed thrusting and right-lateral strike-slip motion; such motion suggests that the Strait of Juan de Fuca is a pull-apart basin. There is up to 1100 m of Pleistocene glacial and marine deposits in the Strait. At the glacial maximum (~14,500 yr BP), the glacier reached the shelf edge through Juan de Fuca Strait. There are recessional moraines within the Strait. Deglaciation of the eastern Strait occurred between ~14,500-13,000 yr BP. Sea level was initially at +75 m, dropping rapidly to -60 m, and then rising to the present elevation at ~5470 yr BP. There is a series of wave-cut terraces that formed during the transgression, the lowest at -50 m, some associated with spits. Post-glacial sediments begin with ice-proximal coarse outwash, passing up to more distal, muddy glacio-marine stratified deposits. Deltas have been built by the transverse feeder drainages along both the north and south margins of the Strait. These bodies are largest along the north side. One of the deltas along the southern side (Elwah River) is skewed to the east, most likely because of the west-to-east wave-driven longshore drift. There is little sediment input now to the eastern Strait because it lacks significant river input. Dunes in sand with a mean size of ~0.5 mm are up to 25 m high occur south of Victoria, with migration to the northeast (landward). Bottom currents here are >100 cm s^{-1}. The sediment is reworked from older deposits. Seismic sections show local erosion. There are sediment drifts around banks (= drumlins) in the eastern part of the Strait. The present-day shorefaces along the margins are wave dominated above ~5 m depth; below -18 m, tidal currents dominate sedimentation generating along-strike current ripples. All depths are dominated by sands. The longshore drift is uniformly to the east (inland). Significant wave heights are <1 m everywhere in the Strait; average maximum storm wave base is ~-20 m. There is 'estuarine circulation' in the summer, but this sometimes reverses in the winter because of poleward and westerly winds. The main energy is tidal, with currents 75-100 cm s^{-1}. The estuarine circulation currents: maximum outward ~50 cm s^{-1} in upper 60 m; inward at ~25 cm s^{-1} at 60-125 m depth, and ~ 10 cm s^{-1} below 125 m. Outflow is strongest on the north side because of Coriolis effect. During strong westerly winds, there is a strong (~ 1 m s^{-1}) inward current at the surface, especially along the southern side. There is strong mixing as the flow passes through Haro Strait, especially during spring tides. There is a non-estuarine (wind-driven) inflow at the sea bed with speeds of 2-5 cm s^{-1}. The salinity of the surface water increases seaward, with a significant increase in the passage through Haro Strait from Georgia Strait which is affected by the input of the Fraser River. This surface fresher layer becomes thinner in the seaward direction. The speed of the surface outflow decreases toward the mouth of the Strait. Only 38% of the tidal energy entering

from the ocean makes it into Georgia Strait; much of the energy is dissipated in Haro Strait. About half of the tidal flux is through Haro Strait; the rest goes through other channels between the San Juan and Gulf islands. The M_2 tide decreases inward to a virtual amphidromic point on land at Victoria, then increases into the Strait of Georgia, with maximum ranges at the north end of the Strait of Georgia. The tidal range on the south coast of Vancouver Island is 2.2 m. There are current-speed maxima adjacent to headlands and in narrow straits between islands. There may be input of Columbia River suspended sediment, and of material eroded by waves, in the bottom water during winter. A strongly asymmetric delta has been documented along the southeastern margin of the strait. It appears that this asymmetry is due to waves arriving from the west, causing an eastward-directed longshore drift.

References

Foreman, M.G.G., Walters, R.A., Henry, R.F., Keller, C.P. and Dolling, A.G. 1995. A tidal model for eastern Juan de Fuca Strait and the southern Strait of Georgia. *Journal of Geophysical Research*, **100**, C1, 721-740.

Frey, S.E. and Dashtgard, S.E. 2011. Sedimentology, ichnology and hydrodynamics of strait-margin, sand and gravel beaches and shorefaces: Juan de Fuca Strait, British Columbia, Canada. *Sedimentology*, **58**, 1326-1346.

Gelfenbaum, G., Stevens, A.W., Miller, I., Warrick, J.A., Ogston, A.S. and Eidam, E. 2015. Large-scale dam removal on the Elwha River, Washington, USA: Coastal geomorphic change. *Geomorphology*, **246**, 649-668.

Hewitt, A.T. and Mosher, D.C. 2001. Late Quaternary stratigraphy and seafloor geology of eastern Juan de Fuca Strait, British Columbia and Washington. *Marine Geology*, **177**, 295-316.

Johannessen, S.C., Masson, D. and Macdonald, R.W. 2006. Distribution and cycling of suspended particles inferred from transmissivity in the Strait of Georgia, Haro Strait and Juan de Fuca Strait. *Atmosphere-Ocean*, **44**, 17-27.

Masson, D. 2006. Seasonal water mass analysis for the Straits of Juan de Fuca and Georgia. *Atmosphere-Ocean*, **44**, 1-15.

Masson, D. and Cummins, P.F. 2004. Observations and modeling of seasonal variability in the Straits of Georgia and Juan de Fuca. *Journal of Marine Research*, **62**, 491-516.

Mayers, I.R. and Bennett, L.C., Jr. 1973. Geology of the Strait of Juan de Fuca. *Marine Geology*, **15**, 89-117.

Mosher, D.C. and Hewitt, A.T. 2004. Late Quaternary deglaciation and sea-level history of eastern Juan de Fuca Strait, Cascadia. *Quaternary International*, **121**, 23-39.

Mosher, D.C. and Thomson, R.E. 2000. Massive submarine sand dunes in the eastern Juan de Fuca Strait, British Columbia. *In*: *International Workshop on Marine Sandwave Dynamics*, Trentesaux, A., and Garland, T. (eds), University of Lille, Lille, France, Proceedings, 131–142.

Ott, M.W. and Garrett, C. 1998. Frictional estuarine flow in Juan de Fuca Strait, with implications for secondary circulation. *Journal of Geophysical Research*, **103**, C8, 15,657-15,666.

Sutherland, G., Garrett, C. and Foreman, M. 2005. Tidal resonance in Juan de Fuca Strait and the Strait of Georgia. *Journal of Physical Oceanography*, **35**, 1279-1286.

Thomson, R.E., Mihály, S.F. and Kulikov, E.A. 2007. Estuarine versus transient flow regimes in Juan de Fuca Strait. *Journal of Geophysical Research*, **112**, C09022, https://doi:10.1029/2006JC003925

Return to List of Straits

5—GOLDEN GATE INLET, SAN FANCISCO

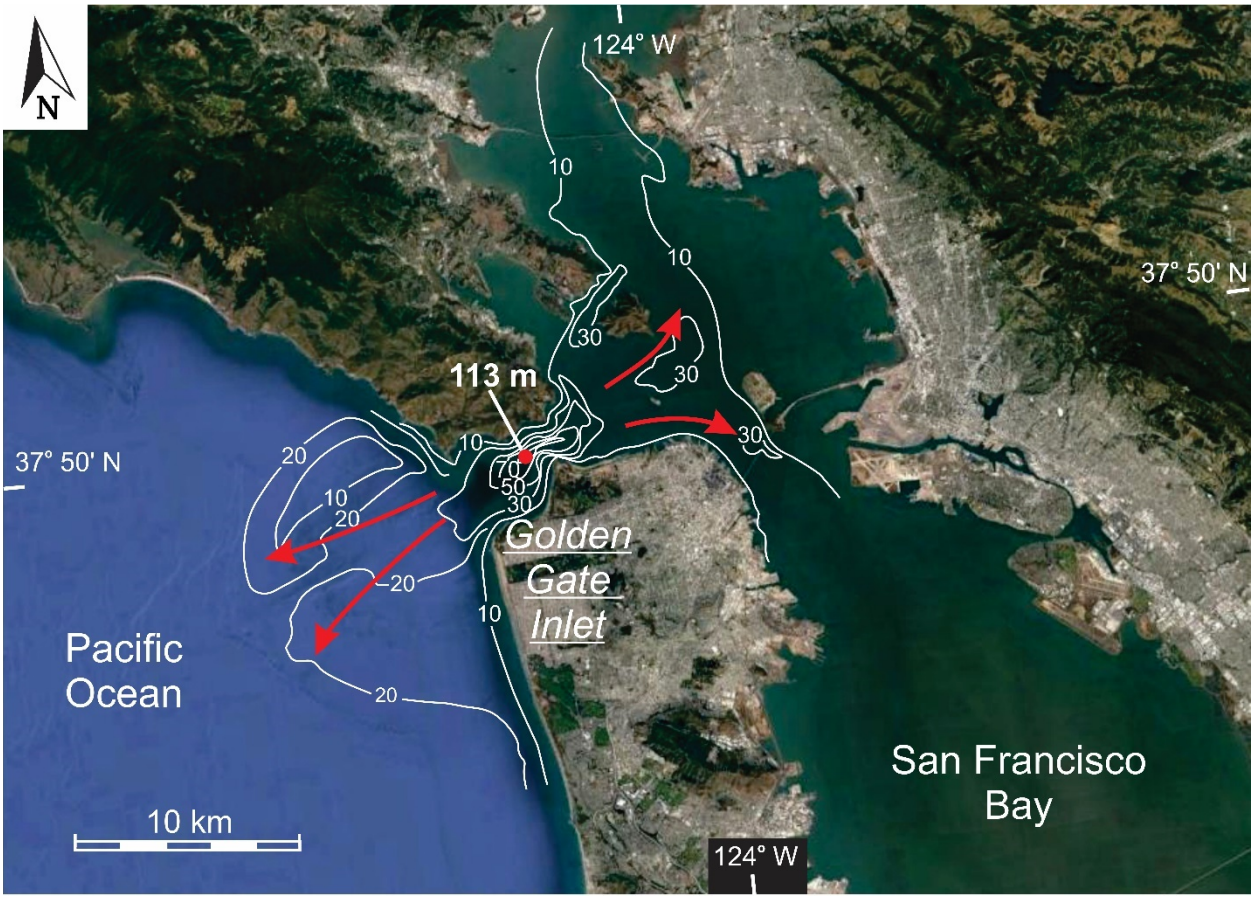

Fig. A5. *<u>The Golden Gate Inlet, San Francisco</u>: The bathymetry shown is modified from Rubin & McCulloch (1980, fig. 1C, based on data from the U.S. Coast and Geodetic Survey) for the main inlet throat and within San Francisco Bay, and from Elias & Hansen (2013, fig. 1) for the ebb-tidal delta seaward of the Golden Gate Inlet. Copyright Elsevier; used with permission. Depths in metres. Satellite image from Google Earth ©. (Data: SIO, NOAA, U.A. Navy, NGA, GEBCO, CSUMB SFLM, CA OPC). The deepest depth in the centre of the inlet scour is 113 m below sea level. There is a well-defined ebb-tidal delta at the seaward end of the strait (Hanes & Bernard 2007; Bernard* et al. *2013a; Elias & Hansen 2013). The corresponding flood-tidal delta is not clearly evident because San Francisco Bay is relatively filled with sediment. Sediment transport is dominated by tidal currents, that are superimposed on a net seaward transport that is presumably driven by the freshwater discharge of the rivers feeding San Francisco Bay (Erikson* et al. *2013).*

Length

ca. 6.6 km long. The narrowest section is a little over 1 km long.

Width

1.5 km wide at its narrowest. At the line of the straight ocean coast, it is 3.8 km wide.

Depth

Deepest point is 113 m deep, with water depths decreasing both landward and seaward. The dunes on the ebb-tidal delta occur in water depths of 30-106 m.

Description

Golden Gate Inlet lies along a suspected fault that runs perpendicular to the main strike-slip faults. The Bay to the east occupies a structural depression between two strike-slip faults... it might be a pull-apart basin that has evolved from a forearc basin. The Golden Gate Inlet is conceptually similar to a 'tidal inlet', although it differs from the classic inlet because it is bedrock constrained, rather than being bounded by mobile barrier islands. The dynamics of the inlet are strongly dominated by tidal currents, which reach 2.5 m s^{-1} in the inlet throat, which is overall ebb dominated, with a net export of sand to the ebb-tidal delta. The current speeds decrease seaward from the inlet, but are still 1 m s^{-1} at the crest of the ebb-tidal delta some 14 km seaward of the Golden Gate Inlet. The 'ebb ramp' is composed of coarse sand to gravel in its proximal part and bears some very large and spectacular dunes that reach up to 10 m high (average 6 m). There is a pronounced seaward fining down the tidal transport path; the crest of the ebb-tidal delta is composed of medium to fine sand. This area is flanked by flood-dominant channels. Waves (mean significant height 2.5 m; maximum 8 m) are important on the crest of the ebb-tidal delta. Like most tidal inlets, the throat of the Inlet is deeply scoured and is floored by bedrock and gravel, so there is no 'sill'. The area landward of the narrows (Central Bay, San Francisco Bay) is lower energy, but still has widespread development of dunes, which are more typically 1-1.5 m high. There is no classic flood-tidal delta because the lagoon is too filled and shallow. There is some 'estuarine circulation' because of freshwater discharge into the 'lagoon', but the freshwater inflow is very small relative to the tidal prism and most workers discount the importance of the estuarine circulation, except perhaps during times of maximum river floods. The sediment comprising the ebb-tidal delta is fluvially supplied sand, which means that the inlet is not a bedload parting, but a through-flow transport path. The dunes on the ebb-tidal delta have heights up to 10 m, and maximum wavelengths of 220 m. Over the last 50 years, the outer margin has eroded, but the 'terminal lobe' away from the dredged ship canal has built higher. There has been extra scour in the inlet throat, with deposition along the coasts.

References

Barnard, P.L., Hanes, D.M., Rubin, D.M., and Kvitek, R.G. 2006. Giant sand waves at the mouth of San Francisco Bay. *Eos*, **87**, 29, 285-289.

Barnard, P.L., Erikson, L.H. and Kvitek, R.G. 2011. Small-scale sediment transport patterns and bedform morphodynamics: new insights from high-resolution multibeam bathymetry. *Geo-Marine Letters*, **31**, 227-236.

Barnard, P.L. Schoellhamer, D.H., Jaffe, B.E. and McKee, L.J. 2013a. Sediment transport in the San Francisco Bay coastal system: An overview. *Marine Geology*, **345**, 3-17.

Barnard, P.L., Erikson, L.H., Elias, E.P.L. and Dartnell, P. 2013b. Sediment transport patterns in the San Francisco Bay coastal system from cross-validation of bedform asymmetry and modelled residual flux. *Marine Geology*, **345**, 72-95.

Elder, W.P. 2013. Bedrock geology of the San Francisco Bay area: A local sediment source for bay and coastal systems. *Marine Geology*, **345**, 18-30.

Elias, E.P.L. and Hansen, J.E. 2013. Understanding processes controlling sediment transports at the mouth of a highly energetic inlet system (San Francisco Bay, CA). *Marine Geology*, **345**, 207-220.

Erikson, L. H., Wright, S.A., Elias, E., Hanes, D.M., Schoellhamer, D.H. and Largier, J. 2013. The use of modeling and suspended sediment concentration measurements for quantifying net suspended sediment transport through a large tidally dominated inlet. *Marine Geology*, **345**, 96-112.

Greene, H.G., Endris, C., Vallier, T., Golden, N., Cross, J., Ryan, H., Dieter, B. and Niven, E. 2013. Sub-tidal benthic habitats of central San Francisco Bay and offshore Golden Gate area—A review. *Marine Geology*, **345**, 31-46.

Hanes, D.M. and Barnard, P.L. 2007. Morphological evolution in the San Francisco Bight. *Journal of Coastal Research*, Special Issue 50: Proceedings of the 9th International Coastal Symposium, Gold Coast, Australia, 469-473.

Rubin D.M. and McCulloch, D.S. 1980. Single and superimposed bedforms: A synthesis of San Francisco Bay and flume observations. *Sedimentary Geology*, **26**, 207-231.

Return to List of Straits

6—STRAIT OF MAGELLAN

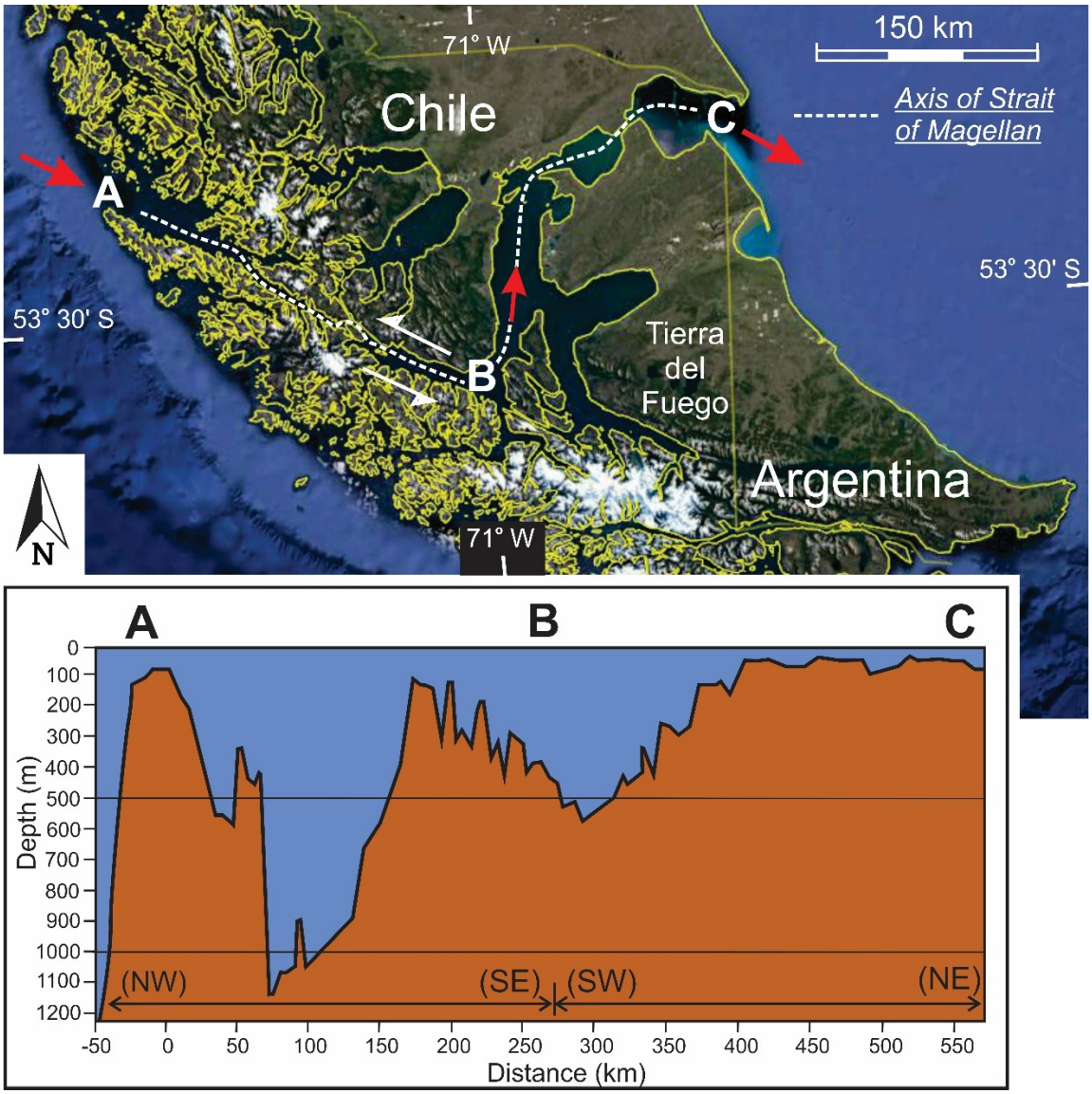

Fig. A6. Strait of Magellan: *The NE-SW segment at the eastern end occupies a rift basin, whereas the narrow SE-NW segment in the west lies along a left-lateral strike-slip fault. Bathymetric profile (A—B—C) along the length of the Straits of Magellan modified from Panella* et al. *(1991, fig. 2). Depths in metres. Satellite image from Google Earth ©. (Data: SIO, NOAA, U.S. Navy, NGA, GEBCO, LDEO-Columbia, NSF. Image: Landsat/Copernicus). The two constrictions that occur in the eastern segment of the Strait (between B and C) are the result of deposition at glacial moraines (McCulloch* et al. *2005; Lovell* et al. *2011). The prevailing flow through the Straits of Magellan is west to east (Panella* et al. *1991; Brun* et al. *2020); this current is part of the Circum-Antarctic circulation that is largely wind-driven. Tidal currents dominate sediment transport at the eastern end of the Strait. Tidal ranges increase inward to the first narrows (west of the letter C), but then decrease to the SW because of frictional dissipation (Medeiros & Kjerfve 1988).*

Length

560 km with a very circuitous, zig-zag path; two main segments-- a generally NE-SW part at the Atlantic end that is ~250 km long with several wider basins and branches; and a SE-NW-oriented western section ~250 m long at the Pacific end that is nearly straight.

Width

Atlantic entrance is 27 km wide. The First Narrows is 4 km wide; the first basin is up to 40 km wide; the Second Narrows is 10 km wide; and the second basin is 31 km wide. The western channel to the Pacific is only 2-5 km wide and passes through an archipelago of islands that allow some connection to the ocean to the south.

Depth

The Atlantic entrance is ~50 m deep. The First Narrows is 50 m deep; the first basin is ~40 m deep; the Second Narrows is 55 m deep; and the second basin averages 20 m deep. The third basin (at the junction of the two segments deepens to the south from 40-550 m. The largest embayment (widest area) has an average depth of 200 m. The westerly channel to the Pacific is up to 1000 m deep! There are a total of 5 basins, separated by 'narrows' in the Atlantic section, and by shallower sills in the Pacific segment. The eastern basin in the E-W segment is 800-1000 m deep; the shoal at its W end is 100-200 m deep; and the westernmost basin rises from ~500 m deep to 50-60 m deep at the shoal at the Pacific end. Overall, the Strait becomes deeper toward the west, with the deepest point (~1100m) in the western third.

Description

The NE-SW segment of the Strait is believed to follow a rift basin that cuts across structural grain, whereas the SE-NW segment follows a left-lateral strike-slip fault. The area was glaciated during MIS 4 (60-70,000 BP and again during the latest glacial maximum. Much of the southern part of the NE-SW segment was ice-filled by northward-flowing glaciers (>700 m thick) during the last glacial maximum and were fronted by glacier-dammed lakes in the isostatically depressed 'moat'. The lakes drained to the Pacific at ~12,700 BP when the glaciers melted back. These lakes were part of the latest glacial advance. The tide on the Atlantic side is semidiurnal and macrotidal (7.1 m mean; 9.0 m springs), whereas the tide on the Pacific side is mixed (mainly semidiurnal) with mean and spring ranges of 1.1 and 1.2 m, respectively. Tidal ranges are amplified into the Strait from the Atlantic, reaching 8.5 m average range, but decrease in a step-wise fashion to the west because of the narrowness of the Strait (termed a 'choking effect'), being only 1.2 m at a distance of 150 km from the Atlantic entrance. Tidal current speeds reach 3 m s^{-1} (and even 4.5 m s^{-1} in the First Narrows) in narrow constrictions. The embayments near the Atlantic end are bordered by wide (up to 7 km) muddy tidal flats, but the channels contain sand bars (and presumably dunes). Sedimentologically, there are 5 components: the first two basins at the Atlantic end are tide-dominated and sandy; the third near the junction of the NE-SW and E-W sections is muddy; the 4th is ~1000 m deep and muddy with tills; and the 5th basin (also nearly 1000 m deep) is muddy with an increasing carbonate content to the west, carried in from the Pacific shelf. Most sediment comes from the ends; lateral input is negligible. The outer half of the Atlantic segment is

floored by sands mainly. Muds occur elsewhere and dominate at depths > ~60 m, except near the Pacific end where the sediments are carbonate sands. Salinity at the Pacific entrance increased at ~8,000 BP, due to the loss of glaciers and less terrestrial runoff—this appears to be consistent with the lack of lateral input of sediment. There is greater lateral input of clastics in the Pacific segment, due to greater rainfall. Sea level was up to 3.5 m above present in the middle Holocene, 5,000-6,000 yr BP. The Atlantic coast is wave dominated, with spits prograding into the mouth of the Strait. The coastline to the south of the mouth is eroding, with littoral drift to the north... the sand is entering the Strait. This erosion is occurring despite the ongoing RSL fall. The opposite spit occurs to the north of the mouth. There is density stratification of the water in the tributary fjords with cold but fresh surface water riding over saltier, warmer water in the main Strait. The main freshwater input is from the southern side (Cordillera de Darwin). Water in the Strait of Magellan is slightly fresher than the open ocean. There is a net west (Pacific) to east (Atlantic) transport of water, which is in the direction of the prevailing winds that probably generate Pacific set-up and Atlantic set-down. There are cross-Strait salinity gradients due to the Coriolis effect... fresher on the northern side where flow is to the east. The eastward flow at the Atlantic mouth is ~0.5 m s^{-1} at the surface. Stratification is well developed in the western segment of the Strait: colder, fresher water on the surface over warmer, saltier Pacific water. The central section is vertically homogeneous due to mixing Atlantic and locally derived colder, fresher water. The eastern section is well mixed Atlantic + local water because of strong tidal currents. No information was available concerning oxygenation of the bottom water in the deep basins.

References

Antezana, T. 1999. Hydrographic features of Magellan and Fuegian inland passages and adjacent subantarctic waters. *Scientia Marina*, *Supplement 1: Magellan-Antarctic: Ecosystems that Drifted Apart*, Arntz, W.E. and Ríos, C. (eds), **63**, p. 23-34.

Brambati, A., Fontolan, G. and Simeoni, U. 1991. Recent sediments and sedimentological processes in the Strait of Magellan. *Bollettino di Oceanologia Teorica ed Applicata*, **IX**, 217-259.

Brun, A.A., Ramirez, N., Pisarro, O. and Piola, A.R. 2020. The role of the Magellan Strait on the southwest South Atlantic Shelf. *Estuarine, Coastal and Shelf Science*, 237, https://doi.org/10.1016/j.ecss.2020.106661

Diraison, M., Cobbold, P.R. and Gapais, E.A. 1997. Magellan Strait: Part of a Neogene rift system. *Geology*, **25**, 703-706.

Harada, N., Ninnemann, U., Lange, C.B., Marchant, M.E., Sato, M., Ahagon, N. and Pantoja, S. 2013. Deglacial-Holocene environmental changes at the Pacific entrance of the Strait of Magellan. *Palaeogeography, Palaeoclimatology, Palaeoecology*, **375**, 125-135.

Lovell, H., Stokes, C.R. and Bentley, M.J. 2011. A glacial geomorphological map of the Seno Skyring-Seno Otway-Strait of Magellan region, southernmost Patagonia. *Journal of Maps*, **7**, 318-339.

Marinoni, L., Setti, M. and Soggetti, F. 1997, Mineralogy of sea-bottom sediments from the Strait of Magellan. *Bollettino di Oceanologia Teorica ed Applicata*, **38**, 281-292.

McCulloch, R.D., Fogwilll, C.J., Sugden, D.E., Mentley, M.J. and Kubik, P.W. 2005. Chronology of the last glaciation in Central Strait of Magellan and Bahía Inútil, southernmost South America. *Geografiska Annaler*, **87A**, 289-312.

Medeiros, C. and Kjerfve, B. 1988. Tidal characteristics of the Strait of Magellan. *Continental Shelf Research*, **8**, 947-960.

Panella, S., Michelato, A., Perdicaro, R., Magazzù, G., Decembrini, F. and Scarazzato, P. 1991. A preliminary contribution to understanding the hydrological characteristics of the Strait of Magellan: Austral Spring 1989. *Bollettino di Oceanologia Teorica ed Applicata*, **IX**, 107-126.

Porter, S.C., Stuiver, M. and Heusser, C.J. 1984. Holocene sea-level changes along the Strait of Magellan and Beagle Channel, southernmost South America. *Quaternary Research*, **22**, 59-67.

Return to List of Straits

7—FLORIDA STAITS

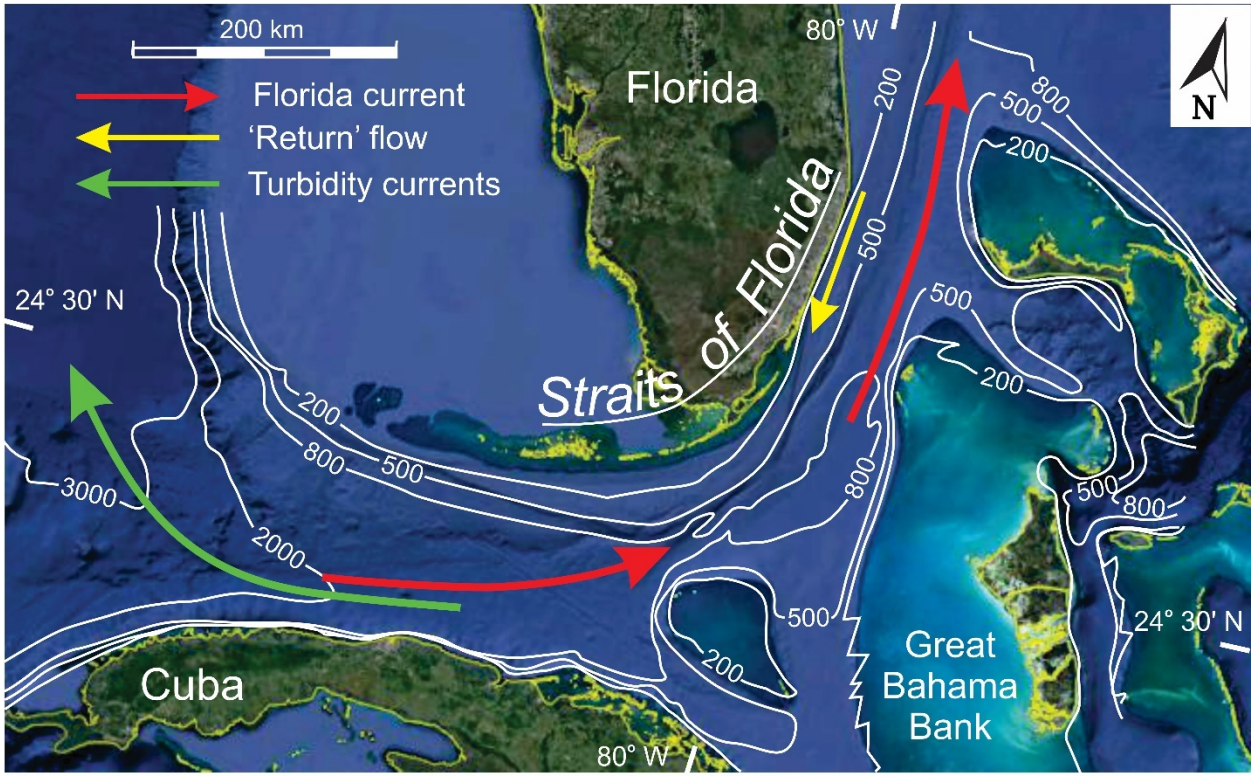

Fig. A7. *Florida Straits: Bathymetry from Hamilton* et al. *(2005, fig. 1; © American Meteorological Society. Used with permission.) Depths in metres. Satellite image from Google Earth © and INEGI. (Data: SIO, NOAA, U.S. Navy, NGA, GEBCO. Image: Landsat/Copernicus). The strait becomes deeper to the south and west, from the more passive northern limb into the tectonically active western limb, which occupies the north-Cuban foreland basin. The cross-sectional profile is asymmetric, with the eastern and southern sides being much steeper than the Florida margin. The dominant current through the Strait of Florida is the Florida Current, which becomes the Gulf Stream in the North Atlantic Ocean (Hamilton* et al. *2005; Czeschel* et al. *2012). The Florida Current is fastest on the eastern side of the N-S segment of the Strait as a result of the Coriolis effect. There is an intermittent, southward-directed current on the western side of the Strait (Gardner* et al. *1989; Soloviev* et al. *2017), the origin of which is not known. A turbidity-current channel system feeds a submarine fan in the southeastern Gulf of Mexico.*

Length

~720 km from southwest of Key West to the northern tip of Little Bahama Bank.

Width

The narrowest point opposite Cay Sal Bank (i.e., the shallow bank located between Cuba and the Bahamas) is ca. 45 km from shelf to shelf; the Strait widens significantly to the west from there, reaching

145 km south of Key West; it also widens to the north to ca. 60 km off Miami and to ca. 80 km off Little Bahama Bank. (All measurements are approximately at the 100 m isobath, so as not to include the marginal shelves).

Depth

The southern Strait is deepest (2100 m) in the west and rises gradually to the east, to 1000 m at the corner where it passes into the northern portion of the Strait. The northern Strait also shallows to the north, being only 715 m deep at its northern end opposite Little Bahama Bank. It is about 750-800 m deep in the most intensely studied section opposite Miami.

Description

The Strait has two parts with different origins: the N-S part is largely due to up-building of the carbonate platforms along the sides with relatively little aggradation of the axis of the Strait, whereas the E-W part is an extension of the north-Cuban foreland basin, bounded by the Florida carbonate platform on the north and the Cuban island-arc province to the south. The bottom water in the northern Strait is colder and less dense than the surface water; flow speeds are up to maybe 1 m s^{-1} (more typically 50-60 cm max., but only 5-20 cm s^{-1} over the contourite drifts). The northward flow occupies most of the N-S Strait and creates contourite drifts. There is a flow to the south on the west side of the Strait (and on the adjacent Florida shelf) that is strong enough at times to generate dunes 1-6 m high; there may also be a contourite drift on the west side. Cold-water coral mounds occur in the deep eastern side of the N-S segment of the Strait and are nucleated on bedrock blocks transported into the Strait from large slump failures on the flank of the Bahamas platform. All sediment in the N-S segment is carbonate sand to ooze that is shed from shallow water, especially from the top of the Bahamas platform. There is significant seasonal and shorter-term variation in the water flux, the cause of which is not certain; seasonal changes are thought to be due either to the strength of the Trade Winds in the equatorial belt, feeding water into the Caribbean, or to local winds. The tides in the Strait are complex and the details of their nature are uncertain.

References

Anselmetti, F.S., Eberli, G.P. and Ding, Z.-D. 2000. From the Great Bahama Bank into the Straits of Florida: A margin architecture controlled by sea-level fluctuations and ocean currents. *GSA Bulletin*, **112**, 829-844.

Brunner, C.A. 1986. Deposition of a muddy sediment drift in the southern Straits of Florida during the Late Quaternary. *Marine Geology*, **69**, 235-249.

Correa, T.B.S., Grasmueck, M., Eberli, G.P., Reed, J.K., Verwer, K. and Purkis, S. 2012. Variability of cold-water coral mounds in a high sediment input and tidal current regime, Straits of Florida. *Sedimentology*, **59**, 1278-1304.

Czeschel, L., Eden, C. and Greatbatch, R.J. 2012, On the driving mechanism of the annual cycle of the Florida Current transport. *Journal of Physical Oceanography*, **42**, 824-839.

Denny, W.M., III, Austin, J.A., Jr. and Buffler, R.T. 1994, Seismic stratigraphy and geologic history of middle Cretaceous through Cenozoic rocks, southern Straits of Florida. *AAPG Bulletin*, **78**, 461-487.

Gardner, W.D., Richardson, M.J. and Cacchione, D.A. 1989. Sedimentological effects of strong southward flow in the Straits of Florida. *Marine Geology*, **86**, 155-180.

Hamilton, P., Larsen, J.C., Leaman, K.D., Lee, T.N. and Waddell, E. 2005. Transports through the Straits of Florida. *Journal of Physical Oceanography*, **35**, 308-322.

Hine, A.C., Wilber, R.J., Bane, J.M., Neumann, A.C. and Lorenson, K.R. 1981. Offbank transport of carbonate sands along open, leeward bank margins: northern Bahamas. *Marine Geology*, **42**, 327-348.

Lee, T.N. and Williams, E. 1988. Wind-forced transport fluctuations of the Florida Current. *Journal of Physical Oceanography*, **18**, 937-946.

Malloy, R.J. and Hurley, R.J. 1970. Geomorphology and geologic structure: Straits of Florida. *GSA Bulletin*, **81**, 1947-1972.

Mayer, D.A., Leaman, K.D. and Lee, T.N. 1984. Tidal motions in the Florida Current. *Journal of Physical Oceanography*, **14**, 1551-1559.

Mullins, H.T., Neumann, A.C., Wilber, R.J., Hine, A.C. and Chinburg, S.J. 1980. Carbonate sediment drifts in northern Straits of Florida. *AAPG Bulletin*, **64**, 1701-1717.

Neumann, A.C. and Ball, M.M. 1970. Submersible observations in the Straits of Florida: Geology and bottom currents. *GSA Bulletin*, **81**, 2861-2874.

Soloviev, A.V., Hirons, A., Maingot, C., Dean, C.W., Dodge, R.E., Yankovsky, A.E., Wood, J., Weisberg, R.H., Luther, M.E. and McCreary, J.P. 2017. Southward flow on the western flank of the Florida Current. *Deep-Sea Research Part I*, **125**, 94-105.

Tournadour, E. Mulder, T., Borgomano, J., Hanqiuez, V., Ducassou, E. and Gillet, H. 2015. Origin and architecture of a mass transport complex on the northwest slope of Little Bahama Bank (Bahamas): Relations between off-bank transport, bottom current sedimentation and submarine landslides. *Sedimentary Geology*, **317**, 9-26.

Wimbush, M. and Lesht, B. 1979. Current-induced sediment movement in the deep Florida Straits: Critical Parameters. *Journal of Geophysical Research*, **84**, C5, 2495-2502.

Return to List of Straits

8—LONG ISLAND SOUND–EAST RIVER

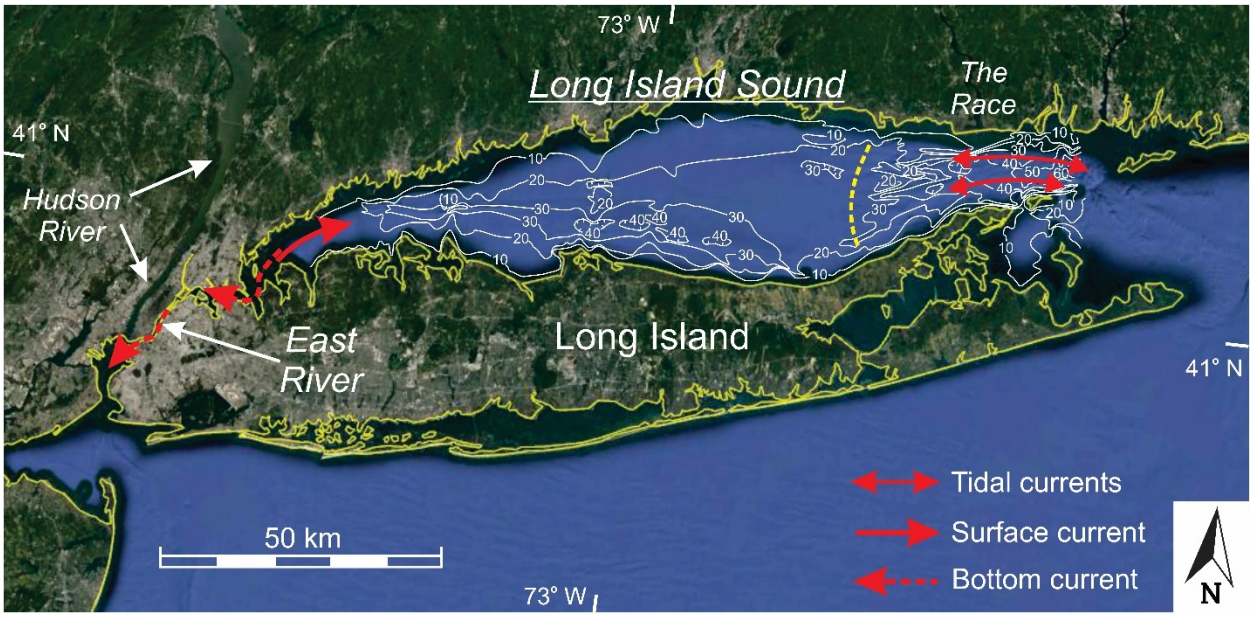

Fig A8. *Long Island Sound–East River: Bathymetry modified from Knebel* et al. *(1999, fig. 2; copyright Elsevier; used with permission; data originally from U.S. Geological Survey maps 40073-E1-TB100 Long Island West and 41073-A1-TB-100 Bridgeport, and U.S. National Ocean Service maps F75 Long Island East and F99 New Haven). Depths in metres. Satellite image from Google Earth ©. (Data: SIO, NOAA, U.S. Navy, NGA, GEBCO. Image: Landsat/Copernicus). Strong tidal currents at the eastern entrance, termed 'The Race', have constructed a series of elongate tidal sand ridges, separated by elongate depressions, that together form a large constriction-related delta (CRD), the western edge of which is shown by the dashed yellow line. Large to very large subaqueous dunes are widespread in this area (Bokuniewicz* et al. *1977). The wider, deeper basin to the west is floored by muddier sediment (Knebel* et al. *1999; Knebel & Poppe 2000). There are also strong tidal currents in the narrow East River (Gunawan* et al. *2014). There is a residual estuarine circulation in the East River and Long Island Sound, with easterly flow at the surface, and westward flow near the bottom, driven by freshwater input by the Hudson River (Blumberg & Pritchard 1997; Blumberg* et al. *1999; Signell* et al. *2000).*

Length

Total length ~ 230 km, including the very tortuous, narrow western part (East River). The main wide part of the Sound is about 150 km long from the eastern narrows, The Race, to the dramatic narrowing at its western end. The East River by itself is ~25 km long.

Width

The system is narrowest at its western end (in New York City) where it is only 0.5 km wide (= the East River). There is another narrows at its eastern end, where it is ~ 13 km wide, called 'The Race'. The wider central part of Long Island Sound is 32.5 km wide.

Depth

Average water depth of main body of Long Island Sound is 24 m, with a 30-60 m-deep axial depression. Depths reach 100 m at the eastern end. East River has a mean depth of 10 m, and a maximum depth >30 m.

Description

The southern side of Long Island Sound is a cuesta of Cretaceous rocks, with the Sound lying along the Cretaceous-Paleozoic basement contact. A series of Quaternary glacial end moraines runs parallel to the length of Long Island. After the glacier retreated, the Sound was occupied by a glacial lake; lake sediments reach 150 m thick locally. The lake drained by 15,500 yr BP. Outwash deltas are widespread along the northern side of the Sound. The lake was followed by a fluvial system, then by an estuary by ~13,500 yr BP. There has been extensive tidal erosion (up to 15 m removed), especially at the eastern end of the Sound. System is in 1/4 wavelength resonance with the M_2 tide, so tidal ranges increase inward (i.e., it is hypersynchronous) from 0.8 m at The Race to 2.6 m at the west end of the Sound during springs. The tidal range decreases to ~1.25-1.4 m at New York harbour. In the East River, tidal currents are greater than 2 m s^{-1} (5-minute average 2.4 m s^{-1} was recorded near the western end) in the narrower western end; they reach 1 m s^{-1} in the broader eastern end. At one measuring site, there was a flood-tide dominance (i.e., toward Long Island Sound). Salinity in the East River increases toward Long Island Sound because of the fresh-water input by the Hudson River at New York. There is weak thermal and salinity stratification in Long Island Sound in the spring and summer, but this is destroyed by surface cooling in the winter. There is no stratification at The Race because of strong tidal mixing. The inner end of the Sound is 5-6 ppt less saline than the mouth. The East River is well mixed to weakly stratified in the western part where currents are strongest. Surface tidal currents at The Race are 1.2 m s^{-1} at springs, reaching 1.6 m s^{-1}. In the wider parts of the Sound, they are typically only 0.2-0.3 m s^{-1}. The flood is shorter than the ebb by about 15 minutes, so there should be a general flood dominance. There is a weak estuarine circulation (eastward at the surface, westward at the bottom with speeds of 5-10 cm s^{-1}. The bottom environments are (from the entrance at The Race, westward): areas of gravelly sediments in areas of erosion and non-deposition near The Race; sands in areas of bedload transport and sediment sorting; to deposition of fine-grained sediment in the central and eastern basins. There is a large area of large dunes (heights to 4 m) just inside the entrance to Long Island Sound, like a subaqueous flood-tidal delta (i.e., a CRD). This pattern defines a tidal transport path entering the Sound. Speeds decrease westward from The Race and there is a general westerly transport of sediment, due to tidal-current asymmetry (the standard deformation of the tidal wave in shallow water), coupled with estuarine circulation (westward inflow of saltier water). The net flow in East River is also to the west. The flow at the connection with Long Island Sound is stratified, but the bottom flow to the west is greater than the surface flow to the east. Flows reverse for days at a time, presumably because of meteorological forcing. The main driver is the head difference between the two ends of the 'river', which is due to tides and wind set-up/set-down. The bed of the East River is floored by bedrock, gravel, gravelly sand, sand and shell debris, with local mussel and *Serpulid* worm colonies. Dunes are likely present. There is a delta of coarse sediment where the East River enters New York harbor. There is net

landward sediment movement into New York Harbor from the sea, forming a flood-tidal delta at The Narrows.

References

Blumberg, A.F., Han, L.A. and St. John, J.P. 1999. Three-dimensional hydrodynamic model of New York harbor region. *Journal of Hydraulic Engineering*, **125**, 799-816.

Blumberg, A.F. and Pritchard, D.W. 1997. Estimates of the transport through the East River, New York. *Journal of Geophysical Research*, **102**, C3, 5685-5703.

Bokuniewicz, H.J, Gordon, R.B. and Kastens, K.A. 1977. Form and migration of sand waves in a large estuary, Long Island Sound. *Marine Geology*, **24**, 185-199.

Coch, N.K. 2016. Sediment dynamics in the Upper and Lower Bays of New York Harbor. *Journal of Coastal Research*, **32**, 756-767.

Coch, N.K., Barton, K.G. and Longoria, A.G. 1991. Holocene evolution of the Hudson River estuary. *Journal of Coastal Research*, **11**, 55-71.

Gunawan, B., Neary, V.S. and Colby, J. 2014. Tidal energy site resource assessment in the East River tidal strait, near Roosevelt Island, New York, New York. *Renewable Energy*, **71**, 509-517.

Knebel, H.J., Signell, R.P., Rendigs, R.R., Poppe, L.J. and List, J.H. 1999. Seafloor environments in the Long Island Sound estuarine system. *Marine Geology*, **155**, 277-318.

Knebel, H.J. and Poppe, L.J. 2000. Sea-floor environments within Long Island Sound: A regional overview. *Journal of Coastal Research*, **16**, 533-550.

Lewis, R.S. and DiGiacomo-Cohen, M. 2000. A review of the geologic framework of the Long Island Sound Basin, with some observations relating to postglacial sedimentation. *Journal of Coastal Research*, **16**, 522-532.

Poppe, L.J., Knebel, H.j., Mlodzinska, Z.J., Hastings, M.E. and Seekins, B.A. 2000. Distribution of surficial sediment in Long Island Sound and adjacent waters: texture and total organic carbon. *Journal of Coastal Research*, **16**, 567-574.

Signell, R.P., List, J.H. and Farris, A.S. 2000. Bottom currents and sediment transport in Long Island Sound: A modeling study. *Journal of Coastal Research*, **16**, 551-566.

Return to List of Straits

9—MINAS PASSAGE AND MINAS CHANNEL, BAY OF FUNDY

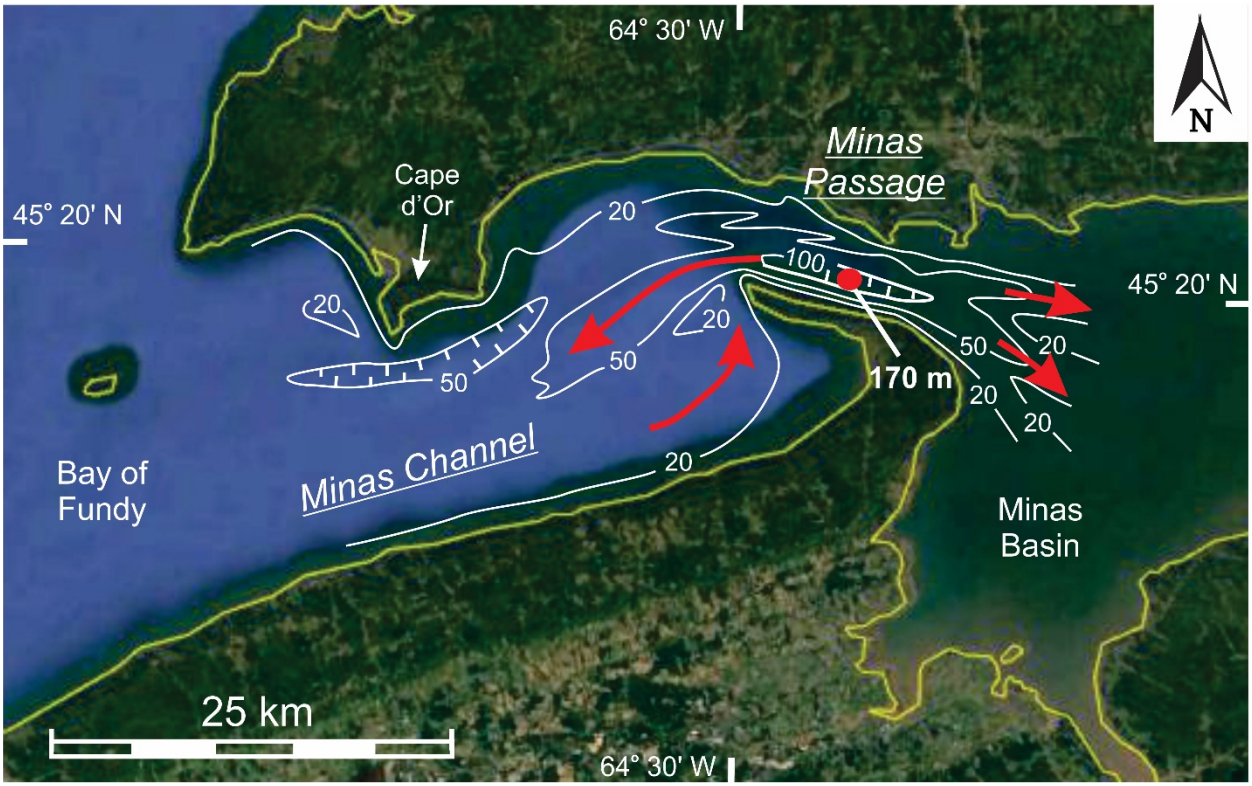

Fig. A9. Minas Passage and Channel: *Bathymetry modified from Shaw* et al. *(2012, fig. 2; copyright Elsevier; used with permission). Depths in metres. Satellite image from Google Earth ©. (Data: SIO, NOAA, U.S. Navy, NGA, GEBCO. Image: Maxar Technologie, CNES/Airbus). The location of the Minas Passage is constrained on its south side by the North Mountain Basalt (Jurassic), that has been folded into a westerly plunging syncline. The Minas Channel cuts across the trend of this unit. Flow in Minas Passage and Minas Channel is strongly tide-dominated; if there is any residual flow because of freshwater discharge within the Minas Basin to the east, it has not yet been documented. The tidal currents have constructed a poorly defined ebb-tidal delta in the transition from Minas Passage to the Minas Channel, with a central ebb-dominant channel, flanked to the SE by a flood-dominant, marginal channel. The elongate tidal bar between the two channels is analogous to a 'channel-margin linear bar' in the Hayes model for ebb-tidal deltas. (Compare with the ebb-tidal delta at the mouth of the Golden Gate Inlet). The closed 20 m isobath to the west of the prominent headland, Cape d'Or, is a banner bank that formed in recirculating eddy shed by this headland.*

Length

Minas Passage: ~15 km; Minas Channel: ~ 35 km, sinuous

Width

Minas Passage: minimum 4.5 km, funnel-shaped at both ends; Minas Channel: minimum 13.4 km, sinuous

Depth

Deepest scour at the narrowest point: 170 m deep. Minas Basin average 19 m; most of its area is 20-50 m deep, with localized deeper tidal scours.

Description

This channel, located at the mouth of the Minas Basin arm of the Bay of Fundy, lies along a major geologic tectonic suture within the Appalachians. This Cobequid-Chedabucto fault experienced left-lateral strike-slip movement during the failed opening of the Bay of Fundy rift in the early to mid-Triassic. Synrift sedimentation in the rift basin (a half graben) was initially lacustrine, with fluvial input from the north side, that extended into the Jurassic. An extrusive basalt unit accumulated to form the North Mountain Basalt, and was then gently folded into a westerly-plunging syncline, creating the hook-like peninsula that separates the Minas Basin from the main Bay of Fundy. The Minas Passage and Channel is a breach in this basalt layer that is the result of post-depositional normal faulting (the so-called Minas Fault). The area was entirely glaciated, and experienced complex changes in glacial flow directions. It was deglaciated by ~14,000 yr BP. Sea level was initially higher than today, then fell to a lowstand before rising to the present level. Tidal range has been increasing from mesotidal over the last 5000 years, but there appears to have been a 'sudden' increase in range in the Minas Basin because of the destruction of a gravel barrier at Minas Passage (Shaw *et al.*, 2010). Since the barrier's destruction, 4.4 km^3 of sediment has been removed by erosion. Now, the natural period of the Bay of Fundy-Gulf of Maine system is ~ 13 hours, which is close to the dominant, M_2 period. Tidal ranges in Minas Basin average 12.4 m; maximum range is 16.2 m. Time and depth-averaged tidal current speeds are up to 3.3 m s^{-1}; maximum speeds are 4-5 m s^{-1}, decreasing into Minas Basin to 1.5 m s^{-1}. (Numerical models predict maximum speeds in MInas Passage up to 5.2 m s^{-1}). Suspended-sediment concentrations are 10-30 g m^{-3} in winter; <10 g m^{-3} in summer. The strongest currents occur at the narrowest part of Minas Passage, but also off the tip of Cape d'Or on the north side of Minas Channel. These are the areas with the deepest scours. Southeast of Cape d'Or, there is a mutually evasive pair of scours. Residual circulation results show two oppositely directed gyres, a counter-clockwise one outside Minas Passage, and a clockwise one in the southern Minas Basin. There is a parting at the west end of Minas Passage, approximately opposite the tip of Cape Split. In Minas Passage, flood dominance occurs along the northern half, whereas ebb dominance occurs along the southern side. In the Minas Channel, residual transport is to the east (flood-dominant) in the southern half, and to the west (ebb-dominant) to the north. These two transport paths are separated by an elongate tidal ridge that is analogous to the 'channel-margin linear bar' of the ebb-tidal delta model. Minas Basin imports coarse sediment, but exports suspended sediment. The scour troughs are incised into an area that is generally 20-30 m deep. The main trough shallows and bifurcates to both the east and west. There are smaller scour toughs near Cape d'Or; they are scoured ~25 m down from the original surface. They have sharp edges. They are cut into glaciomarine sediments that are composed mainly of mud. The scour is floored with bedrock, till, glaciomarine sediments and coarse gravel/boulders. Gravel dunes reach heights of 25 m. Paired banner banks occur at Chignecto Cape and Cape d'Or. The bank at the tip of Cape Split has dunes migrating on opposite directions on either side, in a counter-clockwise sense; it is composed of coarse to very coarse sand. There is a gravel bank on the north flank of Cape Split. All of the banks lie in levee-like locations relative to the main scour, or between the main scour and the smaller scours. There is no

'terminal lobe' as in a tidal delta. There is not much swath bathymetric coverage from Minas Basin, but no dune fields are shown. It is possible that the Minas Basin has lower salinities than the main Bay of Fundy because of river discharge, but there is no report of any estuarine circulation; the tidal mixing is probably too great.

References

Ashall, L.M., Mulligan, R.P. and Law, B.A. 2016. Variability in suspended sediment concentrations in the Minas Basin, Bay of Fundy, and implications for changes due to tidal power extraction. *Coastal Engineering*, **107**, 102-115.

Li, M.Z., Shaw, J., Todd, B.J., Kostylev, V.E. and Wu, Y. 2014> Sediment transport and development of banner banks and sandwaves in an extreme tidal system: Upper Bay of Fundy, Canada. *Continental Shelf Research*, **83**, 86-107.

Mulligan, R.P., Smith, P.C., Hill, P.S., Tao, J. and van Proosdij, D. 2013. Effects of tidal power generation on hydrodynamics and sediment processes in the upper Bay of Fundy. *4th Specialty Conference on Coastal, Estuary and Offshore Engineering*, Montréal, Quebec, Canada, May 29-June 1, 2013, COS-012-1—COS-012-10.

Mulligan, R.P., Smith, P.C., Tao, J. and Hill, P.S. 2019. Wind-wave and tidally driven sediment resuspension in a macrotidal basin. *Estuaries and Coasts,* **42**, 641-654.

Shaw, J., Amos, C.L., Greenberg, D.A., O'Reilly, C.T., Parrot, D.R. and Patton, E. 2010. Catastrophic tidal expansion in the Bay of Fundy, Canada. *Canadian Journal of Earth Sciences*, **47**, 1079-1091.

Shaw, J., Todd, B.J., Li, M.Z. and Wu, Y. 2012. Anatomy of the tidal scour system at Minas Passage, Bay of Fundy, Canada. *Marine Geology*, **323-325**, 123-134.

Stea, R.R. and Wightman, D.M. 1987. Age of the Five Islands Formation, Nova Scotia, and the deglaciation of the Bay of Fundy. *Quaternary Research*, **27**, 211-219.

Wade, J.A., Brown, D.E., Traverse, A. and Fensome, R.A. 1996. The Triassic-Jurassic Fundy Basin, eastern Canada: regional setting, stratigraphy and hydrocarbon potential. *Atlantic Geology*, **32**, 189-231.

Wu, Y., Chaffey, J., Greenberg, D.A., Colbo, K. and Smith, P.C. 2011. Tidally-induced sediment transport patterns in the upper Bay of Fundy: A numerical study. *Continental Shelf Research*, **31**, 2041-2053.

Return to List of Straits

10—NORTHUMBERLAND STRAIT

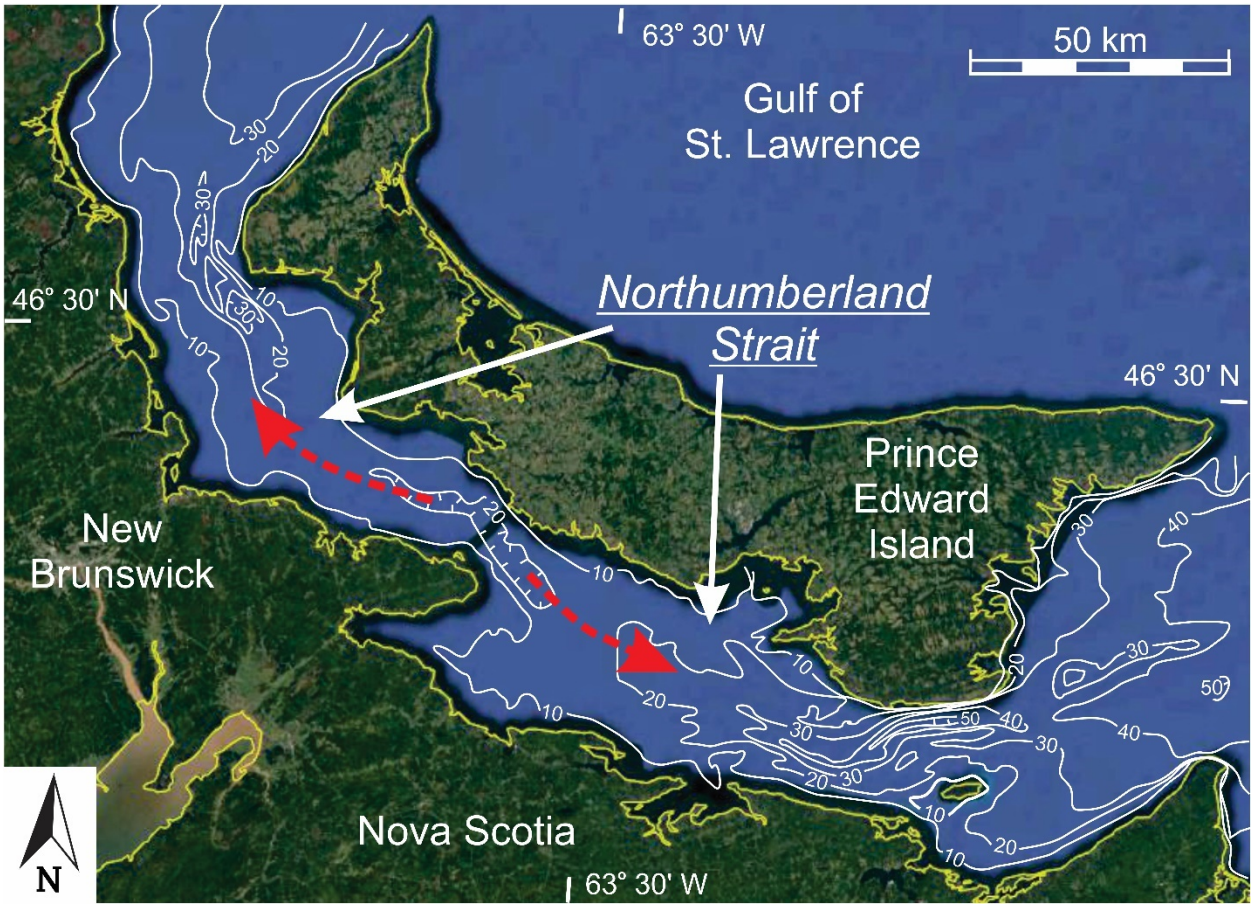

Fig. A10. Northumberland Strait: *Bathymetric contours reproduced with permission of Canadian Science Publishing from Kranck (1972a, fig. 1); permission conveyed through Copyright Clearance Center Inc. Depths in metres. Satellite image from Google Earth ©. (Data: SIO, NOAA, U.S. Navy, NGA, GEBCO. Image: Landsat/Copernicus). The Strait as a whole follows the strike of the Permo-Carboniferous bedrock. The curvilinear depressions at the central narrows are thought to be originally of fluvial origin, cut during the sea-level lowstand. Because the tidal currents are not particularly strong, there is no pronounced deep scour at the narrowest point. The residual transport diverges from the central narrows because of tidal-current asymmetries associated with the tide entering the Strait from both ends (Lauzier 1965; Crowley 1969; Kranck 1972b). Wave energy is weak within the Strait, but a large spit has been constructed by waves at the eastern tip of Prince Edward Island.*

Length

Total length (tip to tip of PEI): 320 km; narrower part: 215 km long.

Width

Narrowest point: 14.5 km; narrows at west end: 21.5 km; narrows at east end: 20.5 km; maximum width: 41.5 km

Depth

Western part: 10-20 m deep; eastern part: > 30 m; shallowest area (~15 km east of the narrows): 18 m deep. There is a curved, linear deep area south of the east end of PEI where depths reach > 50 m.

Description

Northumberland Strait supposedly follows the course of river valleys, perhaps deepened further by glaciation. There is a paleo-drainage divide at the location of the narrowest point, with river valleys heading both west (shorter) and east (longer and deeper). The course of the Strait approximately follows the strike of the Permo-Carboniferous strata that dip gently northward into the Gulf of St. Lawrence, with the Strait following the more easily eroded strata. The thalweg of the western valley is at ~ - 20-40 m; the thalweg of the eastern valley is ~ - 40-60 m. The sea-level lowstand associated with the forebulge was at 5400 years BP at - 15.5 m; since then, there has been sea-level rise. The tide enters the strait from both ends, and are 5 hours out of phase. Tides are more hypersynchronous in the eastern part of the strait, generating larger tides to the east of the narrows than at either end. Tidal range at east end ~ 2 m, whereas near the west end it is 0.6 m. The Coriolis effect has a small but detectable influence on the tides, making them slightly larger on the PEI side. At the narrows, the mean and large tidal ranges are 1.5 m and 2.25 m. Peak tidal-current speeds are ~1 m s^{-1} at this location. The system is thought to be ebb dominated everywhere, which would mean that transport diverges from the point where the tides entering from both ends meet, which is a point 3/4 of the way from the east end. There is a residual flow from west to east through the Strait. The water is brackish throughout because of river input. The bottom sediments are well correlated with average maximum tidal-current speed. Sand (and gravel) occur at the 3 narrow locations (at the central narrows, and at headlands at the west and east ends of the Island), while mud accumulates in the wider areas with slower currents. Mud deposition along the southern side has been ongoing since most recent flooding ca. 3000 years ago, with mud thicknesses reaching > 3 m.

References

Crowley, J.E. 1969. Tidal model of Northumberland Strait. *Journal of the Hydraulics Division*, **95**, 827-838.

Kranck, K. 1972a. Geomorphological development and post-Pleistocene sea-level changes, Northumberland Strait, Maritime Provinces. *Canadian Journal of Earth Sciences*, **9**, 835-844.

Kranck, K. 1972b. Tidal current control of sediment distribution in Northumberland Strait, Maritime Provinces. *Journal of Sedimentary Petrology*, **42**, 596-601.

Lauzier, L.M. 1965. Drift bottle observations in Northumberland Strait, Gulf of St. Lawrence. *Journal of the Fisheries Research Board of Canada*, **22**, 353-368.

Lu, Y., Thompson, K.R. and Wright, D.G. 2001. Tidal currents and mixing in the Gulf of St. Lawrence: an application of the incremental approach to data assimilation. *Canadian Journal of Fisheries and Aquatic Science*, **58**, 723-735.

McRoberts, J.H.E. 1968. Post-glacial history of Northumberland Strait based on benthic foraminifera. *Maritime Sediments*, **4**, 88-95.

Nairn, R.B. and Anglin, C.D. 2002. Confederation Bridge—New scour design methodology for complex materials. *In*: *First International Conference on Scour of Foundations*, Chen, H.-C. and Briaud, J.-L. (eds), Texas Transportation Institute, November 17-20, 2002, College Station, Texas, 978-992.

Scott, D.B., Medioli, F.S. and Miller, A.A.L. 1987. Holocene sea levels, paleoceanography, and late glacial ice configuration near the Northumberland Strait, Maritime Provinces. *Canadian Journal of Earth Sciences*, **24**, 668-675.

Shaw, J, Duffy, G. Taylor, R.B., Chassé, J. and Frobel, D. 2008. Role of a submarine bank in the long-term evolution of the northeast coast of Prince Edward Island, Canada. *Journal of Coastal Research*, **24**, 149-1259.

van de Pol, H.W. 1989. Lithostratigraphy of the Prince Edward Island redbeds. *Atlantic Geology*, **25**, 23-35.

Return to List of Straits

11—STRAITS OF MACKINAC

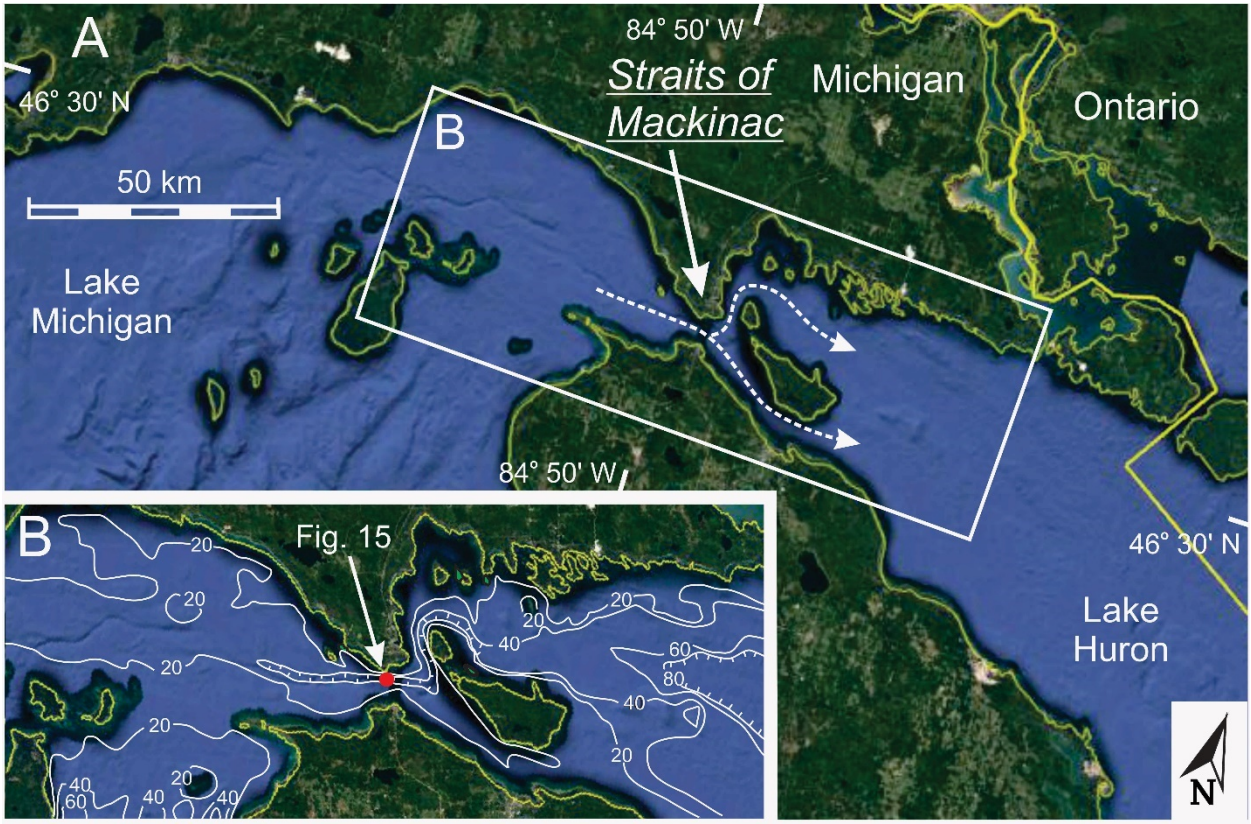

Fig. A11. *Straits of Mackinac: (A) General setting of the Straits of Mackinac. (B) Detailed bathymetry modified from Anderson & Schwab (2013, fig. 1; copyright Elsevier; used with permission). Depths in metres. Satellite images from Google Earth ©. (Image: NOAA, Landsat/Copernicus). The curvilinear, elongate axial depression through the strait that passes north of the islands at the east end is of fluvial origin, with erosion occurring most recently during a low lake-level stage following shortly after deglaciation because isostatic rebound exceeded uplift of the lake's outlet. The strongest currents now are of meteorological origin and show prominent reversals at periods longer than tidal (Anderson & Schwab 2013); the red dot in (B) shows the location at which the currents shown in Fig. 15 of the main paper were obtained. The residual flow is 'estuarine' in character, with surface outflow toward the east [white dashed lines in (A)], and inward (westward) flow at the bed (Saylor & Sloss 1976; Quinn 1977). This circulation is driven by the freshwater input to Lake Michigan.*

Length

Complex pattern because of island at east end, around which the channel splits. ~70 km long going to the north of the islands; ~61 km long to the south of islands (South Channel).

Width

5.6 km N-S at narrowest; absolute narrowest point is 4 km E-W from island to north shore; South Channel to ESE is ~ 6 km wide at narrowest. Saylor and Sloss (1976) give cross-sectional area as a function of depth.

Depth

45-50 m deep (maximum 88 m) in the central, V-shaped channel.

Description

Bedrock (Silurian and Devonian carbonates and shales) strikes parallel to the Straits and dips to the south, into the Michigan Basin. The main bedrock unit beneath the Straits is the Makinaw Breccia that was generated by salt-solution collapse affecting Silurian to middle Devonian strata. A buried river channel passes through the Straits, bending northward around the islands to the east of the main narrows. Along much of its length, it is only 400-800 m wide. Its age is unknown-- it might be pre-glacial, interglacial and/or post-glacial during a low-lake-level phase. The most recent period of occupation was during the Lake Chippewa phase ~9800 yr PB, a lacustrine low-level phase caused by isostatic rebound following deglaciation. Lake level then rose of Nippissing highstand (~3-4 m above present), and then fell to modern level, which has existed for the last ~ 4000 years. The Straits have existed since ~8150 yr BP. In nearby areas to the southwest, shallow water has sand/gravel/bedrock due to wave action, whereas deeper water contains mud. Winter ice reaches an average maximum thickness of 18 inches, with maximum thicknesses of 30 inches. There is little vertical stratification in the eastern half of the Strait, but strong stratification in the narrow western half. Some of the deep water might be more or less stagnant. There is eastward flow in the warmer surface layer, and slower eastward or even westward flow in the denser lower layer. Maximum speeds in each direction are ~8 cm s^{-1}: average eastward is 4.5 cm s^{-1}; average westward 2.8 cm s^{-1}. Net flow is out of Lake Michigan. There are significant flow reversals with instantaneous discharges 30-40 times the averages-- maximum recorded current was 110 cm s^{-1}, currents unlike anywhere else in the Great Lakes. Reversals at inertial, semidiurnal tidal and seiche periods for both lakes (Michigan-- 8.8 hours; Huron-- 6.8 hours). Seiches cause water-elevation differences (up to ~ 10 cm) between the two lakes. Seiches are due to meteorological forcing due to the passage of atmospheric systems. In the open lake, suspended-sediment concentrations are 0.5-2 mg l^{-1}. There is some authigenic calcite precipitation in 'whitings' in the late summer. There is up to 4-5 m of 'lake clay' overlying till in the narrows. Modern mud is apparently absent from the Straits; there might be a thin veneer of sand in the Straits due to modern winnowing. Bottom sediments in the Straits are <10% finer than 60 microns. I did not discover any detailed surveys showing the presence/absence of bedforms in the Straits

References

Anderson, E.J. and Schwab, D.J. 2013. Predicting the oscillating bi-directional exchange flow in the Straits of Mackinac. *Journal of Great Lakes Research*, **39**, 663-671.

Eadie, B.J. and Robbins, J.A. 2005. Composition and accumulation of recent sediments in Lake Michigan. *In*: *State of Lake Michigan: Ecology, Health and Management*, Edsall, T. and Munawar, M. (eds), Michigan State University Press, East Lansing, Michigan, 89-111.

Fisher, T.G. 1999/2000. Geology of the Grand Calumet River region. *Proceedings of the Indiana Academy of Science*, **108/109**, 11-18.

Melhorn, W.N. 1959. Geology of Mackinac Straits in relation to Mackinac bridge. *The Journal of Geology*, **67**, 403-416.

Quinn, F.H. 1977. Annual and seasonal flow variations through the Straits of Mackinac. *Water Resources Research*, **13**, 137-144.

Saylor, J.H. and Sloss, P.W. 1976. Water volume transport and oscillatory current flow through the Straits of Mackinac. *Journal of Physical Oceanography*, **6**, 229-237.

Stanley, G.M. 1938. The submerged valley through Mackinac Straits. *The Journal of Geology*, **46**, 966-974.

Return to List of Straits

12—HUDSON STAIT

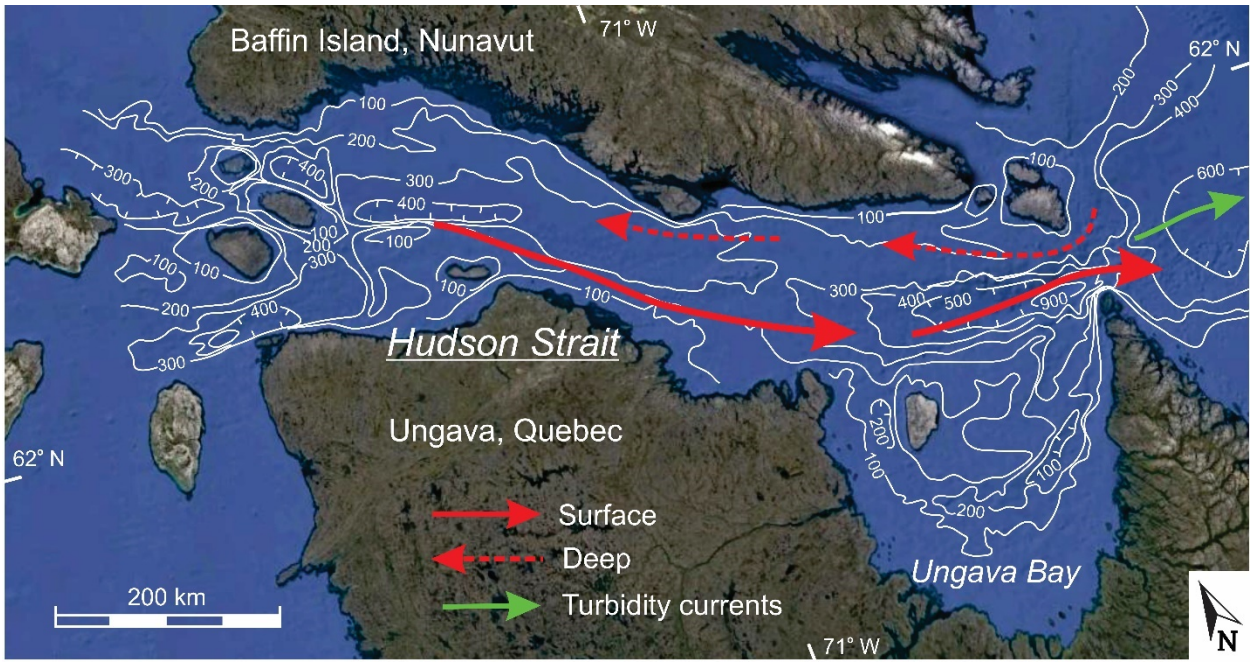

Fig. A12. Hudson Strait: *Bathymetry from Andrews & MacLean (2003, fig. 1; © 2003 Taylor & Francis; bathymetry originally from MacLean (2001),* Natural Resources Canada *– Open Government Licence-Canada). Depths in metres. Satellite image from Google Earth ©. (Data: SIO, NOAA, U.A. Navy, NGA, GEBCO. Image: IBCAO, Landsat/Copernicus). Hudson Strait was the main exit pathway for ice flowing northeastward away from the ice domes in northern Canada (Andrews & MacLean 2003). Deep glacial scour occurred. This channel also experienced extreme melt-water-flow events associated with the catastrophic drainage of glacial Lake Agassiz (Lajeunesse & St-Onge 2008). It was a major conduit for sediment export during glacial periods. The persistent modern flow is driven by the freshwater discharge from Hudson Bay, which creates a strong eastward current along the southern coast because of the Coriolis effect (Drinkwater 1986, 1988; Straneo & Saucier 2008). There is a compensating inward flow along the northern margin. A major deep-sea turbidite system originates at the shelf edge, at the mouth of Hudson Strait. It was active during the glacial maximum.*

Length

750 km-- nearly straight, but slightly curved at its western end.

Width

62 km at its eastern end (off the tip of Ungava Peninsula). 115-150 km wide through most of its length. Western end complicated by several islands; main southern opening 53 km wide. Ungava Bay along the southeastern margin of the Strait has a mouth that is 250 km wide.

Depth

The Strait has a U-shaped cross section, with maximum depths of 300-400 m through most of the Strait, but reaching > 900 m at the eastern end.

Description

The Strait lies along an ancient tectonic lineament, separating two Precambrian crustal blocks. It was a depression in the Paleozoic, and was reactivated as a failed rift (i.e. an aulacogen) during opening of the Labrador Sea in the early Cenozoic. At this time, it was occupied by a major, continental-scale fluvial system (Corradino *et al.*, 2022). It was the main outflow location for ice from the Laurentide Icesheet. There is a strong, net outward flow (0.3 m s^{-1}) along the southern (Quebec) shore and a weaker, net inward flow along the northern shore. The outflow forms 15% of the volume and 50% of the fresh water in the Labrador Current. Tidal current speeds are generally 0.2-1 m s^{-1} but reach 2 m s^{-1} at the eastern end of the Strait. Unconsolidated sediments reach > 130 m thick in the western and eastern deeps. Acoustically transparent deposits interpreted to be till are the mot widespread and thickest. There are multiple 'till tongues' that interfinger with glacio-marine deposits. Glacio-marine deposits also overlie the till tongues. Glacial-fluvial outwash is also important at the eastern and western ends. Final deglaciation occurred by ~11,000-12,000 yr BP. There is ice cover from mid-November until early August. From generalized core logs, the surface sediment drape, which is 1-5 m thick (commonly > 4 m), consists of fine-grained, muddy sediment with some shells and abundant burrows. Diffuse lamination is present locally. There is minor evidence of slumping of the margins of the strait. Current-generated bedforms have not been reported.

References

Andrews, J.T. and MacLean, B. 2003. Hudson Strait ice streams: a review of stratigraphy, chronology and links with North Atlantic Heinrich events. *Boreas*, **32**, 4-17.

Corradino, J., Pullen, A., Leier, A.L. Barbeau, D.L., Jr., Scher, H.D., Weislogel, A., Bruner, A., Leckie, D.A., and Currie, L.D. 2022. Ancestral trans-North American Bell River system recorded in late Oligocene to early Miocene sediments in the Labrador Sea and Canadian Great Plains. *GSA Bulletin*, **134**, 130-144.

Cummins, P.F., Karsten, R.H. and Arbic, B.K. 2010. The semi-diurnal tide in Hudson strait as a resonant channel oscillation. *Atmosphere-Ocean*, **48**, 163-176, https://doi: 10.3137/OC307.2010

Drinkwater, K.F. 1986. Physical oceanography of Hudson Strait and Ungava Bay. *In*: *Canadian Inland Seas*, Martini, I.P. (ed), Elsevier Oceanography Series, **44**, 237-266.

Drinkwater, K.F. 1988. On the mean and tidal currents in Hudson strait. *Atmosphere-Ocean*, **26**, 252-266, https://doi: 10.1080/07055900.1988.9649302

Lajeunesse, P. and St-Onge, G. 2008. The subglacial origin of the Lake Agassiz-Ojibway final outburst flood. *Nature Geoscience*, **1**, 184-188.

Pinet, N., Lavoie, D. and Keating, P. 2013. Did the Hudson Strait in Arctic Canada record the opening of the Labrador Sea? *Marine and Petroleum Geology*, **48**, 354-365.

Straneo, F. and Saucier, F. 2008. The outflow from Hudson Strait and its contribution to the Labrador Current. *Deep-Sea Research 1*, **55**, 926-946.

Vilks, G., MacLean, B., Deonarine, D., Currie, C.G. and Moran, K. 1989. Late Quaternary paleoceanography and sedimentary environments in Hudson Strait. *Géographie Physique et Quaternaire*, **43**, 161-178.

Return to List of Straits

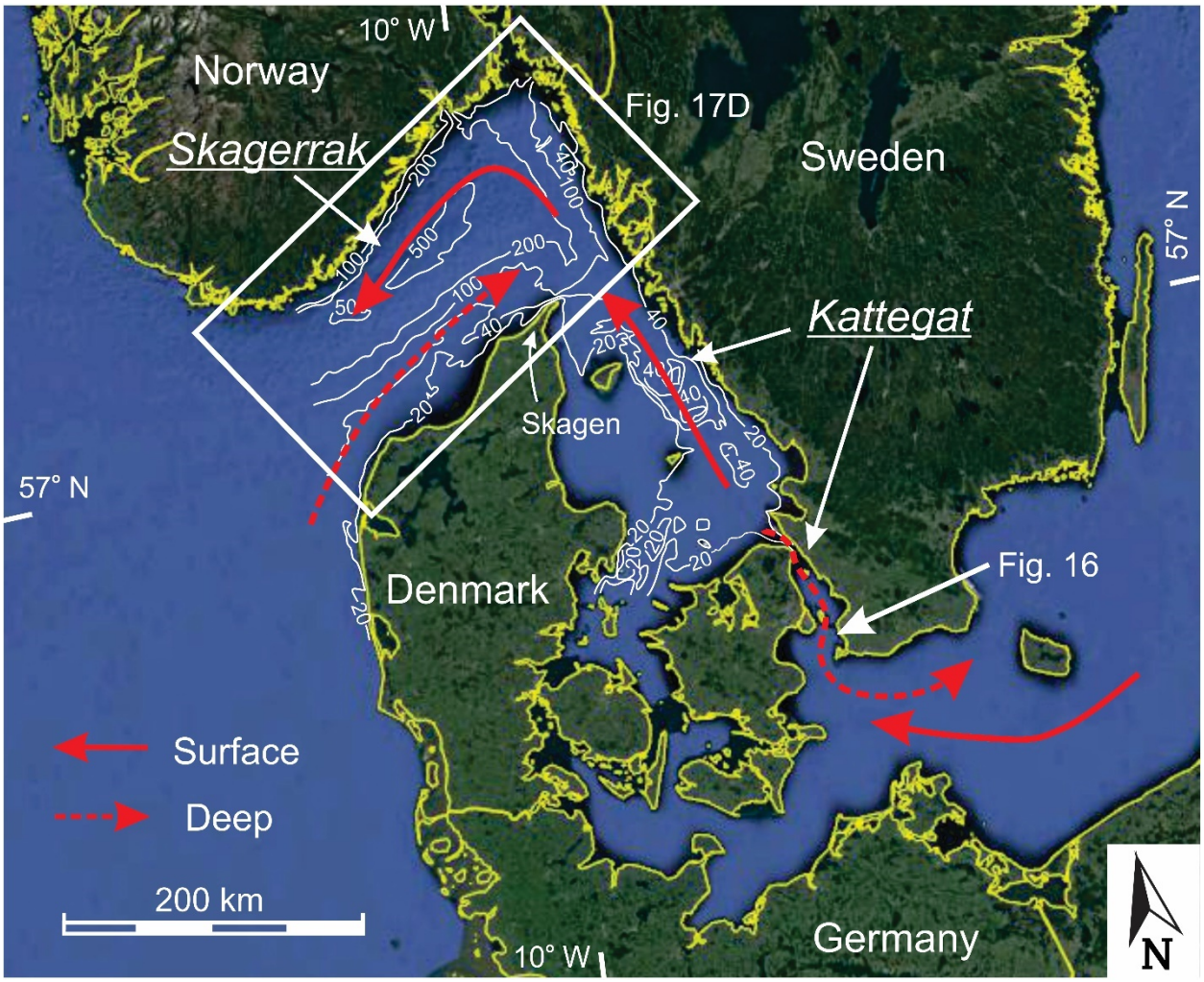

Fig. A13. *Kattegat and Skagerrak: Bathymetry simplified after Kuijpers* et al. *(1993, fig. 1; copyright Elsevier; used with permission). Depths in metres. Satellite image from Google Earth ©. (Data: SIO, NOAA, U.S. Navy, NGA, GEBCO. Image: Landsat/Copernicus). The Skagerrak between Norway and Denmark was occupied by a glacial ice stream (Rise* et al.*1996; Larsson & Stevens 2008) and is a fjord. The Kateggat was not deeply scoured by ice. It was occupied by a (subglacial?) meltwater drainage channel, and by rivers during the post-glacial lowstand (Lykke-Andersen* et al. *1993; Bennike* et al. *2004). The strongest currents through the Kattegat and its various channels are the result of meteorological forcing (Büchmann* et al. *2011; Haid* et al. *2020). The residual currents are an estuarine circulation driven by the freshwater discharge from the Baltic Sea (Gustafsson & Stigebrandt 1996; Sayin & Krauss 1996; Mattsson 1996; Rodhe 1996), with outward flow on the top, and inward flow at the bottom in the Kattegat. In the Skaggerak, the outward flow hugs the northern shore, while the inward flow is banked up against the southern margin (Rodhe 1987, 1996) because of the Coriolis effect. The rectangle shows the location of Figs. 17D in the main text, and the dashed red arrow in the Kattegat shows the line of section in Fig. 16. The wave-formed Skagen spit is probably the largest sand body in this strait.*

Length

Skagerrak: ~260 km long NE-SW. Kattegat: Most direct route through narrow passage into the Baltic, around the southern tip of Sweden-- 610 km.

Width

Skagerrak: 110 km, nearly parallel sided. Kattegat: 55 km at its northern end; widest central part-- 120 km; widest narrow passage-- 16.5 km; narrowest point on second passage (Øresund)-- 4 km; narrowest passage--~ 1 km wide; off the southern tip of Sweden-- 170 km wide, N-S.

Depth

Skagerrak: up to 700 m; average 210 m; has a fjord-like morphology. Kattegat: Most of the strait is < 50 m deep-- mean depth 23 m, and only narrow channels are not < 20 m deep; ~ 100 m in north, ~50 m in south. The narrow channels in the south-- the deepest point is 75 m. Sill depth at the southern end of the main channel is 25.5 m.

Description

The Skagerrak follows a late Paleozoic graben that is continuous with the Oslo graben. It is a pull-apart basin associated with dextral strike-slip movement on a fault zone (NW-SE-trending Sorgenfrei-Tomquist Zone) that is approximately parallel to the Kattegat. This later zone is the present-day contact between sedimentary rocks in Denmark and exposed Precambrian rocks in Sweden. The structure has been reactivated by the Alpine Orogeny, and opening of the Atlantic Ocean. The faults in the Kattegat region are still active today. The chain of islands at the SE end of the Kattegat are due to Mesozoic inversion, dissected by fluvial and glacio-fluvial erosion. The main erosion of the Skagerrak is due to Pleistocene glaciations; channels in the Kattegat are thought to have originated as subglacial meltwater channels. The Skagerrak was ice free by 14-13,000 yr BP. The Kattegat was initially exposed after glacial retreat, and didn't open as a marine strait until ~8500 yr BP; marine sedimentation was preceded by a lake phase in the Baltic. The Kattegat might not have been completely covered by ice; tills are only present in a belt 40-50 km out from Sweden. Others place the glacial limit in mainland Denmark. The northern Kattegat was inundated by 14,000 yr BP. There is 2-layer 'estuarine' circulation, with the pycnocline at 15-20 m depth. The present-day current pattern probably started 4,000 yr BP. It is mainly driven by outflow from the Baltic, with strong wind-driven episodic flows. Surface salinity increases northward: there is a very strong salinity gradient through the Danish Straits. Surface salinity is 15-30 ppt; the salinity of the Baltic Sea water is 8-15 ppt. Deep water has a salinity of 32-34 ppt. Tidal range is < 0.4 m; meteorological water-level fluctuations are as much as ± 1.5 m. There is very little sediment supply from land. Suspended sediment is carried in from both the North Sea and Baltic. The latter sediment is deposited immediately north of the narrow passages in the southernmost Baltic Sea. Shallow-water sediments are coarser than those in deeper water. There may be little or no sedimentation in shallow water. Holocene deposits are thin in the Kattegat... only a few metres thick at most. Sediments in the Kattegat are silty at depths > 20 m (the depth of the pycnocline), except in current-swept channels. In the central part of the Kattegat, there are subaqueous dunes 10-15 m high. Holocene deposits in the Skagerrak are up to 70 m thick. They are weakly stratified, and accumulate mainly in topographic lows...

they don't drape the topography, due to the influence of bottom currents. Bottom-current activity started ~8,000 yr BP. In the Skagerrak, flow is counter-clockwise at all depths (inward along the Danish coast; outward along the Norwegian coast), with speeds maximum at a depth of ~400 m, but extending to the surface. Surface speeds can reach 1-1.5 m s^{-1}, and generate dunes at depths below the wave-dominated shoreface. Along the southern Skagerrak shoreline, there are current-generated dunes (heights < 2 m) in sand down to a depth of at least 70 m. Speeds inferred to reach 1 m s^{-1}; such events occur only infrequently-- once every few months due to meteorological events. The flow reverses at times. Wave-generated structures occur down to 25-30 m. Strong longshore drift to the east (inward) along the Danish coast, that has constructed large Skagen Spit at the Skagerrak-Kattegat junction. Muddy fine sand occurs below 75 m; Holocene sediment in the Skagerrak ranges from 0-100 m thick. Pockmarks are common; some are elongated (= comet marks) due to the current in water depths of 100-500 m on the Danish side of the Skagerrak. There are also clay diapirs associated with some pockmarks. Two references talk about 'sand waves' on the Danish side of the Skagerrak to depths of 270 m, but the seismic sections strongly imply that they are muddy sediment waves! There is an area nearby that has experienced contour-parallel erosion/non-deposition because of contour currents. (Similar contourite drifts occur in the Baltic Sea). Their crests are ~parallel to the depth contours-- part of a contourite sediment drift? Tidal currents in the Kattegat are < 40 cm s^{-1}. Wind-generated flows can reach 3.9 m s^{-1}, and can flow in either direction; these 'instantaneous' flows exceed the net flow by an order of magnitude. During weak winds, flow is stratified, but during strong winds, flow is not stratified. Sand bodies have accumulated at the northern (seaward) end of the narrow channels at the southern end of the Kateggat that are up to 10+ m thick that are building northward with foreset-like bedding-- like an ebb-tidal delta. In the narrow straits, current-generated features include: erosional areas, dunes, sand ribbons and comet marks. The dunes are only active very infrequently. In the widest narrow channel, it appears that outflow is mainly on the east side, with inflow on the west side. The width of the Skagerrak is 10 times the internal Rosby radius (which is 10 km), hence the strong counter-clockwise circulation. From the Baltic Sea to the centre of the Skagerrak, there is an ~14 cm head difference, driving outflow form the Baltic. Surge-like events from the Atlantic can cause strong southerly flows in the Danish straits. Rising sea level increases the inflow of salty oxygenated water; the deeper channels are the main inflow sites. This inflow carries mud from the North Sea into the Baltic. Stronger outflow leads to stronger inflow. The southern sill has an elongate scour depression in its centre. The islands of the Danish Straits create significant flow resistance. Ice is present in the Danish Straits for only 5-10 days each year.

References

Bennike, O., Jensen, J.B., Lemke, W., Kuijpers, A. and Lomholt, S. 2004. Late- and post-glacial history of the Great Belt, Denmark. *Boreas*, **33**, 18-33.

Bøe, R., Rise, L. and Ottesen, D. 1998. Elongate depressions on the southern slope of the Norwegian Trench (Skagerrak): morphology and evolution. *Marine Geology*, **146**, 191-203.

Büchmann, B., Hansen, C. and Söerkvist, J. 2011. Improvement of hydrodynamic forecasting of Danish waters: impact of low-frequency North Atlantic barotropic variations. *Ocean Dynamics*, **61**, 1611-1617.

Christiansen, C., Kuzendorf, H., Otto, C. and Senstius, J. 1993. Recent and subrecent sedimentary conditions in the southern part of the North Sea—Baltic Sea transition. *Boreas*, **22**, 357-366.

Gingele, F.Z. and Leipe, T. 2001. Southwestern Baltic Sea—A sink for suspended matter from the North Sea? *Geology*, **29**, 215-218.

Gustafsson, B. and Stigebrandt, A. 1996. Dynamics of the freshwater-influenced surface layers in the Skagerrak. *Journal of Sea Research*, **35**, 39-53.

Haid, V., Stanev, E.V., Pein, J., Staneva, J. and Chen, W. 2020. Secondary circulation in shallow ocean straits: Observations and numerical modeling of the Danish Straits. *Ocean Modelling*, **148**, 101585, https://doi.org/10.1016/j.ocemod.2020.101585

Kuijpers, A. 1985. Current-induced bedforms in the Danish Straits between Kattegat and Baltic Sea. *Meyniana*, **37**, 97-127.

Kuijpers, A., Werner, F. and Rumohr, J. 1993. Sandwaves and other large-scale bedforms as indicators of non-tidal surge currents in the Skagerrak off Northern Denmark. *Marine Geology*, **111**, 209-221.

Larsson, O. and Stevens, R.L. 2008. Seismic stratigraphy of Late Quaternary deposits in the eastern Skagerrak. *Marine and Petroleum Geology*, **25**, 1023-1039.

Lykke-Andersen, H., Knudsen, K.L. and Christiansen, C. 1993. The Quaternary of the Kattegat area, Scandinavia: a review. *Boreas*, **22**, 269-281.

Mattsson, J. 1996. Some comments on the barotropic flow through the Danish Straits and the division of the flow between the Belt Sea and the Öresund. *Tellus*, **48A**, 456-464.

Nielsen, L.H. and Johannessen, P.N. 2009. Facies architecture and depositional processes of the Holocene-Recent accretionary forced regressive Skagen spit system Denmark. *Sedimentology*, **56**, 935-968.

Rise, L., Olsen, H.A., Bøe, R. and Ottesen, D. 1996. Thickness, distribution and depositional environment of Holocene sediments in the Norwegian part of the Skagerrak. *Norges geologiske undersøkelse Bulletin*, **430**, 5-16.

Ro, H.E., Stuevold, L.M., Faleide, J.I. and Myhre, A.M. 1990. Skagerrak Graben—the offshore continuation of the Oslo Graben. *Tectonophysics*, **178**, 1-10.

Rodhe, J. 1987. The large-scale circulation in the Skagerrak; interpretation of some observations. *Tellus*, **39A**, 245-253.

Rodhe, J. 1996. On the dynamics of the large-scale circulation of the Skagerrak. *Journal of Sea Research*, **35**, 9-21.

Sayin, E. and Krauss, W. 1996. A numerical study of the water exchange through the Danish Straits. *Tellus*, **48A**, 324-342.

Return to List of Straits

14—MENAI STRAIT, WALES

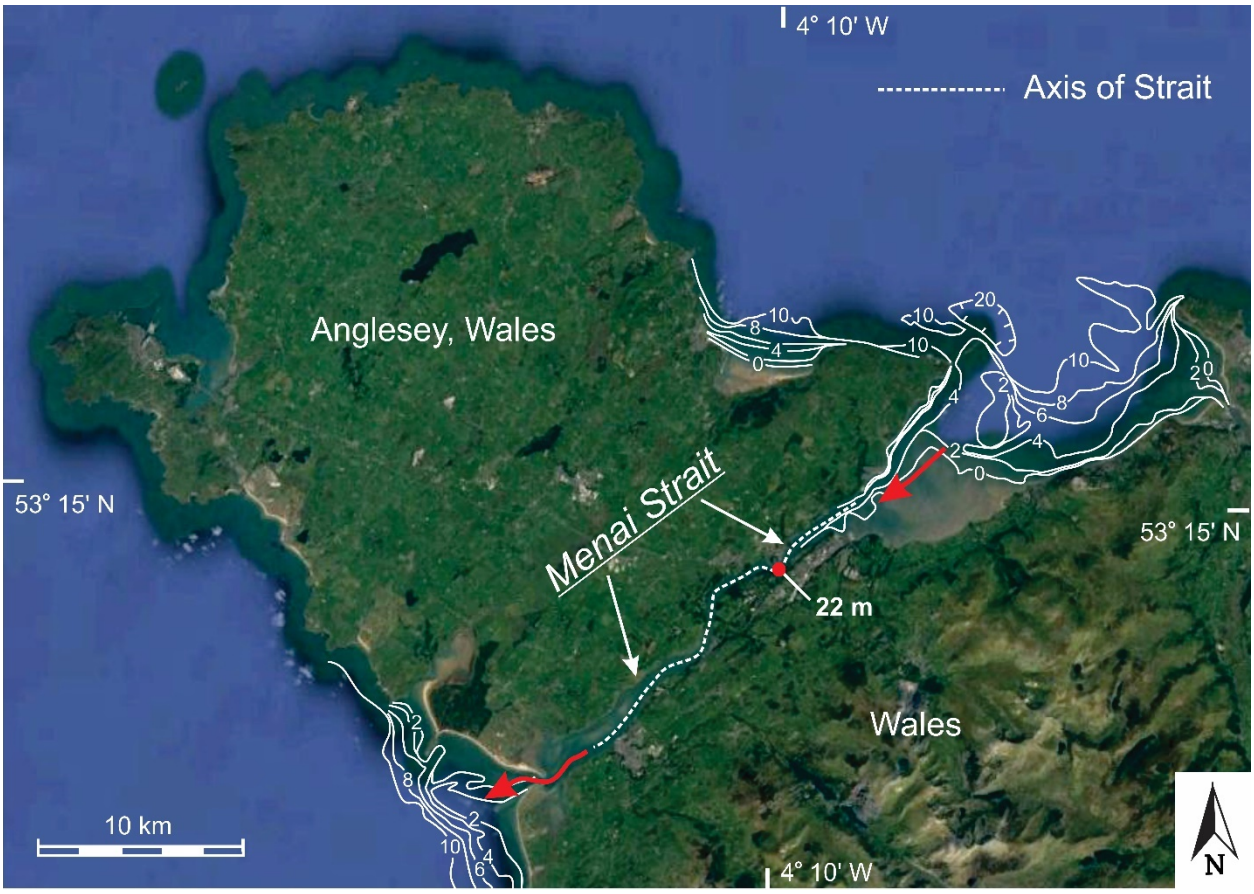

Fig. A14. <u>Menai Strait</u>*: Bathymetry modified after Davies & Robins (2017, fig. 1a; copyright Elsevier; used with permission). Depths in metres. Satellite image from Google Earth ©. (Data: SIO, NOAA, U.S. Navy, NGA, GEBCO. Image: CNES/Airbus). No systematic bathymetric data were obtained for the full length of the Strait itself. The Strait is interpreted to occupy coalesced, lowstand fluvial channels. Estuaries occurred at the ends of the channel earlier in the transgression (Roberts* et al. *2011). A wave-dominated, barrier-inlet system occurs at the southern end, because of exposure to strong wave action, whereas a tide-dominated system occurs at the northern end, because of sheltering from the strongest waves by Anglesey. Strong tidal currents occur along the entire length of the Strait, but phase differences between the two ends of the channel generate a southward-directed residual current (Harvey 1968; Campbell* et al. *1998; Davies & Robins 2017).*

Length

28 km long; slightly sinuous course-- two NE-SW-oriented sections, joined by a narrow, nearly N-S segment.

Width

Nearly parallel sided, but generally widens to the SW. Mean width ~800 m. Narrowest points 230 m and 320 m wide. Over 1 km wide behind spits at southwestern end. Southwestern end nearly closed by two spits prograding from the north and south sides, like a tidal inlet. There appears to be a flood-tidal delta built into the Strait. The northeastern end is funnel-shaped and shallow.

Depth

6-25 m, depending on bedrock depth. Maximum depth in the Strait itself is 22 m, but depths reach 25 m deep in the inlet at the southern mouth (the Fort Belan tidal inlet).

Description

Strait lies along trace of major fault system (Menai Strait Fault System) that is a geological terrane boundary from the Paleozoic. The Strait runs along the trace of Carboniferous limestones. The channel is thought to have been scoured initially by two rivers, one flowing to the SW, the other to the NE, that were joined by stream capture by headward erosion by the river flowing to the NE. Glacial ice flow was to the SW, parallel to the Strait. There may be thin till and fluvio-glacial deposits beneath a discontinuous cover of modern tidal sands. With rising sea level, the Strait was breached at 8.6-8.2 Ka ago. The NE end of the Strait was a flood-dominant estuary before breaching of the divide, and is now an ebb-tidal delta. There is also an ebb-tidal delta offshore from the barrier spits at the SW end of the Strait, but it is much smaller than the one at the NE end. The narrowest constriction is shallow and current speeds there reach 2.5 m s^{-1}. Atmospheric pressure (and secondarily the wind) influences mean water levels in the Strait, causing differences of ~ 40 cm between the two ends. Net water flow is toward the SW, with a residual velocity of 15 cm s^{-1}. Tidal range near the narrows is 6.6 m and 3.4 m at springs and neaps, respectively; at the SW end the ranges are 4.1 m (springs) and 1.8 m (neaps) (i.e., the system is hypersynchronous). The mean tidal range for the M_2 is 1.6 m at the SW end, and 2.5 m at the NE end. The tidal excursion length is 14 km. Maximum tidal current speeds are 0.8 m s^{-1} to NE, and 1.2 m s^{-1} to the SW. There appears to an overall increase in tidal range from the SW to the NE end, with a later high water at the NE end; there is a phase delay of ~40 minutes for passage around Anglesey; thus, there is the meeting of two tidal waves within the Strait. The higher tidal range at the NE end is due to greater resonance in the Irish Sea to the north. Ebb currents are 10-15% stronger than the flood. There is negligible freshwater input. The residual flow can be reversed during strong winds blowing toward the NE. The Stokes Drift is the most important contribution to the net flow to the SW. Turbidity is mainly controlled by wind strength, presumably due to wave resuspension. There are tidal sand bars near the southern end, with dunes on the flank of the channel thalweg. The thalweg seems to be sediment starved (a gravel bed) and the dunes are small, whereas the flank near a sand bar has abundant dunes that are larger where the sand is more abundant. The net southerly transport of sand, which extends through the main channel at the very northern end of the Strait, should leave the northern part of the Strait sediment-starved (the sediment is gravelly there), and lead to sand accumulation at the southern end, which is what seems to be the case in the Google Earth © images. In numerical-model results, there is no transport at all in the northern third of the Strait, in which case the northern ebb-tidal delta is relict. There is 3-8 m of vertical accumulation of sand inside the SW end of the Strait, and up to 40 m of accumulation at the northern end. The amount of aggradation decreases northward in the Strait itself. The sand in the southern part of the Strait has a mean size in fine sand, but it must be coarser fine sand because dunes are widespread.

References

Ali, A. 1992. *Sedimentological, Geophysical and Oceanographic Studies of Postglacial and Contemporary Sedimentary Processes of the NE Menai Strait and Conwy Bay (Wales, U.K.)*. Unpublished Ph.D. thesis, University of Wales, Bangor, Wales, 257 p.

Campbell, A.R., Simpson, J.H. and Allen, G.L. 1998. The dynamical balance of flow in the Menai Strait. *Estuarine, Coastal and Shelf Science*, **46**, 499-455.

Davies, A.G. and Robins, P.E. 2017. Residual flow, bedforms and sediment transport in a tidal channel modelled with variable bed roughness. *Geomorphology*, **295**, 855-872.

Embleton, C. 1964. Deglaciation of Arfon and southern Anglesey, and origin of the Menai Straits. *Proceedings of the Geological Association*, **75,** 407–430.

Gibbons, W. 1987. Menai Strait fault system: An early Caledonian terrane boundary in north Wales. *Geology*, **15**, 744-747.

Harvey, J.G. 1968. The flow of water through the Menai Straits. *Geophysical Journal of the Royal Astronomical Society*, **15**, 517-528.

Roberts, M.J., Scourse, J.D., Bennell, J.D., Huws, D.G., Jago, C.F. and Long, B.T. 2011. Late Devensian and Holocene relative sea-level change in North Wales, UK. *Journal of Quaternary Science*, **26**, 141-155.

Sandford, K. and Mason, G. 2020. Geological model for the Menai Strait tunnel. *Quarterly Journal of Engineering Geology and Hydrogeology*, qjegh2020-047, http://dx.doi.org/10.1144/qjegh2020-047

Simpson, J.H., Berx, B. Gascoigne, J. and Saurel, C. 2007. The interaction of tidal advection, diffusion and mussel filtration in a tidal channel. *Journal of Marine Systems*, **68**, 556-568.

Simpson, J.H., Forbes, A.M.G., and Gould, W.J. 1971. Electromagnetic observations of water flow in the Menai Straits. *Geophysical Journal of the Royal Astronomical Society*, **24**, 245-253.

Solangi, S.H. 1992, *Geophysical/Sedimentological Studies of a Quaternary Tidal Delta System*. Unpublished Ph.D. thesis, University of Wales, Bangor, Wales, 197 p.

Souza, A.J. and Hill, A.E. 2006. Tidal dynamics in channels: Single channels. *Journal of Geophysical Research*, **111**, C09037, https://doi:10.1029/2006JC003469

Return to List of Straits

15—ENGLISH CHANNEL–STRAIT OF DOVER

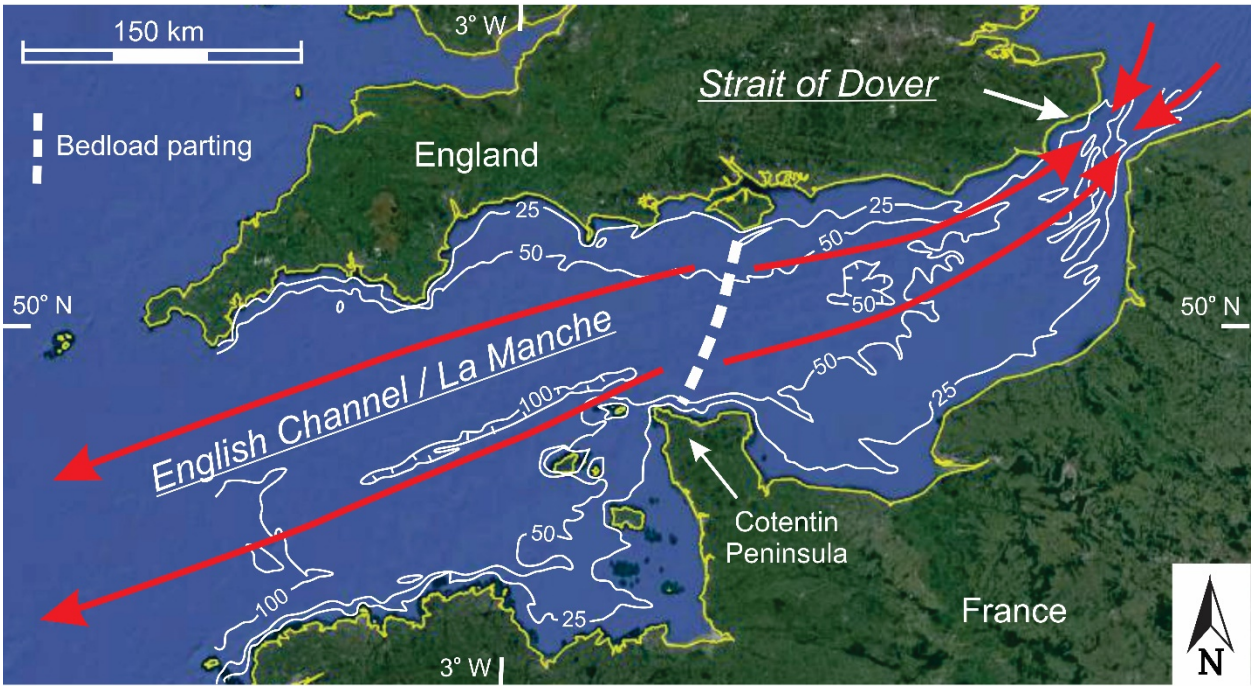

Fig. A15. *English Channel and Strait of Dover: Bathymetry modified after Gibbard & Lautridou (2003, fig. 1; © 2003 John Wiley & Sons, Ltd.). Depths in metres. Satellite image from Google Earth ©. (Data: SIO, NOAA, U.S. Navy, NGA, GEBCO. Image: Landsat/Copernicus). The English Channel as a whole follows the trace of basement faults related to the Hercynian Orogeny. The elongate depression that runs along the axis of the English Channel is interpreted to represent a fluvially formed valley that was eroded during the glacial lowstand (= the Channel River; Antoine* et al. *2003). The strong M_2 tidal currents that flow E-W along the length of the Channel are modulated by the M_4 tidal harmonic (Howarth 1982; Harris* et al. *1995) to generate residual transport paths that diverge at a bedload parting in the centre of the Channel and converge at a bedload convergence to the west of the Strait of Dover (Johnson* et al. *1982). Note that the Strait of Dover not associated with a bedload parting as might be expected. Instead, there is a bedload convergence at or immediately to the west of the narrowest point (Johnson* et al. *1982).*

Length

520 km long

Width

The Channel widens westward. It is 160 km wide at its western end; 30 km wide at the Strait of Dover. It is 90 km wide at the location of the maximum current speeds, off the tip of the Cotentin Peninsula. It is 165 km wide at the Bay of the Seine, and 190 km wide in the Bay of Normandy.

Depth

The Channel deepens westward; its western end (at Cornwall) is ca. 100 m deep. It is ca. 30 m deep in the Strait of Dover, increasing westward to 130 m at the shelf-slope break.

Description

The English Channel runs parallel to old basement faults that originated during the Hercynian-Variscan Orogeny (late Paleozoic) that were inverted during the late Mesozoic and Cenozoic (Alpine orogeny). The Channel was exposed during glacial lowstands and a river flowed westward down its axis (the Channel River). The connection through the Strait of Dover is thought to be due to catastrophic drainage of an ice-dammed lake in the southern North Sea. The main tidal wave enters from the Atlantic Ocean; a smaller one enters through the Strait of Dover. Tidal ranges are larger on the French coast because of the Coriolis effect. At the Strait of Dover, the tidal range is ~ 6 m, and the peak tidal currents are ~1.3 m s^{-1}. Current speeds are generally fastest at headlands and weaker in embayments, but tidal ranges are commonly largest in funnel-shaped embayments such as the Brittany-Normandy Gulf. There are two tidal-current maxima: off the tip of Cotentin Peninsula in the central Channel, and in the Strait of Dover. The western Channel has residual transport to the west; the eastern Channel has transport to the east, with a bedload parting in the centre. There is a bedload convergence in (or just SW of) the Strait of Dover... NOT a parting as is otherwise a common feature of constrictions. In detail, the flow through the Strait of Dover is like an ebb jet, with ebb-dominated (westerly) transport in the middle, and flood-dominated (easterly) transport along both shores. The Strait of Dover appears to be a bypass zone because it lies within a sediment-transport pathway. The area of the bedload parting in the central Channel is sediment deficient with a gravel lag exposed over large areas. Sand abundance increases outward from the parting. Grain size correlates generally with peak tidal-current speeds. The Channel is the primary basis for the tidal transport-path model of Belderson *et al.* (1982; see Fig. 24 of the main paper). Modern carbonate sediment is more abundant in the west. The suspended sediment moves eastward, from the western Channel into the eastern Channel, and from there into the southern North Sea. Thus, the suspended and bedload sediments do not move in the same direction.

References

Antoine, P., Coutard, J.-P., Gibbard, P., Hallegouet, B., Lautridou, J.-P. and Ozouf, J.-C. 2003. The Pleistocene rivers of the English Channel region. *Journal of Quaternary Science*, **18**, 227-243.

Belderson, R.H., Johnson, M.A. and Kenyon, N.H. 1982. Bedforms. *In*: *Offshore Tidal Sands: Processes and Deposits*, Stride, A.H. (ed), Chapman and Hall, London, 27-57.

Gibbard, P.L. and Lautridou, J.P. 2003, The Quaternary history of the English Channel: an introduction. *Journal of Quaternary Science*, **18**, 195-199.

Grochowski, N.T.L., Collins, M.B., Boxall, S.R. and Salomon, J.C. 1993. Sediment transport predictions for the English Channel, using numerical models. *Journal of the Geological Society, London*, **150**, 683-695.

Gupta, S., Collier, J.S., Palmer-Felgate, A. and Potter, G. 2007. Catastrophic flooding origin of shelf valley systems in the English Channel. *Nature*, **448**, July 19, 2007, https://doi:10.1038/nature06018

Harris, P.T., Pattiaratchi, C.B., Collins, M.B. and Dalrymple, R.W. 1995. What is a bedload parting? *In*: *Tidal Signatures in Modern and Ancient Sediments*, Flemming, B.W. and Bartoloma, A. (eds), International Association of Sedimentologists Special Publication, **24**, 2-18.

Howarth, M.J. 1982. Tidal currents on the continental shelf. *In*: *Offshore Tidal Sands: Processes and Deposits*, Stride, A.H. (ed), Chapman and Hall, London, 10-26.

Johnson, M.A., Kenyon, N.H., Ikehara, R.H. and Stride, A.H. 1982. Sand transport. *In*: *Offshore Tidal Sands: Processes and Deposits*, Stride, A.H. (ed), Chapman and Hall, London, 58-94.

Larsonneur, C., Bouysse, P. and Auggret, J.-P. 1982. The superficial sediments of the English Channel and its Western Approaches. *Sedimentology*, **29**, 851-864.

Prandle, D., Ballard, G., Flatt D., Harrison, A.J., Jones, S.E., Knight, P.J., Loch, S., McManus, J., Player, R. and Tappin, A. 1996. Combining modelling and monitoring to determine fluxes of water, dissolved and particulate metals through the Dover Strait. *Continental Shelf Research*, **16**, 237-257.

Reynaud, J.-Y., Tessier, B., Auffret, J.-P., Berné, S., De Batist, M., Marsset, T. and Walker, P. 2003. The offshore Quaternary sediment bodies of the English Channel and its Western Approaches. *Journal of Quaternary Science*, **18**, 361-371.

Smith, A.J. and Curry, D. 1975. The structure and geological evolution of the English Channel. *Philosophical Transactions of the Royal Society of London A*, **279**, 3-20.

Stride, A.H. 1982, Background and outline. *In*: *Offshore Tidal Sands: Processes and Deposits*, Stride, A.H. (ed), Chapman and Hall, London, 1-9.

Velegrakis, A.F., Michel, D., Collins, M.B., Lafite, R., Oikonomou, E.K., Dupont, J.P., Huault, M.F., Lacouturier, M., Salomon, J.C. and Bishop, C. 1999. Sources, sinks and resuspension of suspended particulate matter in the eastern English Channel. *Continental Shelf Research*, **19**, 1933-1957.

Ziegler, P.A. 1987. Celtic Sea—Western Approaches area: an overview. *Tectonophysics*, **137**, 285-289.

Return to List of Straits

16—STRAIT OF GIBRALTAR

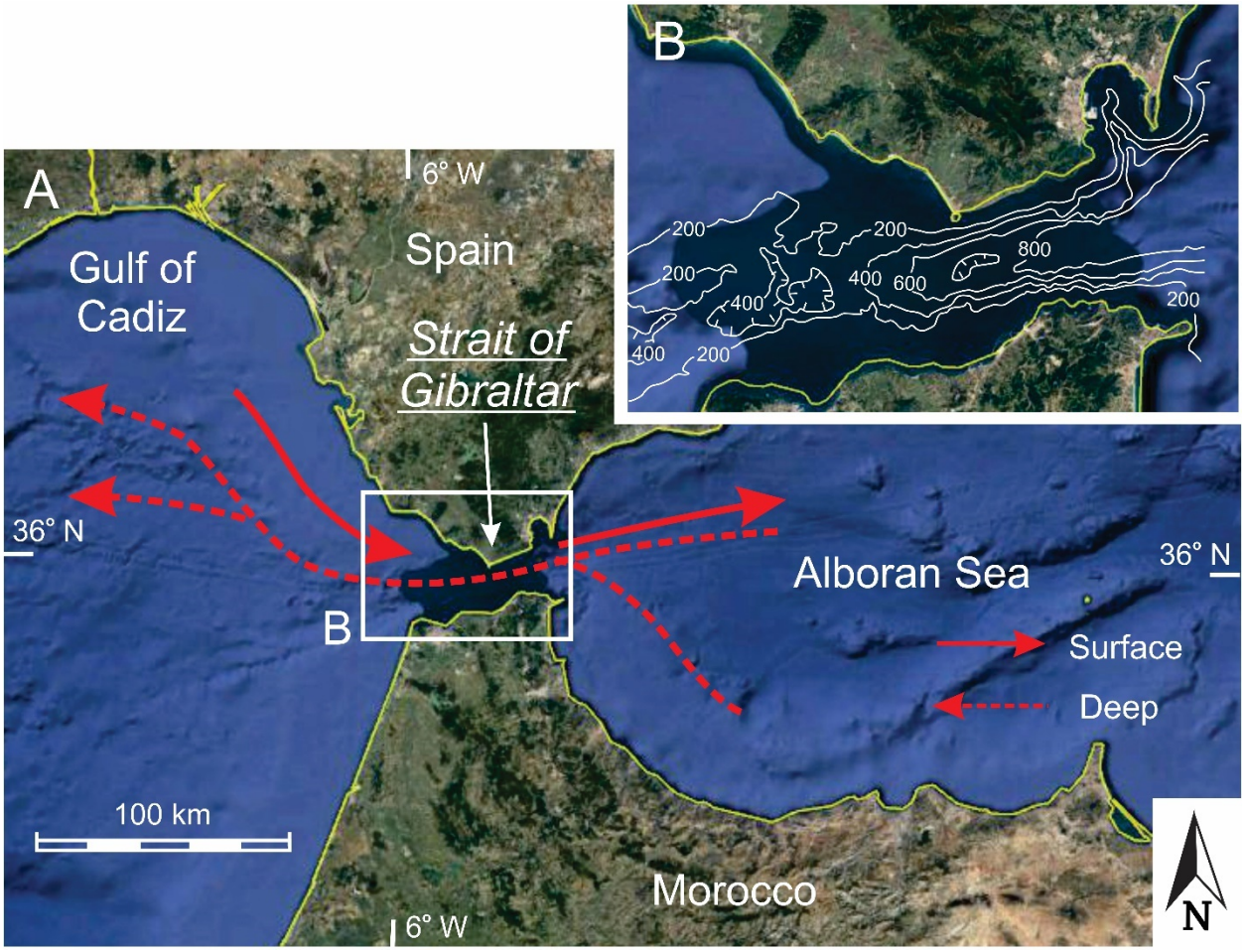

Fig. A16. *Strait of Gibraltar: (A) General setting of the Strait of Gibraltar. (B) Detailed bathymetry taken from Kinder & Bryden (1990, fig. 1; reproduced with permission of Springer Nature). Depths in metres. Satellite image from Google Earth ©. (Data: SIO, NOAA, U.S. Navy, NGA, GEBCO. Image: Landsat/Copernicus). There are strong tidal currents in the Strait of Gibraltar, but flow is dominated by the Mediterranean Outflow (Kinder & Bryden 1990; Price* et al. *1993; Baringer & Price 1999), a dense current generated by excess evaporation within the Mediterranean, that flows westward, downslope, then swings to the north because of the Coriolis effect, hugging the continental slope south of Portugal (Habgood* et al. *2003). There is a compensating inward flow that enters the Mediterranean Sea mainly along the northern side, flowing over the Spanish self before entering the Strait of Gibraltar (Lobo* et al. *2006).*

Length

ca. 50 km long, but length difficult to define exactly because of tapered geometry of both ends.

Width

15 km at its narrowest (at Rock of Gibraltar); 43 km at its wider western end.

Depth

There are two deep channels (north and south), separated by a host-like high. The two channels join at both the eastern and western ends of the Strait. Mean depth 350 m. Main sill is ~ 300 m deep.

Description

The Strait lies along the plate-tectonic suture between the African and Spanish plates. Final opening of the Strait is thought to be due to fluvial erosion during sea-level lowstands. There is a net eastward (inward) flow of fresher water on the surface, and a net outflow at the bottom (the Mediterranean Undercurrent/Outflow). Most near-bed speeds are 10-80 cm s^{-1}, but they increase westward to ca. 1 m s^{-1}. 60% of eastern/inward flux through Strait associated with internal bores/waves along the density interface. Bottom photos show presence of well-sorted sands and gravels; sands are shell/carbonate rich. Bedforms are: ripples/dunes, sand ribbons, obstacle scours and flutes in fine-grained sediment. Almost all sediment transport is to the west, but there are local reversals near southeastern limit of the Strait. There is an outward fining to silty muds at either end of the Strait. The tidal range is ~ 2 m in the Atlantic, and ~ 1 m in the Mediterranean; tidal currents forced mainly from Atlantic end. Meteorological forcing mainly by storms (pressure differences) over the Mediterranean. Measured semidiurnal tidal-current speeds 65-130 cm s^{-1}. There is an asymmetry of tidal range across the Strait because of the Coriolis effect, with larger ranges on the south/right side. The density interface occurs at a depth ranging from > 200 m at Atlantic end, to < 60 m deep in the northeastern part of the Mediterranean end of Strait. Internal tides have ranges of 20-50 m. Outflow from the Strait is deflected to the north over the outer part of the shelf, generating seaward-migrating dunes. The inner part of the Spanish shelf is influenced by the Atlantic Inflow current that occurs in water depths < 100 m, generating southeasterly migrating dunes. The sands on this shelf are mainly bioclastic. The main Mediterranean Outflow descends into deeper water but with a significant northward deflection because of the Coriolis effect. This outflow decreases in speed from > 1 m s^{-1} to only 0.1-0.3 m s^{-1} where the flow detaches from the bed and continues as an interflow. The succession of bedforms is: scour and sand ribbons--> sand waves (dunes) --> muddy sand waves--> mud waves. There are down-slope trending channels with levees like turbidite channels that are formed by the underflow. They have sandy floors and end in lobes composed of sand.

References

Bray, N.A., Winant, C.D., Kinder, T.H. and Candela, J. 1990. Generation and kinematics of the internal tide in the Strait of Gibraltar. *In*: *Physical Oceanography of Sea Straits*, Pratt, L.J. (ed), NATO ASI Series C: Mathematical and Physical Sciences, **318**, 477-491.

Baringer, M.O'N. and Price, J.F. 1999. A review of the physical oceanography of the Mediterranean outflow. *Marine Geology*, **155**, 63-82.

Candela, J. 1990 The barotropic tide in the Strait of Gibraltar. *In*: *Physical Oceanography of Sea Straits*, Pratt, L.J. (ed), NATO ASI Series C: Mathematical and Physical Sciences, **318**, 457-475.

Candela, J. and Winant, C. 1990. Tides in the Strait of Gibraltar. *Journal of Geophysical Research*, **95**, 7313-7335.

Dewey, J.F., Helman, M.L., Turco, E., Hutton, D.H.W. and Knott, S.D. 1989. Kinematics of the western Mediterranean. *In*: *Alpine Tectonics*, Coward, M.P., Dietrich, D. and Park, R.G. (eds), Geological Society, Special Publications, **45**, 265-283.

Kelling, G. and Stanley, D.J. 1972. Sedimentary evidence of bottom current activity, Strait of Gibraltar region. *Marine Geology*, **13**, M51-M60.

Kinder, T.H. and Bryden, H.L. 1990. Aspiration of deep waters through straits. *In*: *Physical Oceanography of Sea Straits*, Pratt, L.J. (ed), NATO ASI Series C: Mathematical and Physical Sciences, **318**, 295-319.

Habgood, E.L., Kenyon, N.H., Masson, D.G., Akhmetzhanov, A., Weaver, P.P.E., Gardner, J. and Mulder, T. 2003. Deep-water sediment wave fields, bottom current sand channels and gravity flow channel-lobe systems: Gulf of Cadiz, NE Atlantic. *Sedimentology*, **50**, 483-510.

Lobo, F.J., Maldonado, A. and Noormets, R. 2010. Large-scale sediment bodies and superimposed bedforms on the continental shelf close to the Strait of Gibraltar: interplay of complex oceanographic conditions and physiographic constraints. *Earth Surface Processes and Landforms*, **35**, 663-679.

Loget, N. and Van Den Driessche, J. 2006. On the origin of the Strait of Gibraltar. *Sedimentary Geology*, **188-189**, 341-356.

Pettigrew, N.R. and Hyde, R.A. 1990. The structure of the internal bore in the Strait of Gibraltar and its influence on the Atlantic inflow. *In*: *Physical Oceanography of Sea Straits*, Pratt, L.J. (ed), NATO ASI Series C: Mathematical and Physical Sciences, **318**, 493-508.

Price, J.F., Baringer, M.O'N., Lueck, R.G., Johnson, G.C., Ambar, I., Parrilla, G., Cantos, A., Kennelly, M.A. and Sanford, T.B. 1993. Mediterranean outflow mixing and dynamics. *Science*, **259**, 1277-1282.

Return to List of Straits

17—MESSINA STRAIT

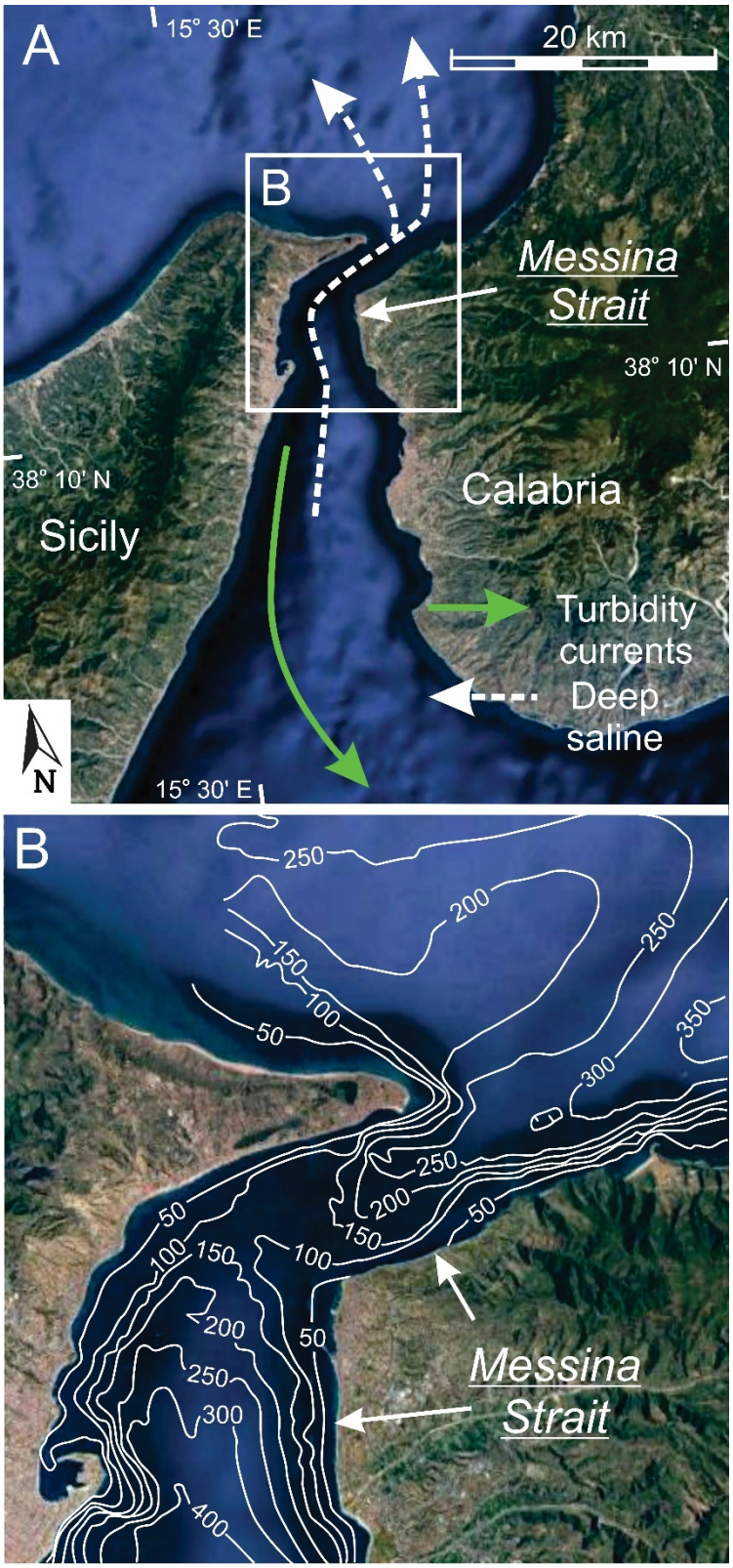

Fig. A17. *Messina Strait: (A) General setting of Messina Strait. (B) Detailed bathymetry simplified slightly from Droghei* et al. *(2017, fig. 1a; used with permission of Springer Nature). Depths in metres. Satellite images from Google Earth ©. (Data: SIO, NOAA, U.S. Navy, NGA, GEBCO. Image: Landsat/Copernicus). The margins of the southern section are very steep and are subject to hyperpycnal flows and slumping (Casalbore* et al. *2011; Ridente* et al. *2014). These mass flows can evolve into turbidity currents that flow southwest-ward along an axial submarine canyon that feeds a submarine fan in the Ionian Sea. The dominant currents in the Strait are tidal in origin (Hopkins* et al. *1984; Bignami & Salustri 1990; Cucco* et al. *2016; Longhitano 2018), their strength arising because of the pronounced constriction and the out-of-phase relationship of the tide at either end of the Strait. In addition, there is a density-driven deep flow to the north, compensated by a surface flow to the south (Cucco* et al. *2014; Dronghei* et al. *2017 Longhitano 2018).*

Length

About 40 km long. It has a dog-leg shape, with a long N-S section in the south that turns abruptly E-W near the Strait's northern end.

Width

Narrow northern part 3.25 km wide; N-S section is funnel-shaped, widening to about 15 km at its southern end.

Depth

Mean depth 120 m; sill depth 80 m. The southern end of the Strait reaches > 1000 m deep.

Description

The Strait occurs along the boundary between the Sicilian and Callabrian tectonic plates, with Sicily moving northward relative to mainland Italy. There is rifting in the northern (E-W) part of the Strait. Tides are out-of-phase by almost a half-cycle (~ 5 hours) at opposite ends of the Strait, leading to strong (up to 2 m s^{-1}) currents. Tidal range is only 10-15 cm in the adjacent ocean basins; an amphidromic point occurs near Messina. There are baroclinic flows because of salinity differences at either end of the Strait, causing oppositely directed residual currents at the top (flow to south at ~ 10 cm s^{-1}) and bottom (flow to north at ~12 cm s^{-1}) of the Strait. There are also internal waves and tidal bores along the density interface (150 m deep), just like at the Strait of Gibraltar. The currents generate large dunes in the narrows of the 'throat', at water depths down to ~ 300 m. The centre of the Strait south of the narrows is the site of an axial submarine canyon, the Messina Canyon, that is fed by multiple small canyons and gullies on both sides. There is essentially no shelf on either side, so short, steep rivers feed almost directly into the slope gullies. Anomalous rainfall is documented as feeding debris flows/hyperpycnal flows (containing coarse sediment) into the slope gullies. This event is associated with slope failures. Many slope failures might also be associated with the Messina earthquake. The axial canyon appears to be incised along most of its length; there are no levees. The sill is strongly erosional. Dunes occur both to the north and south of the sill, in areas where sediment deposition begins as flow speeds decrease. The largest dune fields are suggested by Longhitano (2018) to be at the site of bedload convergences

associated with the interaction of tidal and baroclinic flows. Internal waves traveling northward might contribute to dune formation in the northern dune field, but this is not proven. The main dunes reach 15 m in height. Simple dunes are present along the axis of the Messina Canyon to a depth of 1400 Carbonates comprise < 30% of the sediments.

References

Bignami, F. and Salustri, E. 1990. Tidal currents and transient phenomena in the Strait of Messina: A review. *In*: *Physical Oceanography of Sea Straits*, Pratt, L.J. (ed), NATO ASI Series C: Mathematical and Physical Sciences, **318**, 95-124.

Bottari, A., Carapezza, E., Carapezza, M., Carveni, P., Cefali, F., Lo Giudice, E. and Pandolfo, C. 1986. The 1908 Messina Strait earthquake in the regional geostructural framework. *Journal of Geodynamics*, **5**, 275-302.

Casalbore, D., Chiocci, F.L., Scarascia Mugnozza, G., Tommasi, P. and Sposato, A. 2011. Flash-flood hyperpycnal flows generating shallow-water landslides at Fiumara mouths in Western Messina Strait (Italy). *Marine Geophysical Research*, **32**, 257-271.

Cucco, A., Quattrocchi, G., Olita A., Facioli, L. Ribotti, A. Sinerchia, M., Tedesco, C. and Surgente, R. 2016. Hydrodynamic modelling of coastal seas: the role of tidal dynamics in Messina Strait, Western Mediterranean Sea. *Natural Hazards and Earth System Science*, **16**, 1553-1569.

Dronghei, R., Falcini, F., Casalbore, D., Martorelli, E., Mosetti, R., Sannino, G., Santoleri, R. and Chiocci, F.L. 2017. The role of internal solitary waves on deep-water sedimentary processes: the case of up-slope migrating sediment waves off the Messina Strait. *Nature Scientific Reports*, **6**, 36376, https://doi: 10.1038/srep36376

Goes, S., Giardini, D., Jenny, S., Hollenstein, C., Kahle, H.-G. and Geiger, A. 2004. A recent tectonic reorganization in the south-central Mediterranean. *Earth and Planetary Science Letters*, **226**, 335-345.

Hopkins, T.S., Salusti, E. and Settimi, D. 1984. Tidal forcing of the water mass interface in the Strait of Messina. *Journal of Geophysical Research*, **89**, C2, 2013-2024.

Longhitano, S.G. 2018. Between Scylla and Charybdis (part 1): the sedimentary dynamics of the modern Messina Strait (central Mediterranean) as analogue to interpret the past. *Earth-Science Reviews*, **185**, 259-287.

Ridente, D., Martorelli, E., Bosman, A. and Chiocci, F.L. 2014. High-resolution morpho-bathymetric imaging of the Messina Strati (Southern Italy). New insights on the 1908 earthquake and tsunami. *Geomorphology*, **208**, 149-159.

Santoro, V.C., Amore, E., Cavallaro, L, Cozzo, L., Cozzo, G. and Foti, E. 2002. Sand waves in the Messina Strait, Italy. *Journal of Coastal Research*, **SI 36**,640-653.

Santoro, V.C., Amore, E., Cavallaro, L. and De Lauro, M. 2004. Evolution of sand waves in the Messina Strait, Italy. *Ocean Dynamics*, **54**, 392-398.

Return to List of Straits

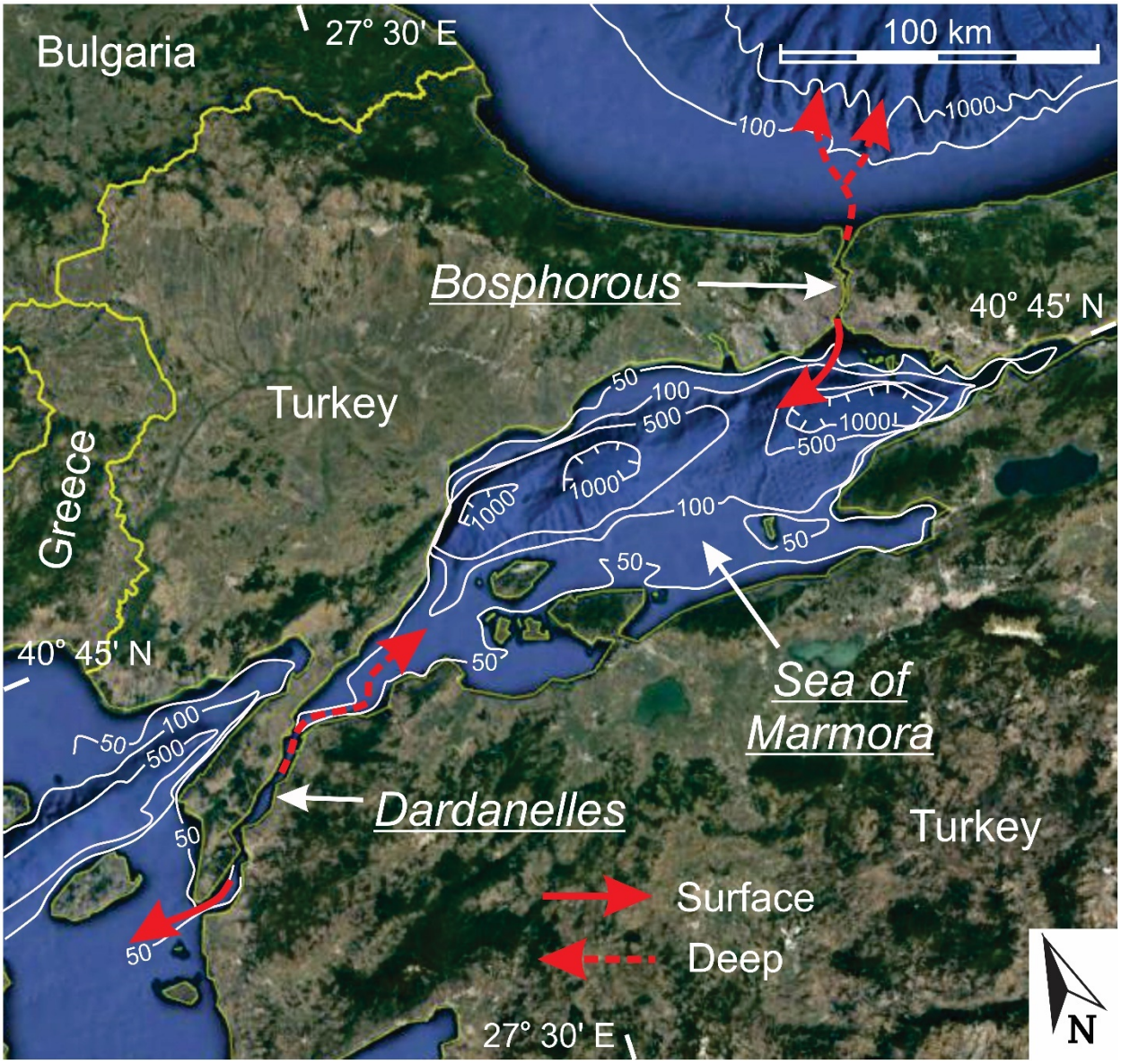

Fig. A18. Dardanelles and Bosphorus: *Bathymetry modified from Hiscott & Aksu (2002, fig. 1; copyright Elsevier; used with permission). See also Unlüata* et al. *(1990, fig. 1). Depths in metres. Satellite image from Google Earth ©. (Data: SIO, NOAA, U.S. Navy, NGA, GEBCO. Image: Landsat/Copernicus). The Dardanelles and Bosphorus began as fluvial channels that have been somewhat enlarged by modern flow (Gökaşan et al. 1997, 2005, 2010), whereas the Sea of Marmara is a pull-apart basin on a strike-slip fault (Görür* et al. *1997). The primary flow in the system is a density-driven outflow from the Aegean Sea into the Black Sea, coupled with the surface outflow of fresher water from the Black Sea in response to its net positive water budget (precipitation > evaporation) (Arisoy & Akyarli 1990; Ünlüata* et al. *1990; Stanev* et al. *2017). The northward flow of denser water into the Black Sea occurs as a bottom-hugging current (Flood* et al. *2009) that is dynamically similar to that exiting the Strait of Gibraltar. Unlike the*

flow in the Strait of Gibraltar, however, the circulation in the Dardanelles–Bosphorus is considered here to be 'estuarine' in character because it is driven mainly by the excess fresh-water input to the Black Sea.

Length

Bosphorus-- 31 km long; Dardanelles-- 62 km; Sea of Marmara-- 240 km; total length -- 333 km.

Width

Bosphorus-- 0.7-3.5 km; Dardanelles-- 1.2- 7 km wide (average 4 km); Sea of Marmara-- 70 km.

Depth

Sea of Marmara-- max. 1300 m; Bosphorus-- mean 35 m (max. 110 m), sill 33 m; the thalweg is defined by the -50m isobath; Dardanelles-- average 35 m deep.

Description

Both the Bosphorus and Dardanelles were apparently formed recently, perhaps in the last glacial cycle. The locations of both are controlled by faulting. The Borphorus was initiated by fluvial erosion, but the southern part is mainly a fault-controlled depresssion (graben). The Dardanelles was formed mainly by erosion caused by overflow of the Meditteranean into the Marmara Sea (according to Turkish workers, although this is inconsistent with other work). Both parts show much evidence of strong, ongoing erosion. The Sea of Marmara is a strike-slip pull-apart rift basin, hence its great depth. The freshwater leaving the Black Sea in the surface layer is much greater in volume than the saline inflow at the bottom. The surface of the Black Sea is ~30 cm higher than the surface of the Marmara Sea, which is 5-27 cm higher than the Aegean Sea (i.e., up to a 57 cm total head). The salinity difference between the outflow (17-20 ppt) and inflow (38-39 ppt) is ca. 20 ppt, which is quite large. The upper layer of the stratified flow becomes saltier toward the Aegean Sea, whereas the lower more salty layer becomes more fresh toward the Black Sea, because of turbulent mixing, including the presence of an hydraulic jump in the lower layer shortly after it enters the Bosphorus. There is considerable temporal variation on time scales from hours to years. The flow in the lower layer never exceeds 1 m s^{-1} (but apparently comes close to this), whereas flow in the upper layer reaches 1.66 m s^{-1}. [Arisoy & Akyarli (1990) has a good plot of current speeds in the lower and upper layers, together with sea-level differences (between the Black Sea and the Sea of Marmara)]. Bottom-layer speeds are of the order of 0.5-0.7 m s^{-1}, which should be sufficient to generate dunes; in the Dardanelles speeds are 5-25 cm s^{-1}. Once the dense flow enters the Black Sea, it continues across the shelf and down the slope in a channel system. Anastomosed channels, braid bars and spill-over deposits are recognized. At the smaller scale, bedforms consist of mud (not sand) and are attributed to mudwaves and/or cyclic steps. Because the flow is thought to be subcritical, they are unlikely to be antidunes, although this is possible. The Sea of Marmara was a lake during sea-level lowstands. The modern flow system was initiated ~ 5 ky BP. There was initially a more vigorous, erosive episode, followed by the less energetic 2-layer flow of today. There are very few dunes on the bed of the Bosphorus, despite the high-energy, erosive conditions. The deposits in the Dardanelles appear to be fine-grained. There are no dunes evident on seismic profiles, and the layering is draping on the 'drifts' that are identified. These drifts have the geometry of subaqueous point bars or

delta-related bodies at the ends of the strait. Tributary rivers are building small deltas into the sides of the Strait.

References

Aksu, A.E., Hiscott, R.N., Mudie, P.J., Rochon, A., Kaminski, M.A., Abrajano, T. and Yaşar, D. 2002. Persistent Holocene outflow from the Black Sea to the eastern Mediterranean contradicts Noah's flood hypothesis. *GSA Today*, **12**, May, 4-10.

Arisoy, Y. and Akyarli, A. 1990. Long term current and sea level measurements conducted at Bosphorus. *In*: *Physical Oceanography of Sea Straits*, Pratt, L.J. (ed), NATO ASI Series C: Mathematical and Physical Sciences, **318**, 225-236.

Flood, R.G., Hiscott, R.N. and Aksu, A.E. 2009. Morphology and evolution of an anastomosed channel network where saline underflow enters the Black Sea. *Sedimentology*, **56**, 807-839.

Gökaşan, E., Demirbağ, E., Oktay, F.Y., Ecevitoğlu, B., Şimşek, M. and Yüce, H. 1997. On the origin of the Bosphorus. *Marine Geology*, **140**, 183-199.

Gökaşan, E., Ergin, M., Özyalvaç, M., Sur, H.İ., Tur, H., Görüm, T., Ustaömer, T., Batuk, F.G., Alp, H., Birkan, H., Türker, A., Gezgin, E., and Özturan, M. 2008. Factors controlling the morphological evolution of the Çanakkale Strait (Dardanelles, Turkey). *Geo-Marine Letters*, **28**, 107-129.

Gökaşan, E., Tur, H., Ecevitoğlu, B., Görüm, T., Türker, A., Tok, B., Çağlak, F., Birkan, H. and Şimşek, M. 2005. Evidence and implications of massive erosion along the Strait of İstanbul (Bosphorus). *Geo-Marine Letters*, **25**, 324-342.

Gökaşan, E., Tur, H., Ergin, M., Görüm, T., Batuk, F.G., Sağcı, N., Ustaömer, T., Emem, O. and Alp, H. 2010. Late Quaternary evolution of the Çanakkale Strait region (Dardanelles, NW Turkey): implications of a major erosional event for the postglacial Mediterranean-Marmara Sea connection. *Geo-Marine Letters*, **30**, 113-131.

Görür, N., Cagatay, M.N., Sakinc, M., Sümengen, M., Sentürk, K., Yaltirak, C. and Tchapalyga, A. 1997. Origin of the Sea of Marmara as deduced from Neogene to Quaternary paleogeographic evolution of its frame. *International Geology Review*, **39**, 342-352.

Hiscott, R.N. and Aksu, A.E. 2002. Late Quaternary history of the Marmara Sea and Black Sea from high-resolution seismic and gravity-core studies. *Marine Geology*, **190**, 261-282.

Hiscott, R.N., Aksu, A.E., Mudie, P.J., Marret, F., Abrajano, T., Kaminski, M.A., Evans, J., Çakiroğlu, A.I., and Yaşar, D. 2007a. A gradual drowning of the southwestern Black Sea shelf: Evidence for a progressive rather abrupt Holocene reconnection with the eastern Mediterranean Sea through the Marmara Sea Gateway. *Quaternary International*, **167-168**, 19-34.

Hiscott, R.N., Aksu, A.E., Mudie, P.J., Kaminski, M.A., Abrajano, T., Yaşar, D. and Rochon, A. 2007b. The Marmara Sea gateway since ~16 ky BP: non-catastrophic causes of paleoceanographic events in the Black Sea at 8.4 and 7.15 ky BP. *In*: *The Black Sea Flood Question*, Yanko-Hombach, V., Gilbert, A.S., Paninn N. and Dolukhanov, P.M. (eds), Springer, New York, 89-117.

Hiscott, R.N., Aksu, A.E., Flood, R.D., Kostylev, V. and Yaşar, D. 2013. Widespread overspill from a saline density-current channel and its interaction with topography on the southwest Black Sea shelf. *Sedimentology*, **60**, 1639-1667.

Kaminski, M.A., Aksu, A.E., Box, M., Hiscott, R.N., Filipescu, S. and Al-Salameen, M. 2002. Late glacial to Holocene benthic foraminifera in the Marmara Sea: implication for Black Sea—Mediterranean Sea connections following the last deglaciation. *Marine Geology*, **190**, 165-202.

Stanev, E.V., Barshorn, S. and Zhang, Y.J. 2017. Cascading ocean basins: numerical simulations of the circulation and interbasin exchange in the Azov-Black-Marmara-Mediterranean Seas systems. *Ocean Dynamics*, **67**, 1003-1025.

Ünlüata, Ü., Oğuz, T., Latif, M.A. and Özsoy, E. 1990. On the physical oceanography of the Turkish straits. *In*: *Physical Oceanography of Sea Straits*, Pratt, L.J. (ed), NATO ASI Series C: Mathematical and Physical Sciences, **318**, 25-60.

Return to List of Straits

19—STRAIT OF HORMUZ

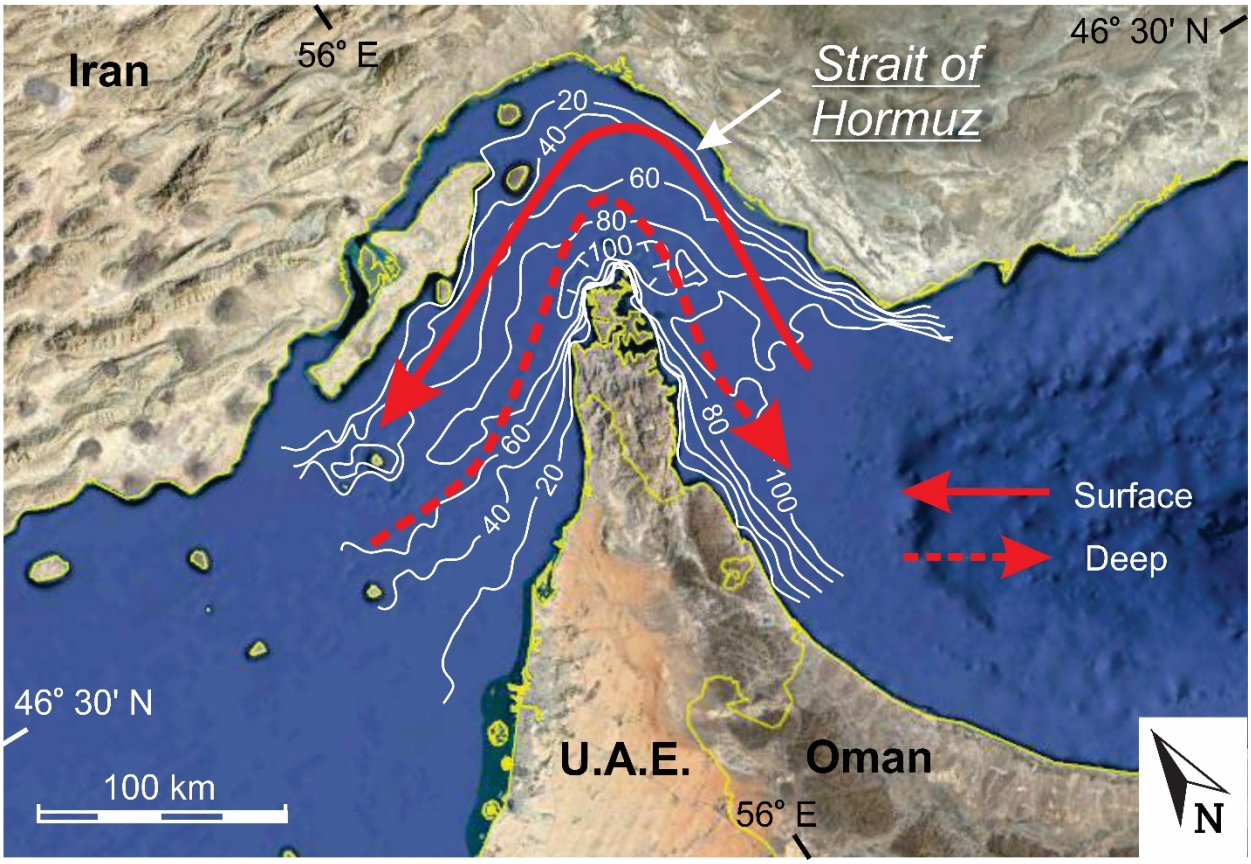

Fig. A19. Strait of Horumuz*: Bathymetry from fig. 1 of Thoppil & Hogan (2009; © American Meteorological Society. Used with permission.) Depths in metres. Satellite image from Google Earth ©. (Data: SIO, NOAA, U.S. Navy, NGA, GEBCO. Image: Landsat/Copernicus). The Strait is tightly curved because erosion has circumvented the northern promontory of the Oman Mountains that are being over-ridden by the southward movement of the thrust sheets of the Iranian fold-and-thrust complex to the north (Matsuyama* et al. *1998; Molinaro* et al. *2004). There is significant tidal flux through the Strait (Reynolds 1993; Azizpour* et al. *2016), supplemented by meteorological forcing. The background circulation is governed by the excess evaporation in the Persian/Arabic Gulf that generates an inverse-estuarine circulation with a seaward-flowing current at the bottom of the Strait, compensated by inflow at the surface (Reynolds 1993; Pous* et al. *2004, 2015; Thoppil & Hogan 2009).*

Length

The total length along the arcuate path is ~240 km.

Width

Narrowest point is 39 km wide; average 56 km wide.

Depth

Most authors say there is no sill in the Strait, but Pous *et al.* (2004) says there are two, one at each end of an elongate deep trough hugging the tip of the tip of the Musandam Peninsula. Pous *et al.* (2004) also say there are depths up to 260 m immediately off the tip of this Peninsula. There is an axial low that is ~110 m deep, descending from < 100 m in the Persian Gulf. The average depth is ca. 90 m.

Description

This narrow Strait marks the nearly right-angle intersection of the NNE-SSW-oriented Oman Mountains (Late Cretaeous age thrusting and obduction) with the NW-SE-oriented Zagros thrust belt of Late Cenozoic age. The Oman Mountains is an 'indentor', deforming the general arcuate geometry of the Zagros belt. The Strait itself lies along the trend of the Zagros foreland basin. Salt diapirism in the northern half (i.e., in the thrust belt) has created islands. There are three energy sources; in order of relative importance they are: tides (100); wind (10); density differences (1). Thus, tides are overwhelmingly the most important source of currents. Most of the dense bottom water is generated by evaporation in the United Arab Emirates coastal area. Current speeds average ca. 5 cm s^{-1}. The flow is that of a 'negative estuary'. When there is inverse-estuarine circulation, the near-bed outgoing current has a peak speed of ca. 25-30 cm s^{-1}; Pous *et al.* (2004) say that outflow speeds are < 0.4 m s^{-1}. The outgoing water is banked up against the Omani coast, whereas the incoming water is banked up against the Iranian coast due to the Coriolis effect. There are internal waves on the pycnocline. There is a net inflow because evaporation exceeds rainfall and river input. The development of high salinity water is seasonal, mainly in winter because of stronger winds. Thus, the export of water at the bottom is also seasonal, with the saltiest water exiting in the winter. The tide is not important in determining the long-term circulation of the Gulf or Strait. The tidal range decreases inward, from > 3m in the Gulf of Oman, to < 2 m in the entrance to the Gulf. Maximum current speeds (Strait-parallel) are 60-75 cm s^{-1}. The tidal currents are dominated by the semi-diurnal components, with the M_2 as the main constituent. The maximum tidal-current speeds increase inward, the opposite to the tidal range. The sites in the Gulf of Oman were flood-tide dominant, whereas those in the Persian Gulf were ebb-tide dominant, meaning that there is a convergence within the Strait of Hormuz. Most of the seafloor sediments in the deepest part of the Strait are relict carbonate grains, with not much modern sediment. The Iranian side of the Strait has a very low percentage of relict grains, perhaps because it is shallower with greater modern-day production.

References

Azizpour, J., Siadatmousavi, S.M. and Chegini, V. 2016. Measurement of tidal and residual currents in the Strait of Hormuz. *Estuarine, Coastal and Shelf Science*, **178**, 101-109.

Johns, W.E., Yao, F., Olson, D>B., Josey, S.A., Grist, J.P. and Smeed, D.A. 2003. Observations of seasonal exchange through the Straits of Hormuz and the inferred heat and freshwater budgets of the Persian Gulf. Journal of Geophysical Research, Oceans, 108, 3391, doi:10.1029/2003JC001881.

Matsuyama, M., Kitade, Y., Senjyu, T., Koike, Y. and Takashi, I. 1998. Vertical structure of a current and density front in the Strait of Hormuz. *In*: *Offshore Environment of the ROPME Sea Area after the War-Related Oil Spill: Results of the 1993–94 Umitaka-Maru Cruises*, Otsuki, A., Abdulraheem, M.Y. and Reynolds, R.M. (eds), Terra Scientific Publishing Company, Tokyo, 23-34.

Michaelis, PL. and Pauken, R.J. 1990. Seismic interpretation of the structure and stratigraphy of the Strait of Hormuz. *In*: *The Geology and Tectonics of the Oman Region*, Robertson, A.H.F., Searle, M.P. and Ries, A.C. (eds), Geological Society, Special Publication, **49**, 387-395.

Molinaro, M., Guezou, J.C., Leturmy, P., Eshraghi, S.A. and Frizon de Lamotte, D. 2004. The origin of changes in structural style across the Bandar Abbas syntaxis, SE Zagros (Iran). *Marine and Petroleum Geology*, **21**, 735-752.

Pous, S., Carton, X. and Lazure, P. 2004. Hydrology and circulation in the Strait of Hormuz and the Gulf of Oman—Results from the GOCP99 experiment: 1. Strait of Hormuz. *Journal of Geophysical Research*, **109**, C12037, https://doi:10.1029/2003JC002145

Pous, S., Lazure, P. and Carton, X. 2015. A model of the general circulation in the Persian Gulf and in the Strait of Hormuz: Intraseasonal to interannual variability. *Continental Shelf Research*, **94**, 55-70.

Reynolds, R.M. 1993. Physical oceanography of the Persian Gulf, Strait of Hormuz, and the Gulf of Oman—Results from the *Mt. Mitchell* expedition. *Marine Pollution Bulletin*, **27**, 35-59.

Sarnthein, M. 1972. Sediments and history of the postglacial transgression in the Persian Gulf and northwest Gulf of Oman. *Marine Geology*, **12**, 245-266.

Stoffers, P. and Ross, D.A. 1979. Late Pleistocene and Holocene sedimentation in the Persian Gulf—Gulf of Oman. *Sedimentary Geology*, **23**, 181-208.

Thoppil, P.G. and Hogan, P.J. 2009. On the mechanisms of episodic salinity outflow events in the Strait of Hormuz. *Journal of Physical Oceanography*, **39**, 1340-1360.

Return to List of Straits

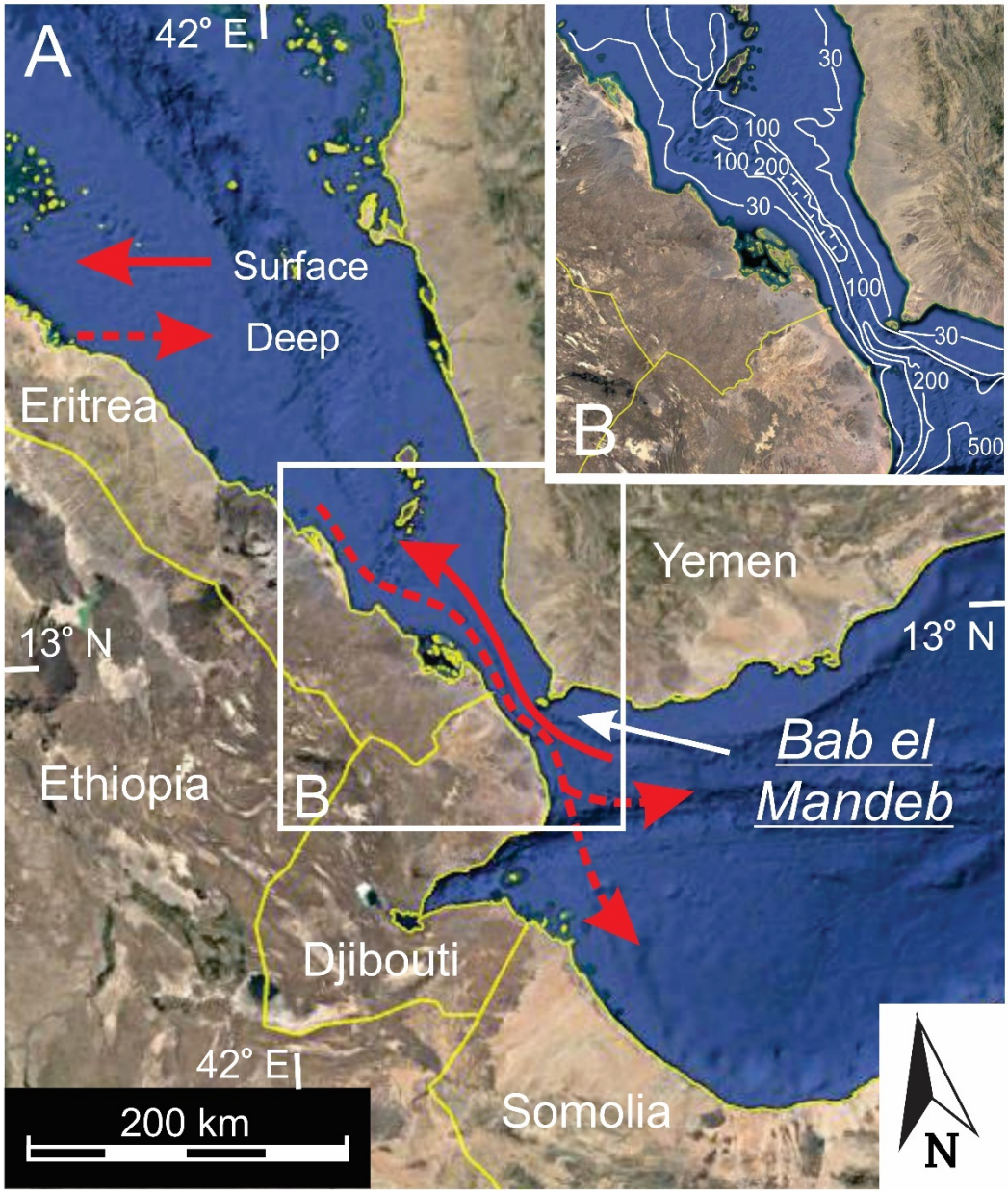

Fig. A20. Bab el Mandeb: *(A) General setting of the Bab el Mandeb strait. (B) Detailed bathymetry modified from Smeed (2004, fig. 3; copyright Elsevier; used with permission). Depths in metres. Satellite images from Google Earth ©. (Data: SIO, NOAA, U.S. Navy, NGA, GEBCO. Image: Landsat/Copernicus). The constriction of the Bab el Mandeb strait is the result of uplift and volcanism related to the presence of a mantle hot spot that is driving the continental separation between the Arabian Peninsula and Africa (Boswell* et al. *2005). Tides and meteorological events contribute significantly to the episodic flow through the strait (Jarosz* et al. *2005a, b; Johns & Sofianos 2012). The residual currents are an inverse-estuarine circulation, with seaward (southward) flow at the bottom, and northward flow at the surface (Sofianos & Johns 2002).*

Length

115 km total

Width

Narrowest point (Perim Narrows): 20.5 km; average width in parallel-sided inner part: 37 km; outer part is funnel shaped, reaching ~ 75 km wide at the entrance. During glacial lowstands, the entrance was only 6 km wide.

Depth

Sill depth 137 m. During glacial lowstands, water depth was only ~17 m.

Description

The Bab el Mandeb Strait is narrow because of thermal uplift, coupled with the large amount of volcanics that erupted here, from the plume that is associated with the opening of the Red Sea-Gulf of Aden system. There is surface-water inflow to the Red Sea, mainly during the southwest monsoon (November-June), and outflow of saltier water at the bottom (i.e., it has inverse-estuarine circulation). Exchange between the Red Sea and Gulf of Aden was greatly reduced during glacial periods. Salinity in the Red Sea might have risen by 10 ppt during the last glaciation. For most of the year, there is 'normal' two-layer flow, but during the summer, a 3-layer flow develops, with outflow at top and bottom, and inflow only in the middle layer. There is an amphidromic point for the M_2 tide in the Strait. Most of the tidal energy from both the Gulf of Aden and the Red Sea is dissipated in the Strait. Tides are much smaller in the Red Sea: the M_2 tidal range outside the Strait is ~ 2 m, whereas inside the Red Sea it is < 1 m. The tidal range reaches 2 m in the Perim Narrows. In the narrowest part of the Strait, K_1 and M_2 current speeds are ca. 40 cm s^{-1}, with a decrease in both directions from this area. Maximum flood-tide current speeds at the narrows reach 1 m s^{-1}. Maximum ebb speeds are 'comparable' to the flood. The internal tide at the narrows for the semi-diurnal and diurnal tides are 8 m and 12 m respectively. (These are smaller than in the Strait of Gibraltar). The pycnocline is at a depth 20-100 m depth. Much of the water exchange between the Gulf of Aden and the Red Sea is atmospherically forced.

References

Androsov, A.A. and Voltzinger, N.E. 2008. Simulation of the internal tide in the Strait of Bab el Mandeb (the Red Sea). *Izvestiya, Atmospheric and Oceanic Physics*, **44**, 121-137.

Bosworth, W., Huchon, P. and McClay, K. 2005. The Red Sea and Gulf of Aden Basins. *Journal of African Earth Sciences*, **43**, 334-378.

Bouilloux, A., Valet, J.-P., Bassinot, F., Joron, J.-L., Dewilde, F., Blanc-Valleron, M.-M. and Moreno, E. 2013. Influence of seawater exchanges across the Bab-el-Mandeb Strait on sedimentation in the Southern Red Sea during the last 60 ka. *Paleoceanography*, **28**, 675-687.

Jarosz, E., Murray, S.P. and Inoue, M. 2005a. Observations on the characteristics of tides in the Bab el Mandab. *Journal of Geophysical Research*, **110**, C03015, https://doi:10.1029/2004JC002299

Jarosz, E., Blain, C.A., Murray, S.P. and Inoue, M. 2005b. Barotropic tides in the Bab el Mandab Strait—numerical simulations. *Continental Shelf Research*, **25**, 1225-1247.

Johns, W.E. and Sofianos, S.S. 2012. Atmospherically forced exchange through the Bab el Mandeb Strait. *Journal of Physical Oceanography*, **42**, 143-1157.

Sofianos, S.S. and Johns, W.E. 2002. An oceanic general circulation model (OGCM) investigation of the Red Sea circulation: 1. Exchange between the Red Sea and the Indian Ocean. *Journal of Geophysical Research*, **107**, C11, 3196, https://doi:10.1029/2001JC001184

Thunell, R.C., Locke, S.M. and Williams, D.F. 1988. Glacio-eustatic sea-level control on Red Sea salinity. *Nature*, **334**, 601-604.

Return to List of Straits

21—MOZAMBIQUE CHANNEL

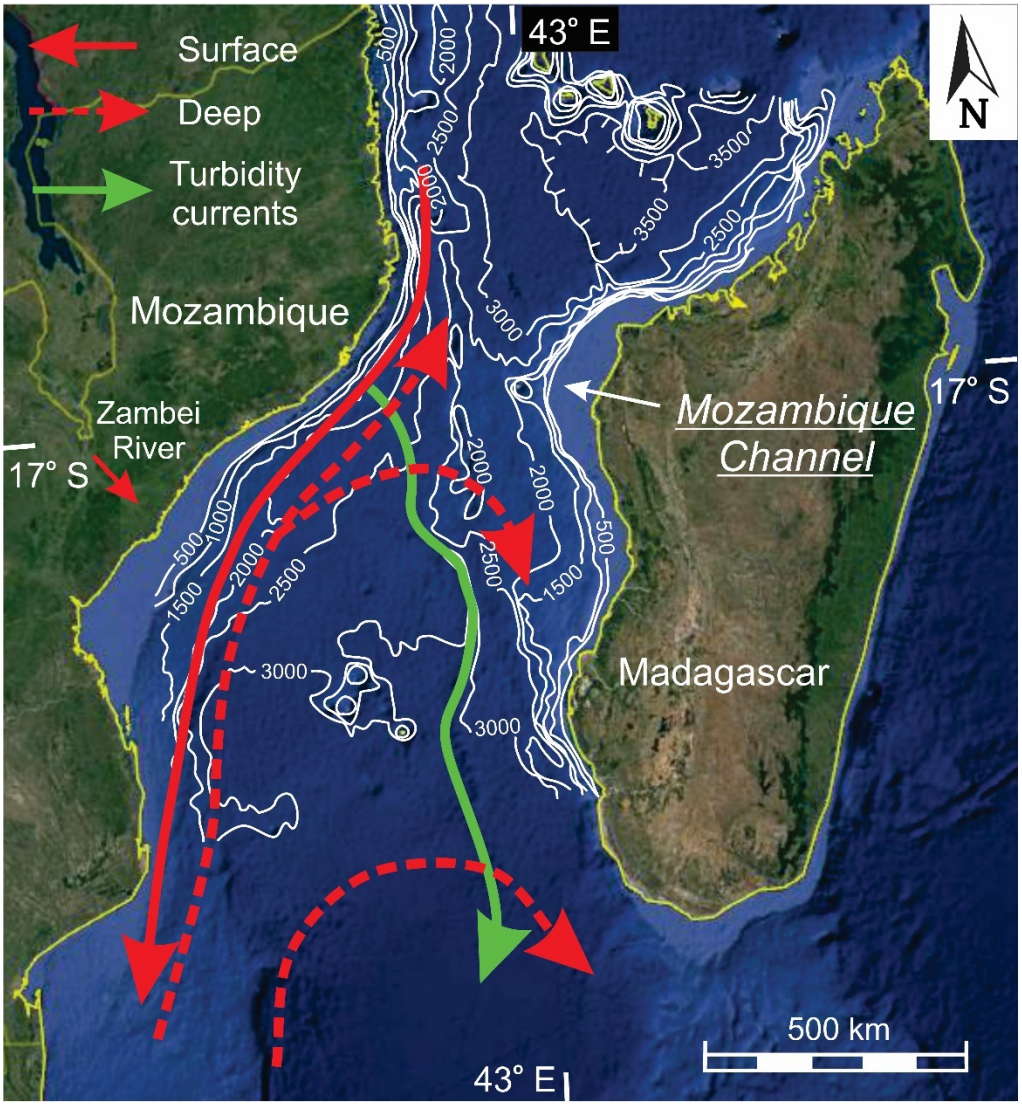

Fig. A21. *Mozambique Channel: Bathymetry after Breitzke* et al. *(2017, fig. 1; used with permission of Springer Nature). Depths in metres. The bathymetric data were derived originally from the ETOPO1 database. Satellite image from Google Earth ©. (Data: SIO, NOAA, U.S. Navy, NGA, GEBCO. Image: Landsat/Copernicus). This strait owes its existence to the arrested separation of the island of Madagascar from Africa (Nairn* et al. *1991). All of the closed 'bulls-eye' features at the north and south ends of the Channel are volcanoes related to the elevated heat flow association with the sea-floor spreading and hotspot activity (Feuillet* et al. *2021). Several thermo-haline ocean currents either pass through or enter and then exit the Channel. The southward-flowing surface current that hugs Africa is the Mozambique Current, which becomes the Agulhas Current in the south; the mid-depth, northward-flowing current is North Atlantic Deep Water; and the deepest current in the south is Antarctic Bottom Water (de Ruijter* et al. *2002; Breitzke* et al. *2017). The Zambezi Valley turbidite channel originates at*

the Zambezi River delta and then heads southward through the Channel, entering the Mozambique Basin in the south (Fierens et al. *2019).*

Length

Because of the flaring of its width at both ends, it is difficult to define its length precisely. The main 'throat' is ca. 300 km long. The entire length of the strait from islands in the north to islands in south is ca. 1200 km.

Width

430 km minimum (at narrows in north); 1000 km in south

Depth

3000 m at narrows (sill); 5000 m in south

Description

Underlain by transitional to oceanic crust. Surface water, the southeast-directed Madagascar Current, flows to the south, mainly along the African coast. It contains large eddies (> 300 km diameter) that extend to the seafloor. This flow is about half the volume of the Indonesian Throughflow (see below). Surface flow is northward along the Madagascar (eastern) side, the opposite of the western side. There is strong bottom-current activity: Antarctic Bottom Water (AABW) and North Atlantic Deep Water (NADW) flow northward, toward the equator, with a speed of ~ 0.2 m s^{-1}, with the flow hugging the African coast because of the Coriolis effect. There is extensive development of giant scours, sediment waves and other erosional/depositional features, beginning during the Pliocene or earlier, but all of the area is covered by a sediment drape today because current speeds have decreased (Breitzke *et al.* 2017). The axis of the Channel is the locus of a deep-sea turbidite channel through which turbidity currents flow southward from the Zambezi delta. Volcanic islands to the north and south of the narrowest part of the Channel are topped by carbonate platforms that shed carbonate debris outward to a distance of about 20 km. Such deposits are nearly circular in overall shape, and consist of pelagic deposits, turbidite channels and lobes, and mass transport complexes.

References

Backeberg, B.C. and Reason, C.J.C. 2010. A connection between the South Equatorial Current north of Madagascar and the Mozambique Channel eddies. *Geophysical Research Letters*, **37**, L04604, https://doi:10.1029/2009GL041950

Breitzke, M., Wiles, E., Krocker, R., Watkeys, M.K. and Jokat, W. 2017. Seafloor morphology in the Mozambique Chanel: evidence for long-term persistent bottom-current flow and deep-reaching eddy activity. *Marine Geophysical Research*, **38**, 241-269.

Counts, J.W., Jorry, S.J., Leroux, E., Miramontes, E. and Jouet, G. 2018. Sedimentation adjacent to atolls and volcano-cored carbonate platforms in the Mozambique Channel (SW Indian Ocean). *Marine Geology*, **404**, 41-59.

de Ruijter, W.P.M., Ridderinkhof, H., Lutjeharms, J.R.E., Schouten, M.W. and Veth, C. 2002. Observations of the flow in the Mozambique Channel. *Geophysical Research Letters*, **29**, 1502, https://doi: 10.1029/2001GL013714

Feuillet, N., Jorry, S., Crawford, W.C., Deplus, C., Thinon, I., Jaques, E. Saurel, J.M., Lemoine, A., Paquet, F., Satriano, C., Aiken, C., Foix, O., Kawalski, P., Laurent, A., Rinnert, E., CathalotDonval, J.-P., Guyader, V., Gaillot, A., Scalabrin, C., Moreira, C., Peltier, A., Beauducel, F., Grandin, R., Ballu. V., Daniel, R., Pelleau, P., Gornez, J., Basançon, S., Geli, L., Bernard, P., Bachelery, P. Fouquet, Y., Bertil, D., Lemarchand, A. and Van der Woerd, J. 2021. Birth of a large volcanic edifice offshore Mayotte, via lithosphere-scale dyke intrusion. *Nature Geoscience*, **17**, 787–795.

Fierens, R., Droz, L., Toucanne, S., Raisson, F., Jouet, G., Babonneau, N., Miramontes, E., Landurain, S. and Jorry, S.J. 2019. Late Quaternary geomorphology and sedimentary processes in the Zambezi turbidite system (Mozambique Channel. *Geomorphology*, **334**, 1-28.

Nairn, A.E. M., Lerche, I. and Iliffe, J.E. 1991. Geology, basin analysis, and hydrocarbon potential of Mozambique and the Mozambique Channel. *Earth-Science Reviews*, **30**, 81-124.

Walford, H.L., White, N.J. and Sydow, J.C. 2005. Solid sediment load history of the Zambezi Delta. *Earth and Planetary Science Letters*, **238**, 49-63.

Return to List of Straits

22-PALK STRAIT

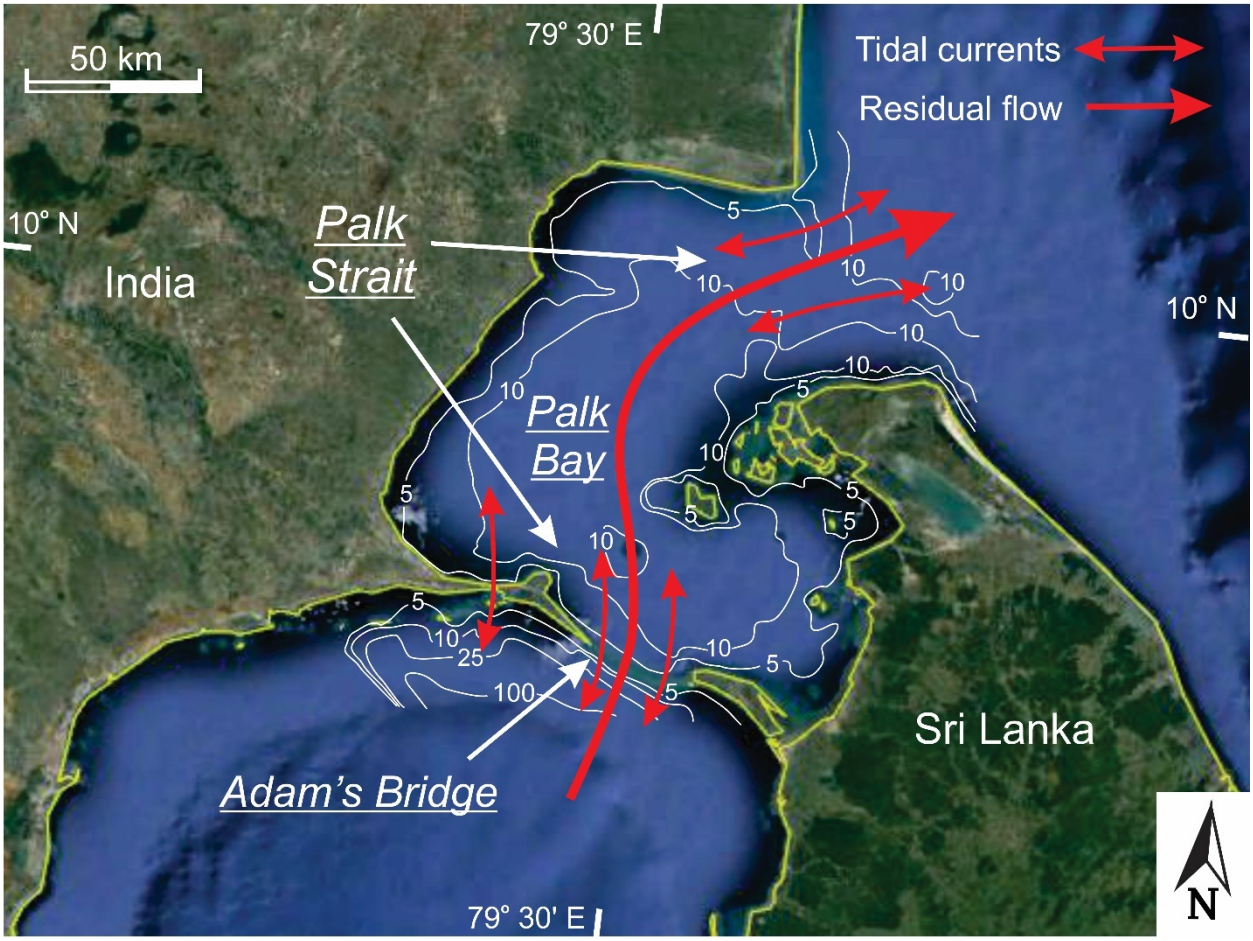

Fig. A22. Palk Strait: *Bathymetry modified after George & Kumar (2019, fig. 1; copyright Elsevier; used with permission), based on data supplied the Indian National Hydrographic Office. Depths in metres. Satellite image from Google Earth ©. (Data: SIO, NOAA, U.S. Navy, NGA, GEBCO. Image: Landsat/Copernicus). Adam's Bridge is a reef tract that is dissected by tidal channels with lobate tidal deltas at both their northern and southern ends (Bahuguna* et al. *2003). The central part of the Bay is very shallow and is affected by locally generated waves (George & Kumar 2019) that probably cause important sediment resuspension. The tidal residual flow is from south to north, but the regional atmospheric pressure gradient reverses this flow in the winter (Scaria* et al. *2015).*

Length

140 km long

Width

65-137 km wide. The channel between the Indian mainland and Rameswaram island at the western end of Adam's Bridge is called the Pamban Strait which is 1.2 km wide. There is a dredged ship canal through it.

Depth

Less than 9.1 m. There is a chain of coral reefs that is termed 'Adam's Bridge'. Pamban Strait is 3-5 m deep. Depth of Palk Bay is rarely > 9 m, and nowhere deeper than 15 m.

Description

The Strait lies along a failed rift between India and Sri Lanka that was initiated in the Cretaceous as India separated from Antarctica. There was counter-clockwise rotation of Sri Lanka initially, followed perhaps by some southward motion. There is a small amount of neotectonic fault movement parallel to Strait. The Strait is blocked by Adam's Bridge which is comprised of a chain of coral reefs (103 patch reefs) separated by tidal channels that are floored by carbonate sand and gravel. Adam's Bridge is ~ 30 km long; 9 km of islands and shallows; 21 km of open water. This reef chain rests on Miocene limestone. A 140 km-long barrier reef occurs along the Indian coast to the south of the Strait. There is converging longshore drift along the Indian coast, building the Mandapam Spit that anchors the western end of Adam's Bridge, but the dominant wave action is from the south, making the north side (Palk Bay) a low-energy depositional area. The island off the tip of this spit is built over a reef core. The line of reefs in Adam's Bridge is suggested as following a former (highstand?) shoreline. There was a mid-Holocene highstand at +2-3m with coral reefs and beachrock at that elevation (raised reefs dated ~4000 yrBP). At a somewhat lower sea level during the post-glacial transgression, the shallow part of Palk Bay was a tidal mudflat, crossed by a network of tidal channels. They appear to represent a somewhat higher-energy tidal phase (relative to today) during flooding of the Bay. Strata above the channels is flat-lying due to passive sedimentation. The south coast of the Indian spit is erosional. The Indian side of the Strait is quite arid, with only ephemeral runoff. There is a seasonal variation in salinity, from a low of ~ 31 ppt, to a high of ~35 ppt, with salinity generally increasing toward Adam's Bridge from the northern mouth. There is relatively little exchange with the Bay to the south through Adam's Bridge. The northern entrance to Palk Bay (the formal Palk Strait) appears to have elongate tidal ridges separated by tidal channels. Sea grass meadows are widespread in Palk Bay. There appears to be a longer-term RSL fall. Tidal-current speeds reach 3 m s^{-1} in the gaps through Adam's Bridge, but Sri Lanka has an amphidromic point on land at its SE tip, so Palk Strait is close to this; hence, tidal ranges are small. The tides are dominantly semi-diurnal. The tide around Sri Lanka is mixed semidiurnal with a spring tidal range of between 0.40 and 0.60 m. The phase difference between the two sides of Adam's Bridge is nearly 12 hours for the dominant M_2 tide. Tidal ranges decrease into the centre of the Bay. The net flux of water across Adam's Bridge is northward, but it is northward in their summer, and southward (but less) in their winter. Modeling of the rare storm (cyclone) surges show that surges of up to +5.4 m are possible along the west side and SE corner of Palk Bay. Very little water comes through Adam's Bridge; most of the surge enters through the northern entrance.

References

Bahuguna, A., Nayak, S. and Deshmukh, B. 2003. IRS views the Adams Bridge (bridging India and Sri Lanka). *Journal of the Indian Society of Remote Sensing*, **31**, 237-239.

George, v. & Kumar, V.S. 2019. Wind-wave measurements and modelling in the shallow semi-enclosed Palk Bay. *Ocean Engineering*, **189**, 106401, https://doi.org/10.1016/j.oceaneng.2019.106401

Joglekar, M.V. 2012. *Channel Dimensions & Paleodischarge Estimates of Buried Channel System in the Palk Bay, East Coast of India*. Unpublished M.Sc. thesis, Goa University, Goa, India, 66 p.

Rajagopal, N. and Ramesh, D. 2012. Coastal geomorphology of Ramanathapuram District, Tamil Nadu—A remote sensing perspective. *Tamil Civilization*, **24**, 81-90.

Ramesh, P.A. and Kannupandi, T. 1997. Recent changes in the coral reef ecosystem of Palk Bay: A conparitive (sic) status of previous reports and researches. *Regional Workshop on the Conservation and Sustainable Management of Coral Reefs*, December 15-17, 1997, M.S. Swaminathan Research Foundation, Chennai, India, C-123-C-130.

Ratheesh-Kumar, R.T., Dharmapriya, P.L. Windley, B.F., Zia, W.J. and Jeevan, U. 2020. The tectonic 'umbilical cord' linking India and Sri Lanka and the tale of their failed rift. *Journal of Geophysical Research: Solid Earth*, **125**, e2019JB018225, https://doi.org/10.1029/2019JB018225

Scaria, S., Murali, K. and Shanmugam, P. 2015. Numerical analysis of tidal dynamics in the region around Gulf of Mannar and Palk Strait. *Ocean Dynamics*, **65**, 487-508.

Stoddart, D.R. and Gopinadha Pillai, C.S. 1972. Raised reefs of Ramanathapuram, South India. *Transactions of the Institute of British Geographers*, **56**, July, 111-125.

Wijeratne, E.M.S. and Pattiaratchi, C.B. 2006. Sea level variability in Sri Lanka waters. *World* Climate Research Program Workshop, Understanding Sea-Level Rise and Variability, Paris, France, 6-9 June, 2006, poster.

Return to List of Straits

23—MALACCA STRAIT AND SINGAPORE STRAIT

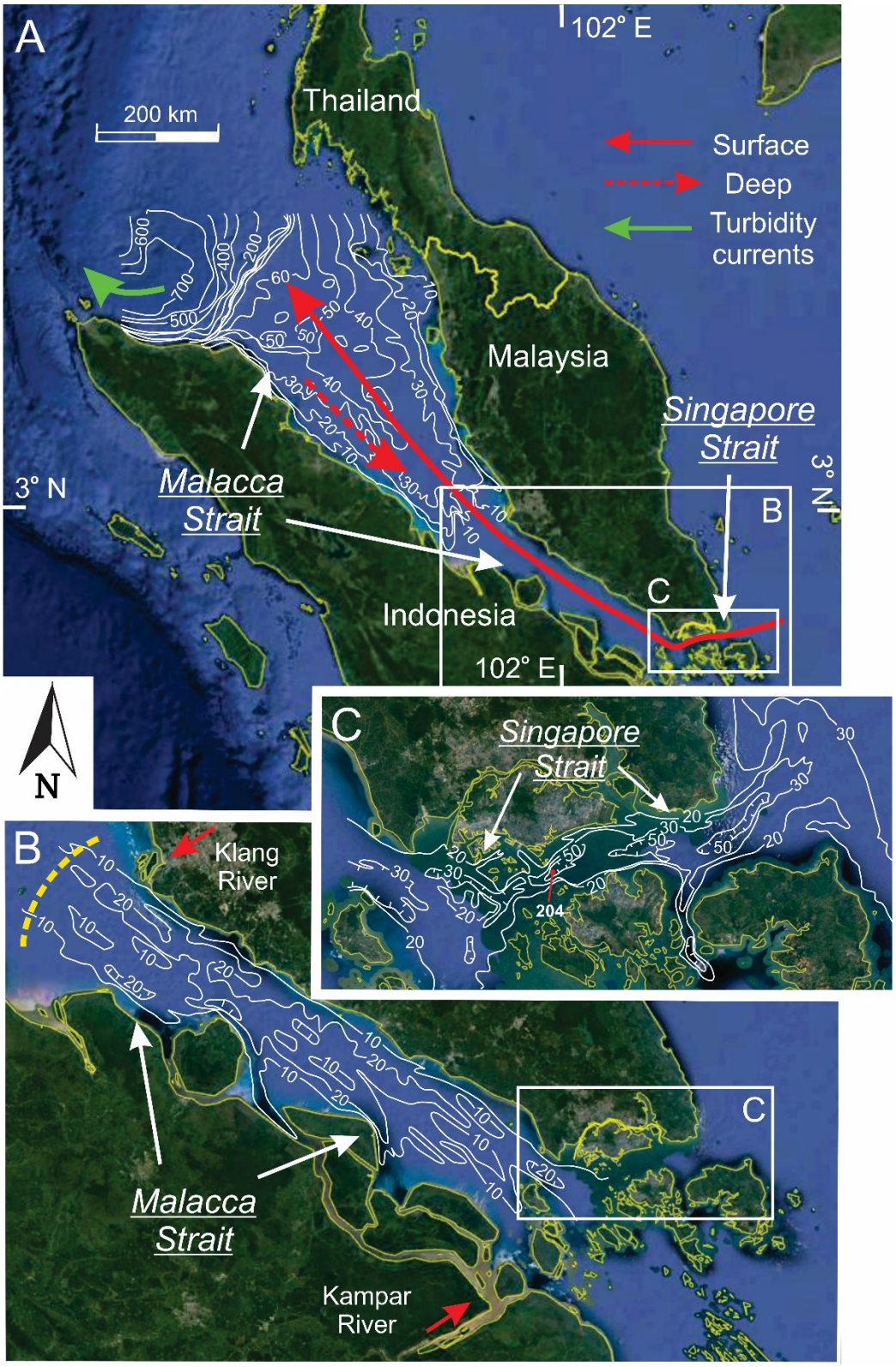

Fig. A23. *Malacca and Singapore Straits: (A) General setting of the entire Malacca-Singapore Strait system, which lies along the axis of a back-arc basin. (B) Greater detail of the narrow eastern part of Malacca Strait. (C) Detail of Singapore Strait. Bathymetric contours for Malacca Strait (A and B) in fathoms, from Keller & Richards (1967, fig. 3). (One fathom = 1.83 m). Bathymetry (in metres) for Singapore Strait (C) modified from Bird* et al. *(2006, fig. 1; copyright Elsevier; used with permission; original data from British Admiralty Chart 2403 'Singapore Straits and Eastern Approaches'). Satellite images from Google Earth ©. (Data: SIO, NOAA, U.S. Navy, NGA, GEBCO. Image: Landsat/Copernicus). The wide, NW part of Malacca Strait was occupied by an axial river during the glacial lowstand, with a delta at the mouth of the Strait (Emmel & Currray 1982), that in turn appears to have fed into a submarine canyon that directed turbidity currents into deep water. The narrow, southeastern part of Malacca Strait (B) shows extensive development of elongate tidal bars, separated by elongate depressions, generated by the strong tidal currents (Keller & Richards 1967; Rizal 2000; van Maren & Gerritsen 2012). In the NW half of this segment of the Strait, these bars are composed of sand, but in the SE they are muddy (Keller & Richards 1967; Chong* et al. *2005, cited in Li* et al. *2015), presumably reflecting the sediment discharge of the nearby Kampar River (the area of turbid water in the south-centre of (B)), which has a highly skewed delta. The dashed yellow line in (B) shows the approximate northwestern edge of the constriction-related delta, which has been termed a 'axial shelf shoal' by Galloway (2002). Singapore Strait contains an over-deepened, erosional scour at its most narrow point (Bird* et al. *2006). Residual flow is from east to west through the strait as a result of the Indonesian Throughflow (Ibrahim & Yanagi 2006; Chen* et al. *2014; Van Sebille* et al. *2014). There is a weak return flow in the wider, NW part of the Strait (Ibrahim & Yanagi 2006), generating an estuarine circulation pattern.*

Length

~ 1130 km in a sinuous path, winding through the islands that block the ESE end at Singapore. Keller & Richards (1968) say it is 805 km long.

Width

The Strait narrows SE-ward gradually. At the northwestern (Adaman Sea) end, it is 230-240 km wide. The south-eastern 300 km of Malacca Strait (west of the islands) is parallel-sided and 45-65 km wide. At the Singapore (southeastern) end, it is blocked by a series of islands with multiple passes into the Java Sea. The widest of these passes is 8.5 km wide, but the main channel (Singapore Strait) is 7 km wide at its narrowest.

Depth

The Strait generally becomes shallower to the southeast. The northwestern end is the continental slope into the Andaman Sea. Most of the wider, north-western half of the Strait is 70-110 m deep. The narrower paralllel-sided southeastern part of Malacca Strait is 35-55 m deep, and is contoured with a pronounced strait-parallel tidal-ridge (?) grain (Keller and Richards 1968). There is a 'choke point' (bathymetric constriction) at the NW end of the straight reach (at Kuala Lumpur). Amongst the islands

at Singapore, depths are typically 30 m deep, although Singapore Deep is up to 204 m deep. (This might have been formed by river flow, perhaps at a confluence, or where flow crossed a fault).

Description

Malacca Strait runs along the length of a back-arc basin. During the Pleistocene lowstand, there were two valleys in the western part of the Strait. In the eastern part, there was up to 40 m of erosional relief. These valleys fed a large delta that prograded into the Andaman Sea. Fluvial erosion is believed to be responsible for the opening of Singapore Strait. Residual water flux is to the west, but reverses with the monsoon: westward in January-March, but eastward for June-August. (This is part of the Indonesian Throughflow (see van Sebille *et al.* 2014).) Flow is tide-dominated through the eastern half of the Strait, with tidal currents reaching 1.4 m s^{-1}. Most of the sediment input is from the southern, Sumatra side, and consists of significant quantities of mud. Sand is the dominant bottom sediment throughout the axis of the Strait in its eastern part, where elongate 'ridges' are present, some of which are composed of mud. The carbonate content of the sediment is generally < 15% because of the high influx of terrigenous sediment from both sides. The Pleistocene-Holocene contact is very close to, or at, the surface through much of the Strait, but a wide coastal plain has developed along the Sumatra coast. Tidal range increases into the Strait from the Andaman Sea, from values of ca. 65-75 cm to >1.5 m at Singapore. Tidal range to the west of Singapore Strait is 2.7 m a springs, but it is 1.4 m to the east. There is a phase difference between the ends of the Strait of Singapore of less than an hour, so this doesn't drive the strong currents. Instead, it appears as if the tidal wave from the Andaman Sea experiences hypersynchronous conditions as it propagates southeastward. There is a 'tidal maximum' at the northwestern end of the straight reach, at Kuala Lumpur. I didn't find information about the asymmetry of tidal currents in Malacca Strait, but standard tidal theory of an incoming tidal wave in shallow water would predict net sand transport to the east in the narrow eastern part of the Strait. HOWEVER, the 'mean currents' (tide only) is predicted to be to the west through all of the narrow, inner part of the Strait (Chen *et al.* 2014). Saltier water enters from the west as a bottom-hugging salt wedge. The water becomes fresher during the northeast monsoon because of water coming from the Java (South China) Sea and river runoff. There are coral reefs growing in the vicinity of Singapore. Singapore Strait consists of a deep channel, with a localized 'deep' (Singapore Deep) reaching down to -204 m. The channel at Singapore appears to be cut by rivers flowing to the east, although Bird *et al.* (2006) suggest it was cut by flow from Malacca Strait. The rivers to the south (e.g., the Kampar River, south of Singapore) has a pronounced turbidity maximum and an impressive tidal bore. Tidal ranges are said to reach 4-5 m locally. The mouth of the Kampar River is partially deflected to the west. The fine fraction likely moves westward with the residual flow, whereas the tidal asymmetry likely carries the sand to the east (i.e., in opposite directions). (Storm) wind stress can be equal to or greater than the tidal currents in the wider western part of the Strait, but are weaker than the tidal currents in the narrower eastern part. In the west, wind generates a Strait-wide counter-clockwise eddy.

References

Bird, M.I., Pang, W.C. and Lambeck, K. 2006. The age and origin of the Straits of Singapore. *Palaeogeography, Palaeoclimatology, Palaeoecology*, **241**, 531-538.

Chen, H., Murali, K. Khoo, B.-C., Lou, J. and Kumar, K. 2005. Circulation modelling in the Strait of Singapore. *Journal of Coastal Research*, **21**, 960-972.

Chen, H., Malanotte-Rizzoli, P., Koh, T.-Y. and Song, G. 2014. The relative importance of the wind-driven and tidal circulations in Malacca Strait. *Continental Shelf Research*, **88**, 92-102.

Chong, V.C., King, B. and Wolanski, E. 2005. Physical features and hydrography. *In*: Ecology of Klang Strait. Sasekumar, A. and Chong, V.C. (eds). Faculty of Science, University of Malaya, Kuala Lumpur, 1-6. [Not seen. Cited in Li *et al.* (2015).]

Emmel, F.J. and Curray, J.R. 1982. A submerged Late Pleistocene delta and other features related to sea level changes in the Malacca Strait. *Marine Geology*, **47**, 197-216.

Hii, Y.S., Law, A.T., Shazili, N.A.M., Abdul Rashi, M.K., Mohd Lokman, H., Yusoff, F.M. and Ibrahim, H.M. 2006. The Straits of Malacca: Hydrological parameters, biochemical oxygen demand and total suspended solids. *Journal of Sustainability Science and Management*, **1**, 1-14.

Ibrahim, Z.Z. and Yanagi, T. 2006. The influence of the Andaman Sea and the South China Sea on water mass in the Malacca Strait. *Le Mer*, **44**, 33-42.

Keller, G.H. and Richards, A.F. 1967. Sediments of the Malacca Strait, southeast Asia. *Journal of Sedimentary Petrology*, **37**, 102-127.

Rizal, S. 2000. The role of non-linear terms in the shallow water equation with the application in three-dimensional tidal model of the Malacca Strait and Taylor's Problem in low geographical latitude. *Continental Shelf Research*, **20**, 1965-1991.

Tay, S.H.X., Kurniawan, A., Ooi, S.K. and Babovic, V. 2016. Sea level anomalies in straits of Malacca and Singapore. *Applied Ocean Research*, **58**, 104-117.

van Maren, D.S. and Gerritsen, H. 2012. Residual flow and tidal asymmetry in the Singapore Strait, with implication for resuspension and residual transport of sediment. *Journal of Geophysical Research*, **117**, C04021, https://doi:10.1029/2011JC007615

Van Sebille, E., Sprintall, J., Schwarzkopf, F.U., Sen Gupta, A., Santoso, A., England, M.H., Biastoch, A. and Böning, C.W. 2014. Pacific-to-Indian Ocean connectivity: Tasman leakage, Indonesian throughflow, and the role of ENSO. *Journal of Geophysical Research: Oceans*, **119**, 1365–1382, https://doi:10.1002/2013JC009525

Return to List of Straits

24—LOMBOK STRAIT

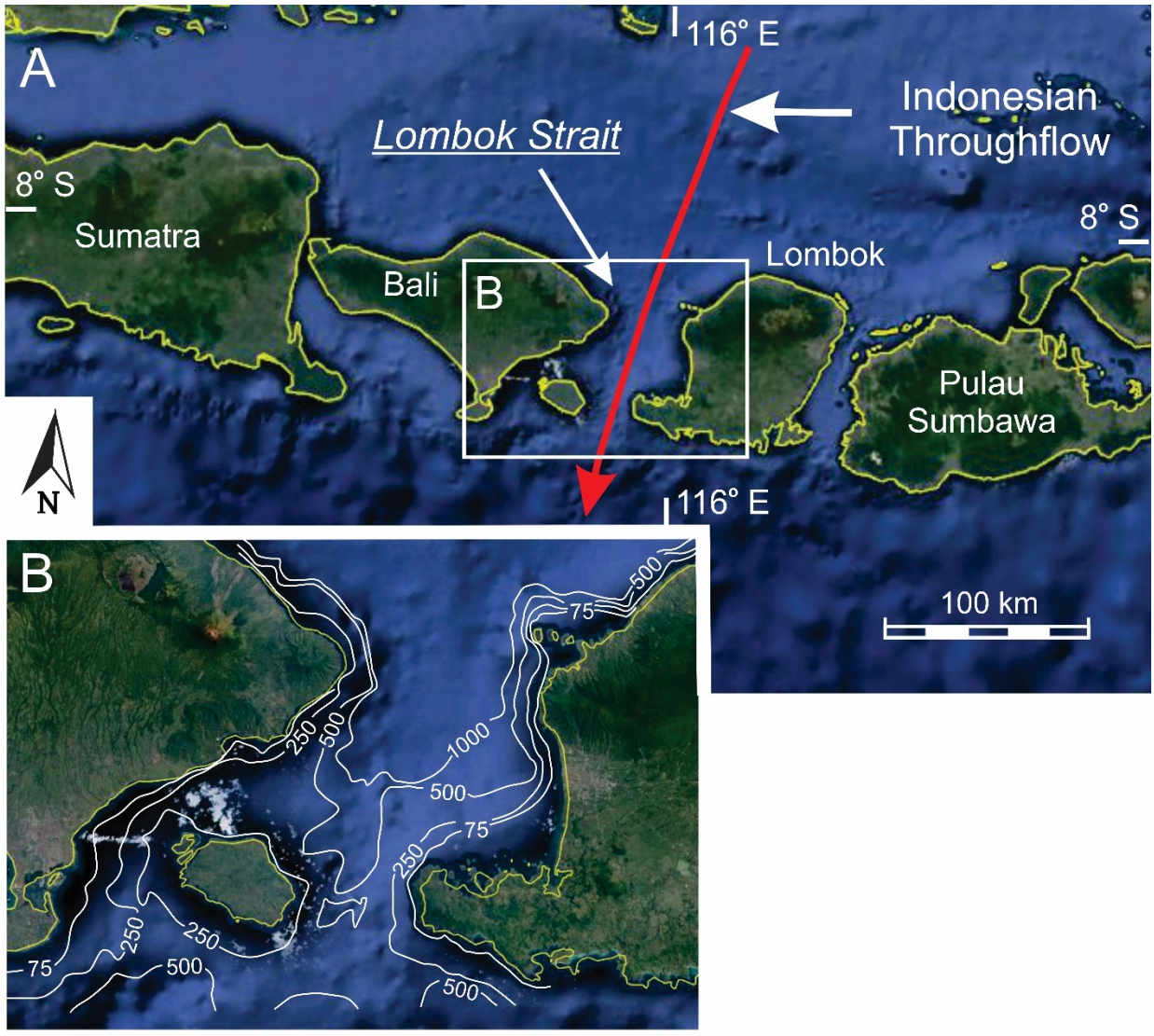

Fig. A24. *Lombok Strait: (A) General setting of Lombok Strait. (B) Detailed bathymetry after Androsov* et al. *(2020, fig. 2a). Depths in metres. Satellite images from Google Earth ©. (Data: SIO, NOAA, U.S. Navy, NGA, GEBCO. Image: Landsat/Copernicus). Lombok Strait represents a fault-controlled, deep-water break in the Indonesian island arc (Suleaman* et al. *2018), lying between arc volcanoes. It lies immediately to the SSW of Makassar Strait, through which the Indonesian Throughflow passes* en route *to Lombok Strait, which is one of the most important passes by which water enters the Indian Ocean (Wyrtki 1987; Murray & Arief 1988; Murray* et al. *1990; Van Sebille* et al. *2014).*

Length

Of the order of 50 km long

Width

35 km at northern (narrow) entrance; 22 km at main southern entrance. It is ~65 km wide in the middle and branches southward around a large island. The external Rossby radius here is about 120 km, which is more than the width of the strait.

Depth

Depths typically 800-1000 m; sill is topographically irregular with maximum depths of ca. 350 m. Bottom topography is quite rugged, presumably due to volcanic activity and the absence of significant sediment cover.

Description

Lombok Strait is the southern extension of Wallace's Line which separates SE Asian and Australian faunas. The Strait lies between two volcanic centres and there is an active fault in the Strait. The Sunda Block of which Bali is a part, is moving to the ESE at 27 mm yr^{-1}. Relative to this movement, Bali itself is moving to the northeast. The Strait has a persistent southerly flow due to ca. 15-20 cm of water-level set-up on the north side of the Indonesian island chain because of the easterly Trade Winds. This 'Indonesian Throughflow' is due to large-scale set-up on the western side of the Pacific due to Trade Winds. The pressure gradient has a strong seasonal variation being highest in July and August (i.e., strongest flow then). Current speeds typically are c. 70 cm s^{-1}, but reverse strongly at times due to typhoons in Timor Sea to the south. A well-developed plume of Pacific water extends 30 km south of the Strait into the Indian Ocean. On the southern sill, tidal flows reach speeds of > 3 m s^{-1}. The external Rossby Radius at this latitude is 90 km (says 120 km in one reference). This is 3x the width of the strait, so it is a 'narrow strait' because of this and there shouldn't be much cross-strait difference in flow. Corals grow in shallow water along the Strait margins. The seafloor in deeper water is exposed volcanic bedrock, with local hemipelagic mud.

References

Androsov, A., Voltzinger, N., Kuznetsov, I. and Fofonova, V. 2020. Modeling of nonhydrostatic dynamics and hydrology of Lombok Strait. *Water*, **12**, 3092; dhttps://oi:10.3390/w12113092

Karang, I.W.G.A., Chonnaniyah and Osawa, T. 2019. Landsat 8 observation of the internal solitary waves in the Lombok Strait. *Indonesian Journal of Geography*, **51**, 251-260.

Murray, S.P. and Arief, D. 1988. Throughflow into the Indian Ocean through the Lombok Strait, January 1985—January 1986. *Nature*, **333**, 444-447.

Murray, S.P., Arief, D., Kindle, J.C. and Hurlburt, H.E. 1990. Characteristics of circulation in an Indonesian Archipelago strait from hydrography, current measurements and modeling results. *In*: *Physical Oceanography of Sea Straits*, Pratt, L.J. (ed), NATO ASI Series C: Mathematical and Physical Sciences, **318**, 3-23.

Murty, S. A., Goodkin, N. F., Wiguna, A. A. and Gordon, A. L. 2018. Variability in coral-reconstructed sea surface salinity between the northern and southern Lombok Strait linked to East Asian winter

monsoon mean state reversals. *Paleoceanography and Paleoclimatology*, **33**, 1116–1133, https://doi.org/10.1029/2018PA003387

Suleaman, C., Hidayati, S., Omang, A., and Priambodo, I.C. 2018. Tectonic model of Bali Island inferred from GPS data. *Indonesian Journal of Geoscience*, **5**, 80-91.

Van Sebille, E., Sprintall, J., Schwarzkopf, F.U., Sen Gupta, A., Santoso, A., England, M.H., Biastoch, A. and Böning, C.W. 2014. Pacific-to-Indian Ocean connectivity: Tasman leakage, Indonesian throughflow, and the role of ENSO. *Journal of Geophysical Research: Oceans*, **119**, 1365–1382, https://doi:10.1002/2013JC009525

Wyrtki, K. 1987. Indonesian through flow and the associated pressure gradient. *Journal of Geophysical Research*, **92**, 12,941-12,946.

Return to List of Straits

25—MAKASSAR STRAIT

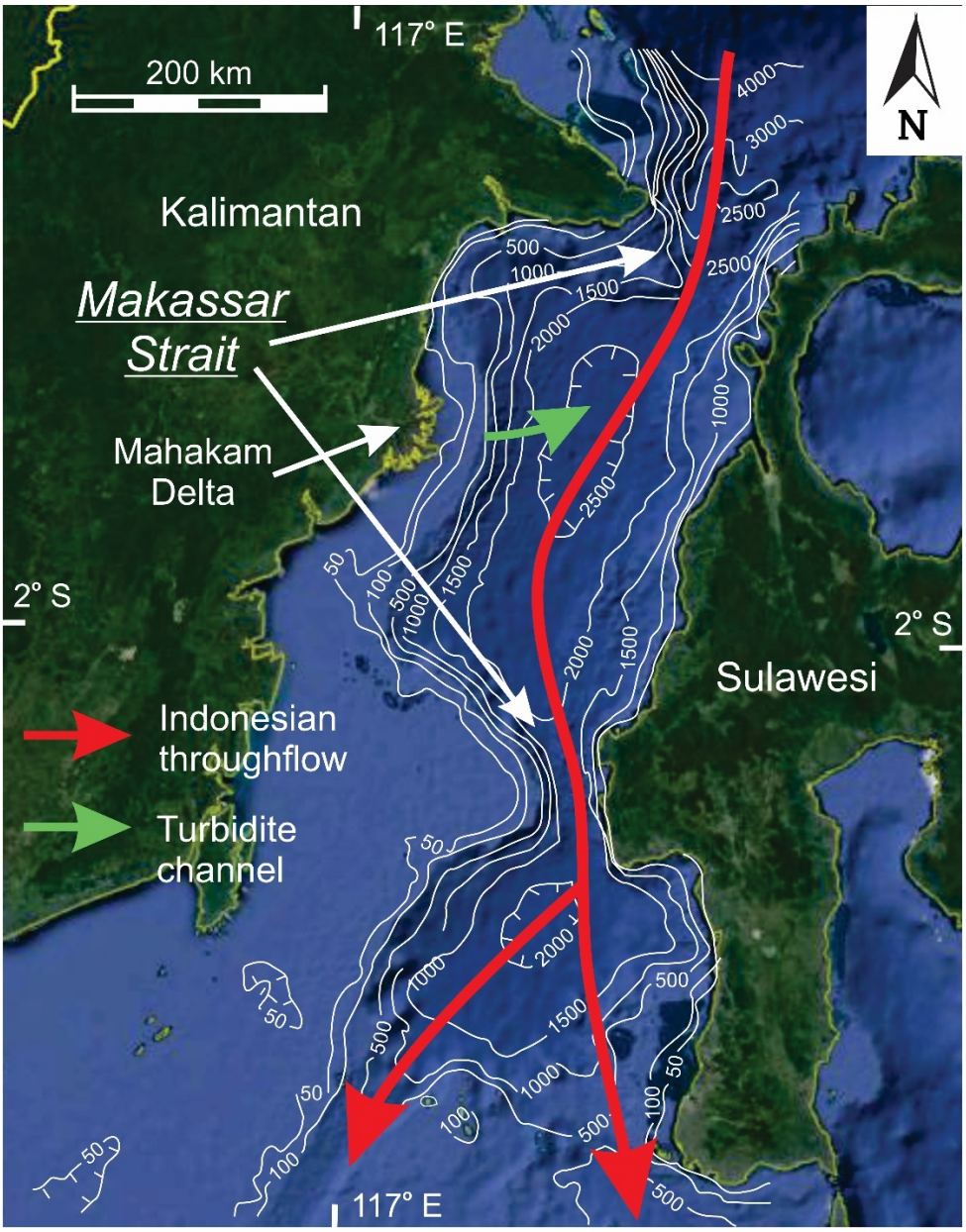

Fig. A25. *Makassar Strait: Bathymetry from Waworuntu* et al. *(2001, fig. 1; bathymetry reproduced with permission). Depths in metres. Satellite image from Google Earth ©. (Data: SIO, NOAA, U.S. Navy, NGA, GEBCO. Image: Landsat/Copernicus). Makassar Strait is asymmetric in cross-section profile, especially in the south. The western side, with its wide shelf, overlies continental crust, whereas the eastern side is flanked by an active thrust complex associated with subduction farther to the east (Ckoke* et al. *1999; Guntoro 1999). The Strait consists of two* en echelon *basins, separated by a strike-slip fault zone that defines the narrow choke point between the basins. Makassar Strait is one of the most significant pathways by which the Indonesian Throughflow passes from the western Pacific into the Indian Ocean (Sustano & Gordon 2005; Mayer & Damm 2012; Van Sebille* et al. *2014). Most of the flow occurs*

through the deep-water basins, with relatively weaker currents over the shallow western shelf. Because of this, the well-known Mahakam delta, which borders the Strait on the northern part of its western side (Roberts & Sidow 2012), is not strongly asymmetric. Coral reefs are abundant on the outer part of the western shelf. A turbidite channel-levee complex that is surrounded by a wide field of sediment waves has been constructed by eastward-flowing turbidity currents in the northern Makassar Basin (Posamentier et al. *2000). This channel appears to originate offshore from the Mahakam Delta, and its offshore extent has not been mapped.*

Length

~470 km from the northern constriction to the first major widening at the southern end (where the deep trough is narrowest).

Width

130-370 km. Labani Channel between the two basins is 44 km wide below the level of the shelves.

Depth

Central trough-- 1500-2300 m deep. The narrowest constriction between the two basins (Labani Channel) is ~2000 m deep. The main sill is the Dewakang Sill-- 550-650 m deep at the southern end of the southern basin. The western shelf is wide--25-220 km, widening southward, and typically < 30 m deep. The outer edge of the shelf promontory has a coral reef < 10 m deep. The shelf on the east side is <10-20 km wide.

Description

Most workers consider to the Strait to be caused by rifting, with the Strait experiencing back-arc spreading. Recent work has interpreted it as a foreland basin, bounded on both sides (W=Kalimantan; E=Sulawesi) by thrust complexes. The shelf edge on the east is definitively a thrust front. The western margin, which is an extension of continental crust, is most likely a rifted/extensional margin. There may be oceanic crust beneath the deep basins. Another interpretation is that the extension is due to trench roll-back. The narrows between the northern and southern basins (the Labani Channel) is the location of a strike-slip fault. Tsunamis are moderately common. Some of them may be caused by slumping caused by the earthquakes, given that some tsunamis are too large for the magnitude of the fault movement. Tsunamis are most important on the east side because of the narrow shelf and proximity to active faults; the west side is relatively safer. Sea level reached its present elevation at ~ 5 ka BP. Significant wave height is < 0.6 m because of the limited fetch and equatorial location. Tides (M_2 and K_1) in Makassar Strait are small (increase from ~0.35 m at south end to ~ 0.6 m at north end). The amplitudes of the M_2 and S_2 tides are 0.55 m and 0.35 m respectively. Tidal currents are very weak through most of the strait, but are strong (> 0.5 m s^{-1}) along the Sulawesi coast, and flow to the south throughout the entire tide. The Strait is the most important path for the Indonesian Throughflow, carrying 50-80% of the total flux. Most of the flow is in the upper 400-700 m, with southward-directed current speeds of 0.5-0.8 m s^{-1}. Speeds sometimes reach > 1 m s^{-1}; they don't appear to impinge on the western shelf very much, although perhaps on outermost edge locally: the current does tend to hug the

western side of the deep trough. All of the southward flow is above the height of the Dewakang Sill. Speeds at the bottom are very weakly to the north; stronger northerly flow occurs at 800-1000 m depth. (Measurements come from the narrowest section of the deep-water trough, the Labani Channel). In the deep-water North Makassar Basin, at the base of slope and beyond, there is a leveed turbidite channel system that is highly sinuous and feeds frontal splays. There are large overbank wedges that spill out on the outside of meander bends. They are covered by sediment waves, many of which are believed to have been formed by the upper, dilute part of overbank turbidity currents. Some waves are, however, thought to be due to prevailing oceanic currents. Debris flows/mass transport complexes are abundant. The turbidite channel is 250-1000 m wide, with flow to the north. The Mahakam delta is a lobate, tidally influenced, river-dominated delta. (Tidal range averages 1.2 m, but varies from 0.5 m at neaps to a maximum of 3 m at springs). It has prograded approximately 60 km in the Holocene, nearly but not quite reaching the local shelf edge at the present time. The distribution of mud is asymmetric because of the influence of a southerly directed current that reaches 80 cm s^{-1} on the delta front. Beyond the influence of siliciclastic mud, the shelf is floored with carbonate, including abundant *Halimeda* buildups that average 20 m in relief. There is more coralline algae near the shelf edge. At the shelf edge, reefs have a relief of up to 80-100 m. There are repeated cycles of deltaic deposits and carbonates on the shelf, as a result of repeated sea-level cycles.

References

Cloke, I.R., Milsom, J. and Blundell, D.J.B. 1999. Implications of gravity data from East Kalimantan and Makassar Straits: a solution to the origin of the Makassar Straits? *Journal of Asian Earth Sciences*, **17**, 61-78.

Guntoro, A. 1999. The formation of the Makassar Strait and the separation between SE Kalimantan and SW Sulawesi. *Journal of Asian Earth Sciences*, **17**, 79-98.

Mahfud, J., Haditiar, Y., Ikhwan, M., Wafdan, R., Setiawan, I. and Rizal, S. 2019. Numerical simulation of the M_2 tide in the Makassar Strait. *Earth and Environmental Science*, **348**, 01209, https://doi:10.1088/1755-1315/348/1/012095.

Mayer, B. and Damm, P.E. 2012. The Makassar Strait throughflow and its jet. *Journal of Geophysical Research*, **117**, C07020, https://doi:10.1029/2011JC007809

Posamentier, H.W., Meizarwin, Wisman, P.S. and Plawman, T. 2000. Deep water depositional systems—Ultra-Deep Makassar Strait, Indonesia. *Gulf Coast Section SEPM Foundation, 20th Annual Research Conference* '*Deep-Water Reservoirs of the World*', Houston, Texas, December 3-6, 2000, 806-816.

Prasetya, G.S., De Lange, W.P. and Healy, T.R. 2001. The Makassar Strait tsunamigenic region, Indonesia. *Natural Hazards*, **24**, 295-307.

Roberts, H.H. and Sydow, J. 2012. Late Quaternary stratigraphy and sedimentology of the offshore Mahakam delta, east Kalimantan (Indonesia). *In*: *Tropical Deltas of Southeast Asia—Sedimentology, Stratigraphy, and Petroleum Geology*, Sidi, F.H., Nummedal, D., Imbert, P., Darman, H. and Posamentier, H.W. (eds), SEPM, Special Publications, **76**, 125-145.

Susanto, R.D. and Gordon, A.L. 2005. Velocity and transport of the Makassar Strait throughflow. *Journal of Geophysical Research*, **110**, C01005, https://doi:10.1029/2004JC002425

Van Sebille, E., Sprintall, J., Schwarzkopf, F.U., Sen Gupta, A., Santoso, A., England, M.H., Biastoch, A. and Böning, C.W. 2014. Pacific-to-Indian Ocean connectivity: Tasman leakage, Indonesian throughflow, and the role of ENSO. *Journal of Geophysical Research: Oceans*, **119**, 1365–1382, https://doi:10.1002/2013JC009525

Waworuntu, J.M., Garzoli, S.L. and Olson, D.B. 2001. Dynamics of the Makassar Strait. *Journal of Marine Research*, **9**, 313-325.

Return to List of Straits

26—VITIAZ STRAIT

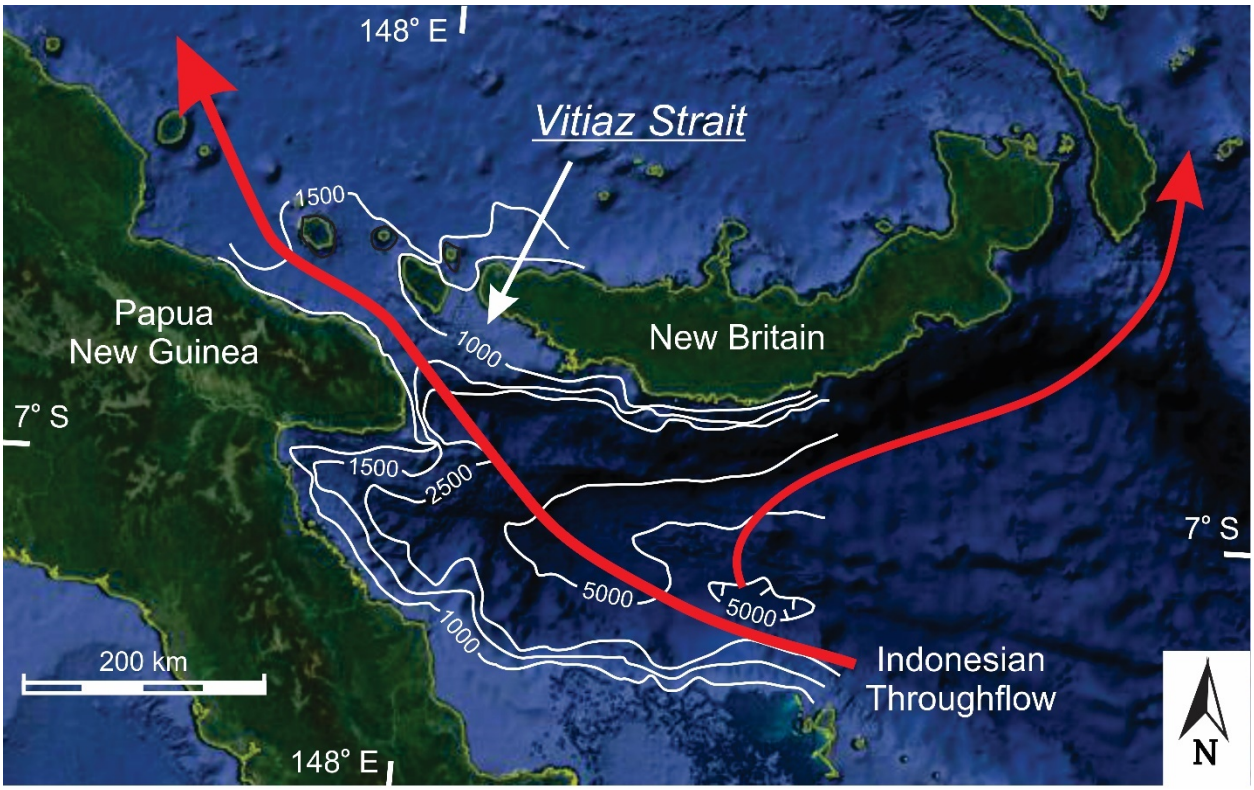

Fig. A26. *Vitiaz Strait: Bathymetry adapted from fig. 1 of Tchilobou* et al. *(2020). Because of scale differences between the original and derived images, and the subtle colour gradations indicating depths in the original figure, contour locations are only approximate. Depths in metres. Satellite image from Google Earth ©. (Data: SIO, NOAA, U.S. Navy, NGA, GEBCO. Image: Landsat/Copernicus). Vitiaz Strait is a deep, structurally controlled passage that is partially blocked by volcanoes associated with the Bismarck arc (Davies* et al. *1987; Whitmore* et al. *1997). This Strait is a major passage for movement of water from the western Pacific into the SE Asian seas,* en route *to the Indian Ocean (i.e., the Indonesian Throughflow) (e.g. Cravatte* et al. *2011). Current speeds for this flow exceed 1 m* s^{-1} *(Lindstrom* et al. *1987, 1990).*

Length

ca. 150 km

Width

Main part of strait about 90 km wide (42 km wide at the 200 m depth), but splits into two channels to the WNW around Umboi Island. The SW channel is about 45 km wide; the NE channel is 24 km wide.

Depth

A little more than 1200 m deep.

Description

This Strait is a break in the island arc associated with northwestward subduction of Solomon Sea oceanic crust. There is active volcanism associated with this subduction, including within the Strait itself. This break in the arc might be related to the rifting that is thought to have generated the Finisch Deep to the southeast, or to ongoing right-lateral strike-slip motion through the Strait. There is a persistent westerly flow due to the persistent easterly Trade Winds. Current speeds are up to 1.2 m s^{-1} (average 70-90 cm s^{-1} in the core of the flow). The core of this flow is at 150-300 m depth; in the Strait surface currents reach 1.8 m s^{-1}. This flow is a major component of the global water circulation in the equatorial Pacific: it is the principal source of water for the Equatorial Undercurrent (EUC) that flows eastward across the entire Pacific. The flow through Vitiaz Strait also feeds the Indonesian Throughflow which in turn feeds the westerly/southerly flow through straits farther to the west (e.g., Malacca and Lombok straits). The barotropic M_2 tides are nearly zero in the Solomon Sea (< 10 cm), and there doesn't appear to be much of a phase difference across the Vitiaz Strait, so tidal currents are presumably weak. The baroclinic M_2 tide is only 3-5 cm amplitude, and the highest amplitudes occur in the centre of the Solomon Sea, not near Vitiaz Strait. There is some elevated tidal energy concentration at Vitiaz Strait, but it is much smaller than farther east near the entrance to the Solomon Sea. The sediments under the Strait are highly faulted. The seafloor is covered by fine-grained sediment with shells, faecal pellets, and volcanic sand. Nearby, there are isolated coral reefs on former volcanic islands.

References

Cravatte, S., Ganachaud, A., Duong, Q.-P., Kessler, W.S., Eldin, G. and Dutrieux, P. 2011. Observed circulation in the Solomon Sea from SADCP data. *Progress in Oceanography*, **88**, 116-130.

Creswell, G.R. 2000 Coastal currents of northern Papua New Guinea, and the Sepik River outflow. *Marine and Freshwater Research*, **51**, 553-564.

Davies, H.L., Lock, J., Tiffin, D.L., Honza, E., Okuda, Y., Murakami, F. and Kisimoto, K. 1987. Convergent tectonics in the Huon Peninsula region, Papua New Guinea. *Geo-Marine Letters*, **7**, 143-152.

Krause, D.C. 1965. Submarine geology north of New Guinea. *Geological Society of America Bulletin*, **76**, 27-42.

Lindstrom, E., Butt, J., Lukas, R. and Godfrey, S. 1990. The flow through Vitiaz Strait and St. George's Channel, Papua New Guinea. *In*: *Physical Oceanography of Sea Straits*, Pratt, L.J. (ed), NATO ASI Series C: Mathematical and Physical Sciences, **318**, 171-189.

Lindstrom, E., Lukas, R., Fine, R., Firing, E., Godfrey, S., Meyers, G. and Tsuchiya, M. 1987. The western equatorial Pacific Ocean circulation study. *Nature*, **330**, 533-537.

Tchilibou, M., Gourdeau, L., Lyard, F., Morrow, R., Larrouy, A.K., Allain, D. and Djath, B. 2020. Internal tides in the Solomon Sea in contrasted ENSO conditions. *Ocean Science*, **16**, 615-635.

Whitmore, G.P., Johnson, D.P., Crook, K.A.W., Galewsky, J. and Silver, E.A. 1997. Convergent margin extension associated with arc-continent collision: The Finsch Deep, Papua New Guinea. *Tectonics*, **16**, 77-87.

Return to List of Straits

27—TORRES STRAIT

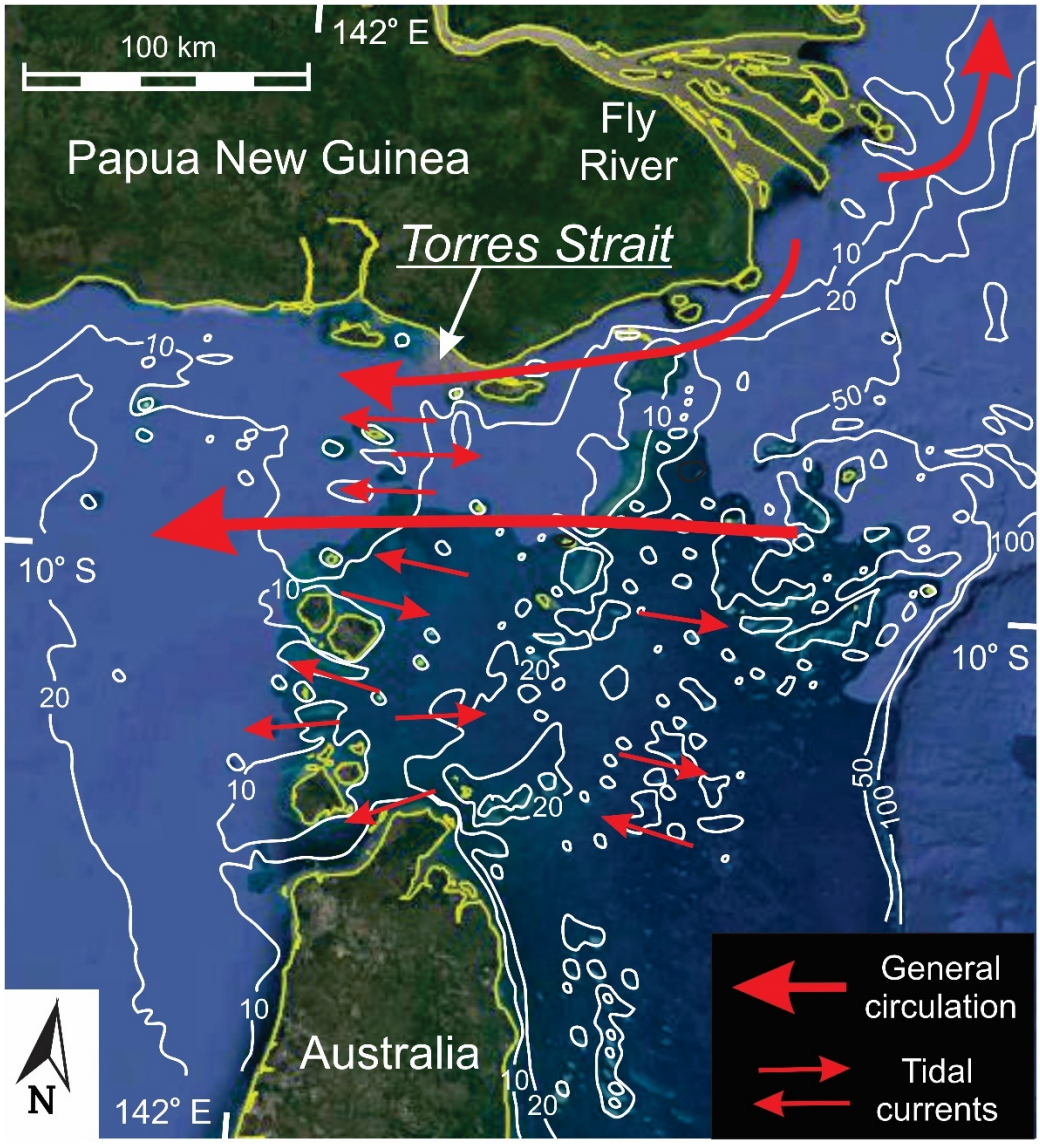

Fig. A27. Torres Strait: *Bathymetry modified from fig. 1 of Daniell & Hughes (2007; copyright Elsevier; used with permission). Depths in metres. Satellite image from Google Earth ©. (Data: SIO, NOAA, U.S. Navy, NGA, GEBCO, LDEO-Columbia, NSF. Image: Landsat/Copernicus). Torres Strait is very shallow (generally < 10 m deep at the sill), and flow through it is significantly impeded by multiple bedrock islands and coral reefs (Wolanski* et al. *1988): all of the small circular to elliptical bodies throughout the eastern part of the Strait are coral reefs that represent the northern extension of the Great Barrier Reef (Woodroffe* et al. *2000). Tidal currents are the dominant energy source for sediment redistribution (Harris 1988; Daniell & Hughes 2007; Hemer* et al. *2004), but they are superimposed on a pervasive but weak, east-to-west current (Wolanski* et al. *1988; Saint-Cast 2008) that is part of the regional Indonesian Throughflow. In addition, a part of the outflow of the Fly River in Papua New Guinea moves along the northern flank of the Strait; most of the outflow moves to the northeast.*

Length

ca. 170 km (nearly the same as the width)

Width

Total width: 140 km; width between Thursday and Moa Islands, the main channel: 28 km, of which Wolanski *et al.* (1988) estimate that 71% is blocked by reefs and islands. The islands rise up to 100 m above water level and represent a ridge of Carboniferous volcanics and Mesozoic sedimentary rocks.

Depth

Typically < 15 m; sill depth ~ 12 m (Harris 1988); there are large areas that are only 6-9 m deep. The sill is located approximately in the centre of the strait, with gradual slopes to the east and west. The centre of strait has several islands (especially along the south side) that compartmentalize flow into several 'channels'. Reefs are common on the sill, and also farther to the east, closer to the Great Barrier Reef.

Description

Torres Strait might occupy the back-bulge depression related to the PNG foreland basin. The main source of energy is tidal currents that have near-bed speeds that reach 0.8-1.5 m s^{-1}, due to water-surface elevation differences at either end of the strait that reach 6 m. Maximum tidal range: 3.9 m. Ebb is to the east; flood is to the west. The prevailing wind for most of the year (May to November) causes a net westward flow of water that causes a net migration of banks and dunes to the west. There are, however, local areas with eastward migration of dunes due to the presence of mutually evasive tidal transport paths. Dunes in areas reverse their migration direction with the seasonal change in wind direction. Significant wave heights are < 1.5 m for most of the year (maximum is ~ 3.5 m) and there is no swell because of the Great Barrier Reef-- only locally generated waves are present during the Trade Wind season. The very shallow water of the Strait, coupled with the presence of reefs and islands, means that only 30% of the tidal-wave energy from either side propagates through the Strait. Most sediments are bioclastic carbonates (> 80%), with terrigenous-clastic deposits only close to 'sources' (mainly rivers from Papua New Guinea presumably, as well as coastal erosion). There are areas of mud off the Fly River delta and in the SE part of the Strait; elsewhere the bottom sediments are sands and gravels, except in scour areas where there is bedrock exposure and/or lag gravels. The concept of bedload parting and tidal sediment-transport pathways is used, with sediment grain size decreasing down the transport path. There is a turbidity maximum in the centre of Torres Strait composed mainly of sediment resuspended from the sea bed (i.e., carbonate mud). Bedforms come in 4 types: 1) linear sand banks; 2) elongate dune trains; 3) dune fields; and 4) sand ribbons. Reef growth is prolific in Torres Strait. Sediment from Papua New Guinea (PNG) is present only within 5-10 km of the PNG coast; very little is coming into Torres Strait from the Fly River. There are extensive areas of sea grass in the Strait, commonly with sea grass occurring in the troughs of starved dunes. These starved dunes migrate 0.59 m/day, whereas full-bedded dunes migrated only 0.13 m/day. The modelled mud content of the sediment is low, increasing outward from the sill towards the ends.

References

Daniell, J.J., Harris, P.T., Hughes, M.G., Hemer, M. and Heap, A. 2008. The potential impact of bedform migration on seagrass communities in Torres Strait, northern Australia. *Continental Shelf Research*, **28**, 2188-2202.

Daniell, J.J. and Hughes, M. 2007. The morphology of barchan-shaped sand banks from western Torres Strait, northern Australia. *Sedimentary Geology*, **202**, 638-652.

Harris, P.T. 1988. Sediments, bedforms and bedload transport pathways on the continental shelf adjacent to Torres Strait, Australia-Papua New Guinea. *Continental Shelf Research*, **8**, 979-1003.

Harris, P.T. 1991. Reversal of subtidal dune asymmetries caused by seasonally reversing wind-driven currents in Torres Strait, northeastern Australia. *Continental Shelf Research*, **11**, 655-662.

Harris, P.T. & Baker, E.K. 1991, The nature of sediment forming the Torres Strait turbidity maximum. *Australian Journal of Earth Sciences*, **38**, 65-78.

Heap, A.D. and Sbaffi, L. 2008. Composition and distribution of seabed and suspended sediments in north and central Torres Strait, Australia. *Continental Shelf Research*, **28**, 2174-2187.

Hemer, M.A., Harris, P.T., Coleman, R. and Hunter, J. 2004. Sediment mobility due to currents and waves in the Torres Strait-Gulf of Papua region. *Continental Shelf Research*, **24**, 2297-2316.

Saint-Cast, F. 2008. Multiple time-scale modelling of the circulation in Torres Strait—Australia. *Continental Shelf Research*, **28**, 2214-2240.

Wolanski, E., Ridd, P. and Inoue, M. 1988. Currents through Torres Strait. *Journal of Physical Oceanography*, **18**, 1535-1545.

Woodroffe, C.D., Kennedy, D.M., Hopley, D., Rasmussen, C.E. and Smithers, S.G. 2000. Holocene reef growth in Torres Strait. *Marine Geology*, **170**, 331-346.

Return to List of Straits

28—BASS STRAIT

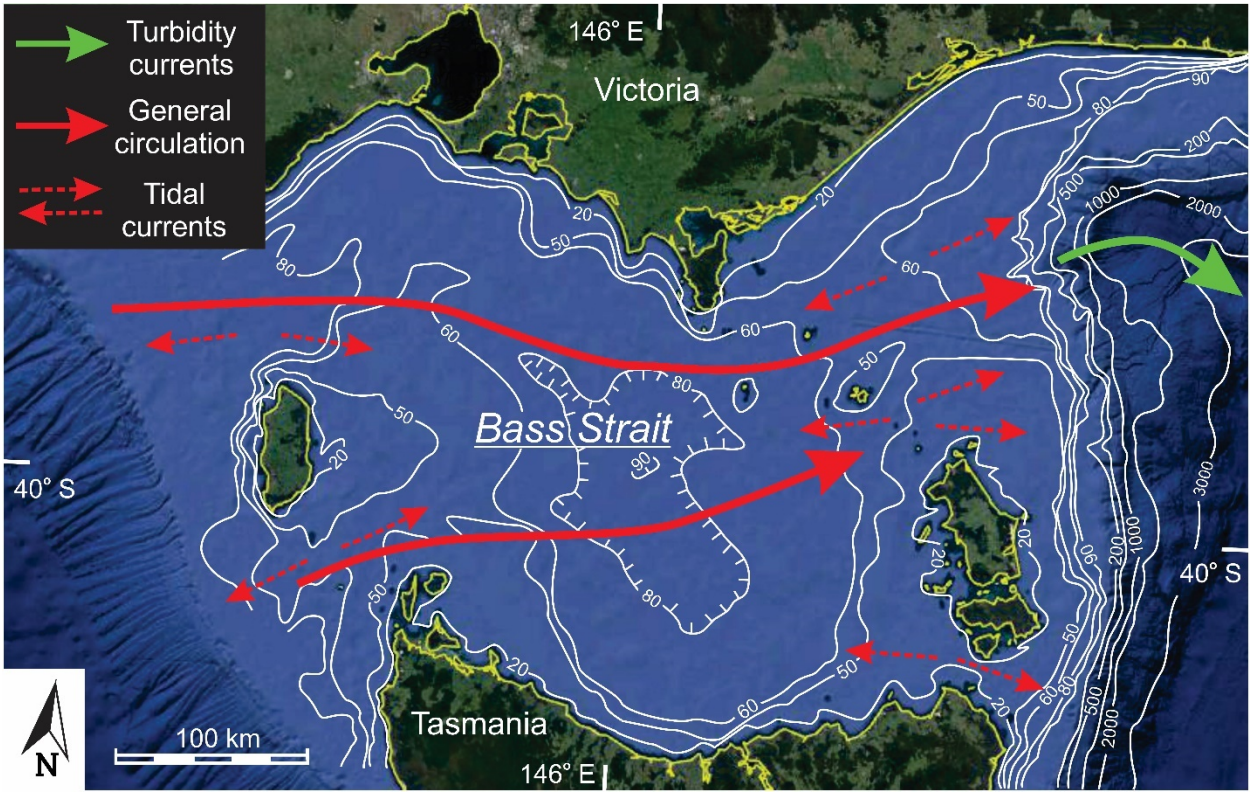

Fig. A28. Bass Strait*: Bathymetry from Malikides* et al. *(1988, fig. 1; used by permission of Taylor & Francis Ltd.). Depths in metres. Satellite image from Google Earth ©. (Data: SIO, NOAA, U.S. Navy, NGA, GEBCO, LDEO-Columbia, NSF. Image: Landsat/Copernicus). The Strait consists of a sill at either end, separated by central depression (Bass Basin) that is the remnant of a rift basin associated with the attempted separation of Tasmania from mainland Australia (Young* et al. *1991; Royer & Rollet 1997). Tidal currents are strong on the two sills (Malikides* et al. *1988, 1989), but currents in the Bass Basin are weak (Passlow* et al. *2006). There is a weak west-to-east current through the Strait, caused by the regional wind regime (Middleton & Black 1994). The head of a submarine canyon occurs at the NE corner of the Strait, an association that occurs in several of the straits examined in this study (e.g. Strait of Juan de Fuca, Malacca Strait and Cook Strait). See Fig. 22A of the main text for the distribution of carbonate content in the surficial sediments.*

Length

300-350 km, along a somewhat sinuous path

Width

210 km at its widest in the area of the central basin; main western opening-- 83 km; eastern opening complicated by many islands, the largest of which is Flinders Island.

Depth

Strait has complex morphology, with sills at either end, separated by a deep central basin. The basin is up to 90 m deep. The eastern sill is 50-60 m deep at its deepest (large parts are < 20 m deep), whereas the deepest part of the western sill is 60-80 m deep.

Description

The Strait is a failed rift associated with the initial stages of the separation of Australia from Antarctica. Initial rifting was in the Cretaceous, forming a half graben in the Bass Basin, with some dextral shear. The stress regime became dextral transpressive in the Eocene, but the effects are minimal in Bass Strait. The tidal range (= 2 x amplitude) is almost everywhere < 2 m, and < 1 m in many places. Only in very isolated locations is it > 2 m. Tidal current speeds are ~ 1 m s^{-1} at the surface. There is a net west-to-east net flow through the Strait because of the prevailing wind (a wind-driven current), which is in the opposite direction to the so-called 'Tasman Leakage' around the southern tip of Tasmania. There is, however, almost no transport through Bass Strait because it is too shallow. There is an eastward drift of water along the northern coast, at a speed of 2.3 cm s^{-1}. Modeling shows that the dominant flow is apparently to the east, with faster speeds over the shallow sills, and quite slow speeds in the deeper basin. Even the fast speeds are only ~10-15 cm s^{-1}. The sediment contains 50-92% modern and relict carbonate of cool-water origin (skeletal debris derived from bryozoans, molluscs and foraminifera), with quartz as the subordinate constituent. The quartz is said to probably originate from the granites of the islands. In general, the siliciclastic content is highest around islands and along the coasts; carbonates are greatest farther from the modern shoreline. The mixing is probably due to the reworking of palimpsest, lowstand clastics by tidal currents and waves. Sediment delivery to the strait is limited; river mouths on the Australian side are unfilled wave-dominated estuaries. The one larger river on the Tasmanian side might be about to construct a delta, but it lies in an indentation on the side of the Strait so it does not interact with the currents. The margins of the Strait are wave-dominated beaches. The finest sediment occurs in the deeper central basin and especially on the concave Tasmanian side, where mean sizes are silt. The shallower sills are covered by sand-sized sediment, with the coarsest sand in the shallowest water and especially the western entrance. On the eastern 'sill', compound dunes occur (heights 2-12 m; average 6 m) in 40-46 m of water. Tidal-dominance is concentrated mainly on the sills; elsewhere in the Strait, sediment movement is mainly by waves. Four sediment types recognized: 1) bryozoan and lithoclastic sand and gravel; 2) Bioclastic and lithoclastic fine sand; 3) quartz sand; and 4) carbonate sandy mud and muddy sand. The main area of net accumulation is in the central basin.

References

Malikides, M., Harris, P.T., Jenkins, C.J. and Keene, J.B. 1988. Carbonate sandwaves in Bass Strait. *Australian Journal of Earth Sciences*, **35**, 303-311.

Malikides, M., Harris, P.T. and Tate, P.M. 1989. Sediment transport and flow over sandwaves in a non-rectilinear tidal environment: Bass Strait, Australia. *Continental Shelf Research*, **9**, 203-221.

McIntoch, P.C. and Bennett, A.F. 1984. Open ocean modeling as an inverse problem: M_2 tides in Bass Strait. *Journal of Physical Oceanography*, **14**, 601-614.

Middleton, J.F. and Black, K.P. 1994. The low frequency circulation in and around Bass strait: a numerical study. *Continental Shelf Research*, **14**, 1495-1521.

Passlow, V., O'Hara, T, Daniell, J., Beaman, R.J. and Twyford, L.M. 2006. *Sediments and Benthic Biota of Bass Strait: An Approach to Benthic Habitat Mapping*. Geoscience Australia, Record 2004/23, 97 p.

Royer, J.-Y. and Rollet, N. 1997. Plate-tectonic setting of the Tasmanian region. *Australian Journal of Earth Sciences*, **44**, 543-560.

van Sebille, E., Sprintall, J., Schwarzkopf, F.U., Sen Gupta, A., Santoso, A., England, M.H., Biastoch, A. and Böning, C.W. 2014. Pacific-to-Indian Ocean connectivity: Tasman leakage, Indonesian throughflow, and the role of ENSO. *Journal of Geophysical Research: Oceans*, **119**, 1365–1382, https://doi:10.1002/2013JC009525

Veevers, J.J., Powell, C.McA. and Roots, S.R. 1991. Review of seafloor spreading around Australia. I. synthesis of the patterns of spreading. *Australian Journal of Earth Sciences*, **38**, 373-389.

Weeks, L.G. and Hopkins, B.M. 1967. Geology and exploration of three Bass Strait Basins, Australia. *The American Association of Petroleum Geologists Bulletin*, **51**, 742-760.

Young, I.M., Trupp, M.A. and Gidding, M.J. 1991. Tectonic evolution of Bass Strait—Origins of Tertiary inversion. *Exploration Geophysics*, **22**, 465-468.

Return to List of Straits

29—COOK STRAIT

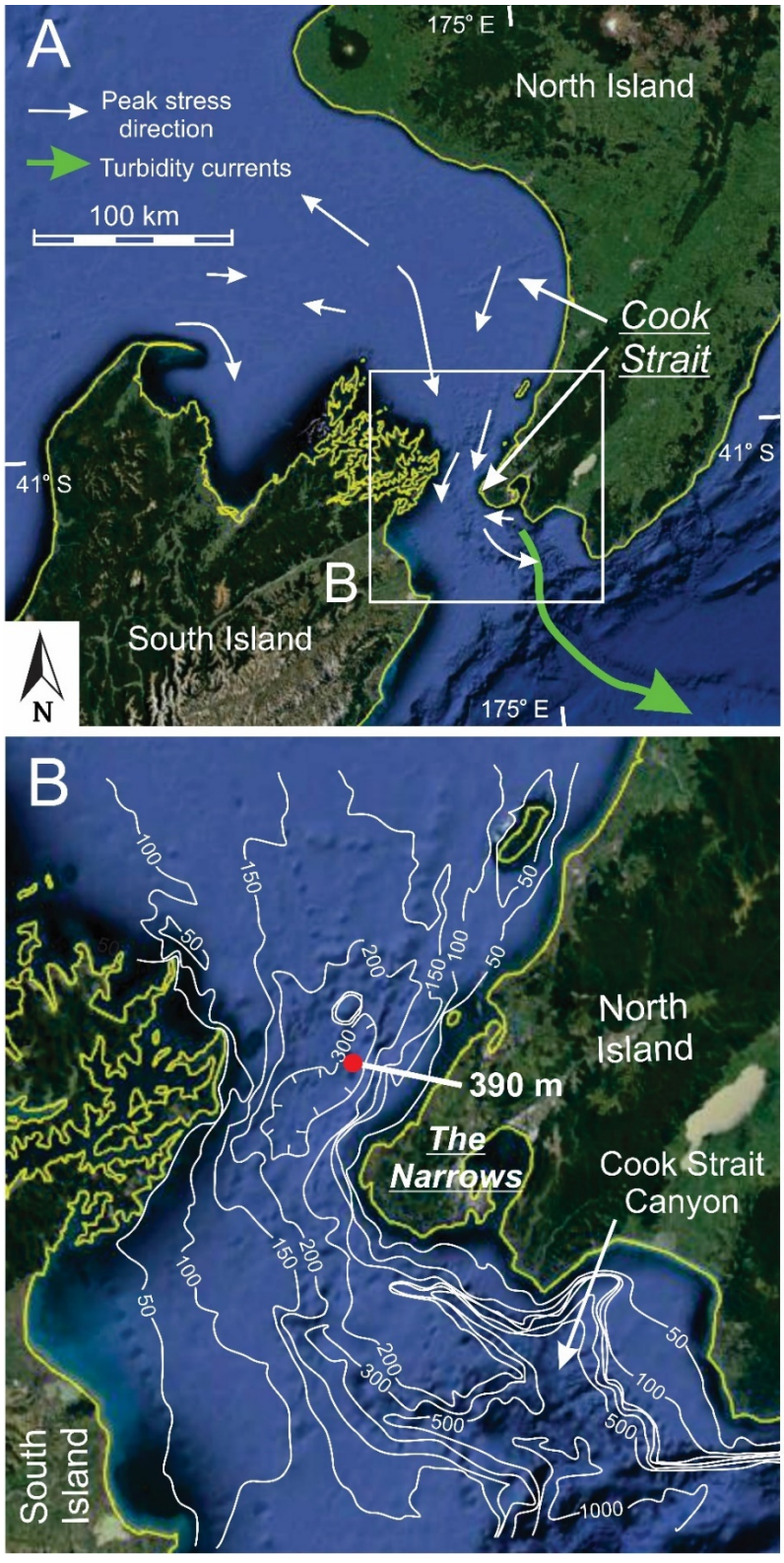

Fig. A29. *Cook Strait: (A) General setting of Cook Strait. (B) Detailed bathymetry taken from Carter (1992, fig. 1; used by permission of Taylor & Francis Ltd.). Bathymetry originally derived from Mitchell & Lewis (1980); reproduced with permission of the New Zealand National Institute of Water & Atmospheric Research Ltd. (NIWA). See also Lamarche et al. (2011, fig. 1). Depths in metres. Satellite images from Google Earth ©. (Data: SIO, NOAA, U.S. Navy, NGA, GEBCO, LDEO-Columbia, NSF. Image: Landsat/Copernicus). The shelf surface to the northwest of the central narrows in Cook Strait is relatively smooth and largely featureless. Within 'The Narrows', there is one or two deep scours with localized depths of nearly 400 m (Carter 1992; Lamarche* et al. *2011). To the south of the constriction, the shelf is deeply incised by the Cook Strait Submarine Canyon (Mountjoy* et al. *2014). Tidal currents are strong within the central constriction (Heath 1978; Bowman* et al. *1980; Walters* et al. *2010). The background flow is from north to south through the Strait and results from wind forcing and general oceanic circulation (Heath 1971, 1986; Reid 1996; Walters* et al. *2010).*

Length

'The Narrows' is ~ 30 km long. The entire Strait (Greater Cook Strait) is approximately 120 km long, with a zig-zag course. The overall orientation is North-South.

Width

Minimum width-- 22 km. Area to the north of the Narrows is strongly funnel-shaped, being ~95 km wide at the northern tip of the South Island. The area to the south of the narrows is more parallel-sided, with a width of ~ 60 km.

Depth

Cook Strait doesn't appear to have a single discrete 'sill'. Instead, there is an elongate deep in the centre of the Narrows, with depths > 200 m: the Narrows Basin is 380 deep, and has a 225 m-deep sill at its southern end. Depths on either side, and to both the north and south are less than 100 m deep. The head of Cook Strait Canyon extends into the eastern side of the southern approach to the Strait, with water depths > 600 m on the shelf. The shallowest connection between the two Islands is in the NW approaches, where the arcuate 'sill' is 70-90 m deep.

Description

The Narrows formed as a result of plate-tectonic movements that aligned various sedimentary basins. The subsidence of the Narrows basin, the critical break in the New Zealand mountain chain, is due to the splaying of strike-slip faults, allowing down-drop of the area between the splays (a sort of pull-apart basin). Residual currents are in opposite directions on either side of the Strait: southward on the west side, and northward on the east side. Three oceanic currents intrude into the Strait. Tidal flux was greatest during interglacial highstands, causing deep scour in the Narrows, and low or absent during glacials, allowing sediment (mud) deposition. During the last post-glacial sea-level rise, the strongest tidal action might have occurred early in the Holocene, with a decrease to today. Present-day tidal ranges are microtidal at both ends of the Strait, and decrease inward to a minimum of ~ 0.4 m at the Narrows. Maximum tidal-current speeds in the Narrows are > 1 m s^{-1} (highest stated value 3.5 m s^{-1}).

[Walters *et al.* (2010, fig. 5) present good map of average current speeds!] Peak tidal-current strengths appear to be directed southward at all locations shown (Lewis *et al.* 1994). Residual tidal flow through the Narrows is southward. There is a residual, weak northerly flow north of the Narrows, but an eddy exists SW of the Narrows. Tidal currents dominate over wind-driven currents over most of the area. Tidal processes on the shelf are responsible for depositing sediment in the upper part of Cook Strait Canyon, leading to failure and down-canyon transport by earthquake-generated turbidity currents. There is a sinuous belt of gravel that passes through the Narrows. Wedges of muddy and sandy sediment are prograding in protected embayments supplied by rivers; these wedges become coarser grained as they prograde into more exposed locations. There is sand transport southward into the Narrows, but to the south of it, there appears to be more complicated transport paths, perhaps mimicking those of an ebb-tidal delta with marginal areas having northward transport into the Narrows. Swath bathymetry (Lamarche et al. 2011) shows large to very large dunes apparently migrating SSWward into the deep depression at the Narrows. (Note that the text says that dunes in this area are migrating to the NE). This direction contradicts the Longhitano model, but is consistent with the residual throughflow documented by Walters *et al.* (2010). There is an interesting scour depression in the western part of the southeastern approaches where dunes occur in the erosional holes, in a situation reminiscent of the case when a mud layer is breached to expose sand. The 'shelf' west of the Narrows is 'smooth' with no dunes.

References

Bowman, M.J., Kibblewhite, A.C. and Ash, D.E. 1980. M_2 tidal effects in greater Cook Strait, New Zealand. *Journal of Geophysical Research*, **85**, C5, 2728-2742.

Carter, L. 1992. Acoustical characterization of seafloor sediments and its relationship to active sedimentary processes in Cook Strait, New Zealand. *New Zealand Journal of Geology and Geophysics*, **35**, 289-300.

Heath, R.A. 1971. Hydrology and circulation in central and southern Cook Strait, New Zealand. *New Zealand Journal of Marine and Freshwater Research*, **5**, 178-199.

Heath, R.A. 1978. Semi-diurnal tides in Cook Strait, New Zealand. *New Zealand Journal of Marine and Freshwater Research*, **12**, 87-97.

Heath, R.A. 1986. In which direction is the mean flow through Cook Strait, New Zealand—evidence of 1 to 4 week variability? *New Zealand Journal of Marine and Freshwater Research*, **20**, 119-137.

Lamarche, G., Lurton, X., Verdier, A.-L. and Augustin, J.-M. 2011. Quantitative characterization of seafloor substrate and bedforms using advanced processing of multibeam backscatter—Application to Cook Strait, New Zealand. *Continental Shelf Research*, **31**, S93-S109.

Lewis, K.B., Carter, L. and Davey F.J. 1994. The opening of Cook Strait: Interglacial tidal scour and aligning basins at a subduction to transform plate edge. *Marine Geology*, **116**, 293-312.

Mitchell, J.S. and Lewis, K.B. 1980. Cook Strait bathymetry. 2nd ed. New Zealand Oceanographic Institute chart coastal series 1:200 000.

Mountjoy, J.J., Micallef, A., Stevens, C.L. and Stirling, M.W. 2014. Holocene sedimentary activity in a non-terrestrially coupled submarine canyon: Cook Strait Canyon system, New Zealand. *Deep-Sea Research II*, **104**, 120-133.

Proctor, R. and Carter, L. 1989. Tidal and sedimentary response to the Late Quaternary closure and opening of Cook Strait, New Zealand: results from numerical modeling. *Paleoceanography*, **4**, 167-180.

Reid, S. 1996. Pressure gradients and winds in Cook Strait. *Weather and Forecasting*, **11**, 476-488.

Walters, R.A., Gillibrand, P.A., Bell, R.G. and Lane, E.M. 2010. A study of tides and currents in Cook Strait, New Zealand. *Ocean Dynamics*, **60**, 1559-1580.

Return to List of Straits

30—TARAMA STRAIT

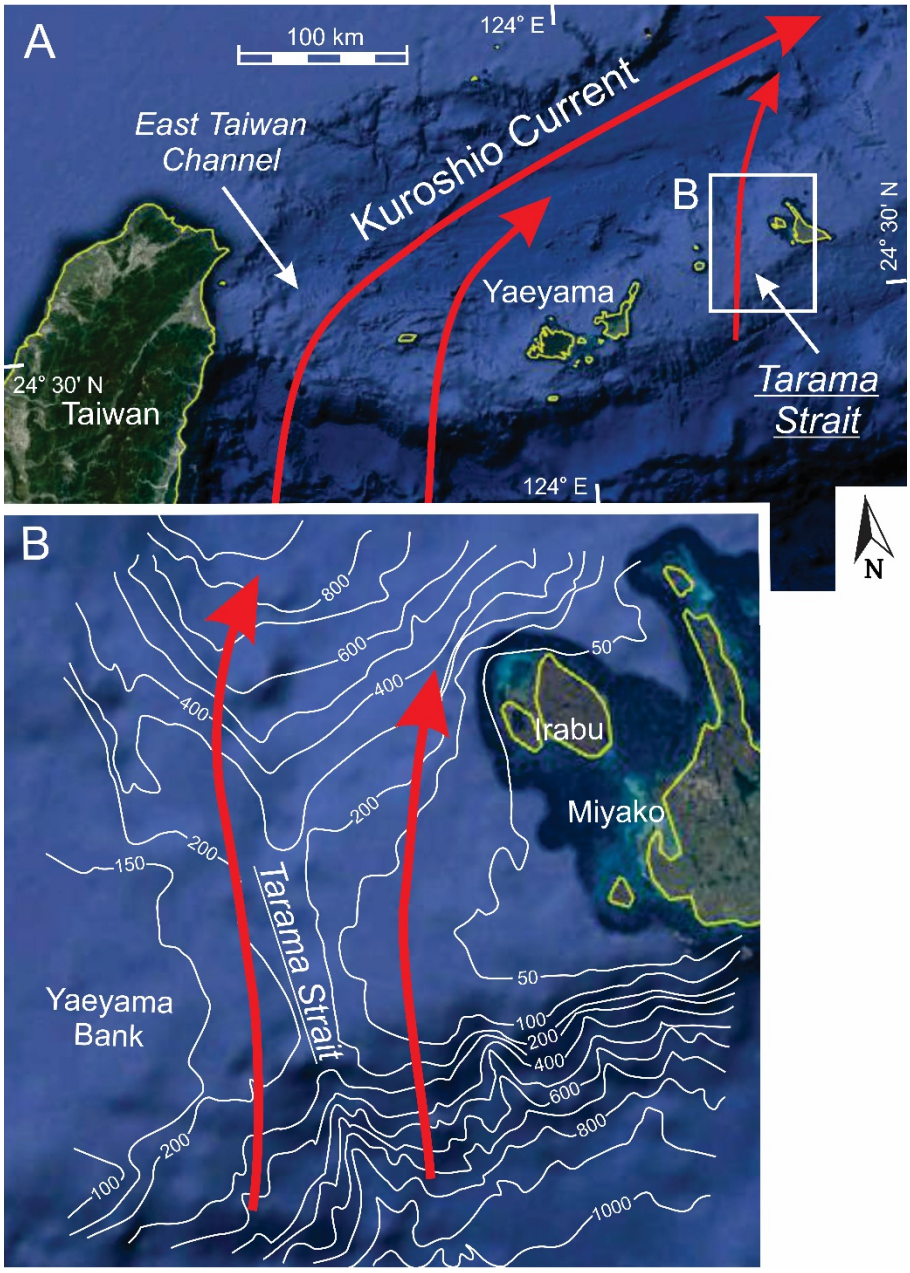

Fig. A30. <u>Tarama Strait</u>: *(A) General setting of Tarama Strait, which lies to the east of Taiwan. (B) Enlarged view of the Strait. Bathymetry modified from Tsuji (1993, fig. 2; copyright Elsevier; used with permission). Depths in metres. Satellite images from Google Earth ©. (Data: SIO, NOAA, U.S. Navy, NGA, GEBCO, LDEO-Columbia, NSF. Image: Landsat/Copernicus). This strait lies between volcanic edifices in the southwestern part of the Ryukyu Arc (Kizaki 1978). It experiences significant wave action from the open Pacific Ocean, and moderately strong tidal-current action (Tsuji 1993). It is also a subsidiary pathway by which the Kuroshio Current passes from the Pacific Ocean, through the Arc, into the Okinawa Trough and East China Sea (Kao* et al. *2006).*

Length

~30 km long N-S.

Width

Entire channel -45 km wide, but the axial part that is >200 m deep is only 3-4 km wide.

Depth

Deepest part is > 200 m deep, but the flanks are < 100 m deep, with terraces at depths of 0-5 m, 20-25 m, 45-55 m and 90-100 m.

Description

The Strait occupies a low area between two volcanoes. Average current speeds typically 15-35 cm s^{-1}, with maximum values of ca. 50-80 cm s^{-1}. Flow of the Kuroshio Current is to north. Tidal currents at high tide (flood) flow to the NNW and to the SSE a low tide. Wave action in storms might also be important to considerable depths. M_2 tidal range is 0.5-0.6 m along most of the Arc. Bedrock outcrops are present down to -60 m. Gravelly sediment occurs down to -150 m. 2D dunes occur on the 90-100 m terrace. Mud is most abundant in shallow protected areas and in the greatest depths. There is little mud from 200-400 m depth. Facies are: (1) reef (hermatypic corals, coralline algae, bryozoans, and sponges; (2) near reef sand; (3) muddy sand-sandy mud (occurs in shallow protected areas); (4) rhodolith and large foraminiferal gravelly sand (mainly on the 90-100 m terrace; rhodoliths average 3.5 cm, max. 11 cm diameter); (5) bryozoan sand; (6) planktonic foraminiferal sand; and (7) planktonic foraminiferal muddy sand facies.

References

Arai, K., Matsuda, H., Sasaki, K., Machiyama, H., Yamguchi, T., Inoue, T., Sato, T., Takayanagi, H. and Iryu, Y. 2016. A newly discovered submerged reef on the Miyako-Sone platform, Ryukyu Island Arc, Northwestern Pacific. *Marine Geology*, **373**, 49-54.

Bassi, D., Nebelsick, J.H., Checconi, A., Hohenegger, J. and Iryu, Y. 2009. Present-day and fossil rhodolith pavements compared: Their potential for analysing shallow-water carbonate deposits. *Sedimentary Geology*, **214**, 74-84.

Kao, S.J., Wu, C.-R., Hsin, Y.-C. and Dai, M. 2006. Effects of sea level change on the upstream Kuroshio Current through the Okinawa Trough. *Geophysical Research Letters*, **33**, L16604, https://doi:10.1029/2006GL026822

Kizaki, K. 1978. Tectonics of the Ryukyu Arc. *Journal of Physics of the Earth*, **26** Supplement, S301-S307.

Kubo, A. and Fukuyama, E. 2003. Stress field along the Ryukyu Arc and the Okinawa Trough inferred from moment tensors of shallow earthquakes. *Earth and Planetary Science Letters*, **210**, 305-316.

Tsuji, Y. 1993. Tide influenced high energy environments and rhodolith-associated carbonate deposition on the outer shelf and slope off the Miyako Islands, southern Ryukyu Island Arc, Japan. *Marine Geology*, **113**, 255-271.

Return to List of Straits

31—TOKARA STRAIT

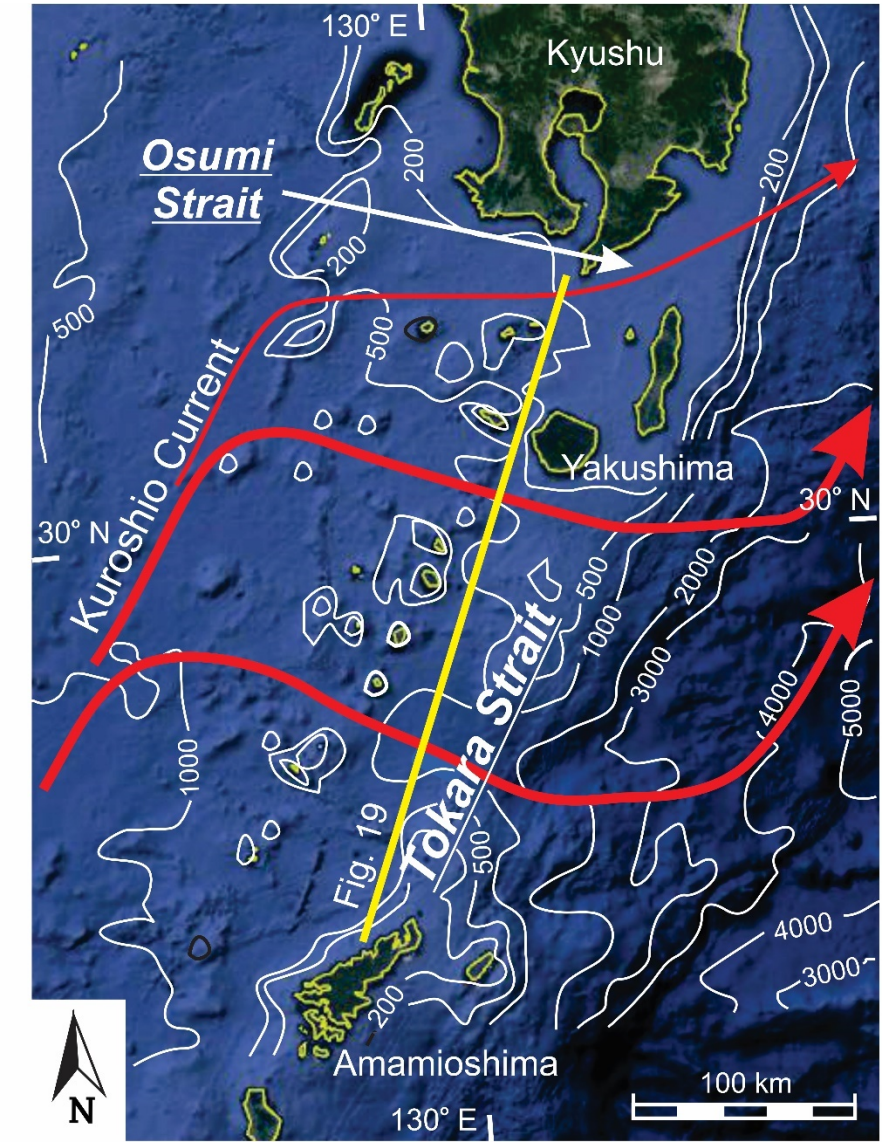

Fig. A31. *Tokara Strait: Bathymetry after Zhu* et al. *(2017, fig. 1c; © American Geophysical Union). Depths in metres. The bathymetric data were derived originally from the ETOPO1 database. Satellite image from Google Earth ©. (Data: SIO, NOAA, U.S. Navy, NGA, GEBCO. Image: Landsat/Copernicus). Tokara Strait is a complex, topographically low segment of the northern Ryukyu Arc. The islands and Isolated circular to elliptical features that occur throughout the Strait are volcanoes. Significant wave action and weak to moderate tidal currents (Zhu* et al. *2017) affect sedimentation in the area. This area is the main pathway by which the Kuroshio Current passes from the back-arc Okinawa Trough and East China Sea into the open Pacific Ocean (Kubota* et al. *1995; Feng* et al. *2000; Liu* et al. *2019). Currents at the surface can be quite strong, but decrease in strength with depth, and weak reverse flow is possible in the deepest channels (cf. Liu* et al. *2019). The yellow line shows the section along which the currents in Fig. 19 of the main paper were obtained.*

Length

Only ~25 km from -200 m isobath to the same depth on the other side of the ridge.

Width

Very wide area (290 km along the Arc; up to 450 km depending on how it is defined and including Osumi Channel) with few islands, all of which are small (< 10 km diameter), so this area is mostly open water. The main, deepest part of this section is 95 km wide and lies a short distance north of the island of Amamioshima.

Depth

Average depth 635 m; shallowest depths at any transect of the Arc is < 100 m, but some transects have minimum depths of 200-300 m. The maximum depth in the Strait is 1077m.

Description

Kizaki (1978) places a strike-slip offset in the ridge in Tokara Strait; alternatively, the channel is the result of arc-parallel extension (Kubo and Fukuyama 2003; Osozawa *et al.* 2012). The Kuroshio Current, which is the Pacific Ocean equivalent of the Gulf Stream, flows northward along the northern side of the arc in the eastern part of the East China Sea, entering partly through straits in the southern part of the Arc, but then flows between the islands and passes through the arc, mainly in its most northerly part (i.e. Tokara Strait and Osumi Channel) and then continues to flow to the NE on the east side of the islands of Japan. This current is like the Gulf Stream and it is warmer and fresher than the surrounding water, which is the cause of its movement. Speeds of this current at the surface are 50-120 cm s^{-1} in Osumi Strait, but 0.7 m s^{-1} maximum in Tokara Channel. The flow splits into 2 threads in Tokara Strait because of the presence of a seamount in the middle. There is a seasonal variation in the strength of this current, with maximum speeds in summer and minimum in autumn, which is attributed to seasonal variation in the bathymetry-parallel wind stress. There is a southwestward underflow current in the southern part of the Strait that parallels the isobaths. Tidal currents: M_2 currents have twice the strength of the diurnal components. Speeds of the M_2 tidal currents are 27 cm s^{-1}; the diurnal currents reach 21 cm s^{-1}. These speeds are near the surface. Near the island of Okinawa, the surface sediments are sand in water depths <800 m; below that, the grain size becomes increasingly finer as the depth increases. The shallow-water sands around the islands are dominated by carbonate material (commonly 90%), dominated by corals and foraminifera. Reefs fringe most of the islands; the most northern reef is on the north flank of Tokara Strait.

References

Feng, M., Mitsudera, H. and Yoshikawa, Y. 2000. Structure and variability of the Kuroshio Current in Tokara Strait. *Journal of Physical Oceanography*, **30**, 2257-2276.

Ikeda, E., Iryu, Y., Sugihara, K., Ohba, H. and Yamada, T. 2006. Bathymetry, biota and sediments of the Hirota Reef, Tane-ga-shima—the northernmost coral reef in the Ryukyu islands. *Island Arc*, **15**, 407-419.

Kao, S.J., Wu, C.-R., Hsin, Y.-C. and Dai, M. 2006. Effects of sea level change on the upstream Kuroshio Current through the Okinawa Trough. *Geophysical Research Letters*, **33**, L16604, https://doi:10.1029/2006GL026822

Kizaki, K. 1978. Tectonics of the Ryukyu Arc. *Journal of Physics of the Earth*, **26** Supplement, S301-S307.

Kubo, A. and Fukuyama, E. 2003. Stress field along the Ryukyu Arc and the Okinawa Trough inferred from moment tensors of shallow earthquakes. *Earth and Planetary Science Letters*, **210**, 305-316.

Kubota, M. Yokota, H. and Okamoto, T. 1995. Mechanism of the seasonal transport variation through the Tokara Strait. *Journal of Oceanography*, **51**, 441-458.

Liu, Z.-J., Namamura, H., Zhu, Z.-H., Nishina, A. Guo, W. and Don, M. 2019. Tempo-spatial variations of the Kuroshio Current in the Tokara Strait based on long-term ferryboat ADCP data. *Journal of Geophysical Research: Oceans*, **124**, 6030-6049. https://doi.org/10.1029.2018JC014771

Osozawa, S., Shinjo, R., Armid, A., Watanabe, Y., Horiguchi, T. and Wakabayashi, J. 2012. Palaeogeographic reconstruction of the 1.55 Ma synchronous isolation of the Ryukyu Islands, Japan, and Taiwan and inflow of the Kuroshio warm current. *International Geology Review*, **54**, 1369-1388.

Varlamov, S.M., Guo, Z., Miyama, T., Ichikawa, K., Waseda, T. and Miyazawa, Y. 2015. M_2 baroclinic tide variability modulated by the ocean circulation south of Japan. *Journal of Geophysical Research: Oceans*, **120**, 3681-3710, https://doi:10.1002/2015JC010739

Yamanouchi, H. 1998. Sandy sediment distribution on coral reefs and beaches at several islands of the Ryukyu Island Arc. *Geographical Review of Japan*, **71**, 72-82.

Zhu, X.-H., Nakamura, H., Don, M., Nichina, A. and Yamshiro, T. 2017. Tidal currents and Kuroshio transport variations in the Tokara Strait estimated from ferryboat ADCP data. *Journal of Geophysical Research*, **122**, https://doi:10.1002/2016JC012329

Return to List of Straits

32—OSUMI CHANNEL

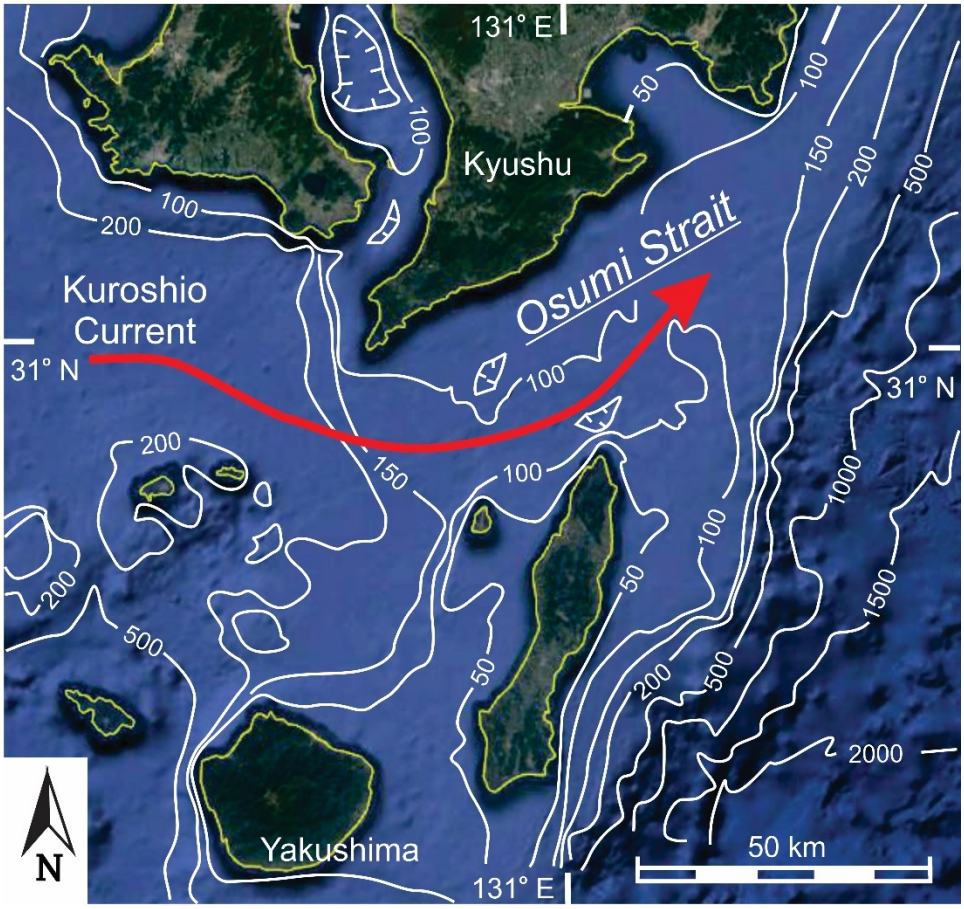

Fig. A32. <u>Osumi Channel</u>*: Bathymetry from Ikehara (1992, fig. 1). Depths in metres. Satellite image from Google Earth ©. (Data: SIO, NOAA, U.S. Navy, NGA, GEBCO, LDEO-Columbia, NSF; Image. Landsat/Copernicus). Osumi Channel is a relatively shallow pass through the Ryukyu Arc, with volcanic islands and shoals occurring especially along its southern side. It is occupied by a minor branch of the Kuroshio Current as it passes eastward from the back-arc area into the Pacific Ocean, nevertheless current speeds are appreciable (Ikehara 1988, 1989; Varamov* et al. *2015). Tidal currents are also present, but are not especially strong, and the currents do not reverse because of the over-riding influence of the Kuroshio Current (Ikehara 1988).*

Length

~130 km long

Width

35 km wide at its narrowest; its SW end is subdivided by two islands.

Depth

Much of it is 80-100 m deep; the deepest hole is 174 m deep.

Description

The Strait was exposed during the lowstand and flooded at ~15,000 yr BP. Perhaps there were estuaries at the ends of the Strait before the sill was flooded? Sedimentation is now dominated by a branch of the Kuroshio Current (the Osumi Branch Current). Its speeds reach maximum values of 1-2.5 m s^{-1} at the surface; more typical speeds are 0.30-0.75 m s^{-1}. It is suggested that the currents were stronger when sea-level was lower, earlier in the transgression, than they are at present. The sediment becomes distinctly finer to the northeast, in the downcurrent direction, from coarse sand and gravel at the southwest end, passing to medium to fine sand near the downstream end of the strait. This decrease is due to a decrease in current speed. Dune bedforms are present at least locally in Osumi Strait, the most northern of the straits; they migrate to the northeast. The distribution of bedforms is similar to that of a tidal transport path: erosion --> sand ribbons --> dunes (large --> small) --> fine sand with current ripples --> mud. Most dunes occur on current-parallel sandbodies (8-10 km long, 3-5 km wide, 15-30 m high) that lie along the flanks of the Strait. The dunes are thought to be partly relict from a stronger current regime earlier in the transgression.

References

Ikehara, K. 1988. Ocean current generated sedimentary facies in the Osumi Strait, south of Kyushu, Japan. *Progress in Oceanography*, **21**, 515-524.

Ikehara, K. 1989. The Kuroshio-generated bedform system in the Osumi Strait, southern Kyushu, Japan. *In*: *Sedimentary Facies in the Active Plate Margin*, Taira, A. and Masuda, F. (eds), Terra Scientific Publishing Co., Tokyo, 261-273.

Ikehara, K. 1992. Formation of duned sand bodies in the Osumi Strait, south of Kyushu, Japan. *Journal of the Sedimentological Society of Japan*, **36**, 37-45.

Ikehara, K. and Kinoshita, Y. 1994. Distribution and origin of subaqueous dunes on the shelf of Japan. *Marine Geology*, **120**, 75-87.

Kizaki, K. 1978. Tectonics of the Ryukyu Arc. *Journal of Physics of the Earth*, **26** Supplement, S301-S307.

Kubo, A. and Fukuyama, E. 2003. Stress field along the Ryukyu Arc and the Okinawa Trough inferred from moment tensors of shallow earthquakes. *Earth and Planetary Science Letters*, **210**, 305-316.

Taira, A. 2001. Tectonic evolution of the Japanese island arc system. *Annual Reviews of Earth and Planetary Science*, **29**, 109-134.

Varlamov, S.M., Guo, Z., Miyama, T., Ichikawa, K., Waseda, T. and Miyazawa, Y. 2015. M_2 baroclinic tide variability modulated by the ocean circulation south of Japan. *Journal of Geophysical Research: Oceans*, **120**, 3681-3710, https://doi:10.1002/2015JC010739

Return to List of Straits

33—BUNGO CHANNEL–HAYASUI STRAIT

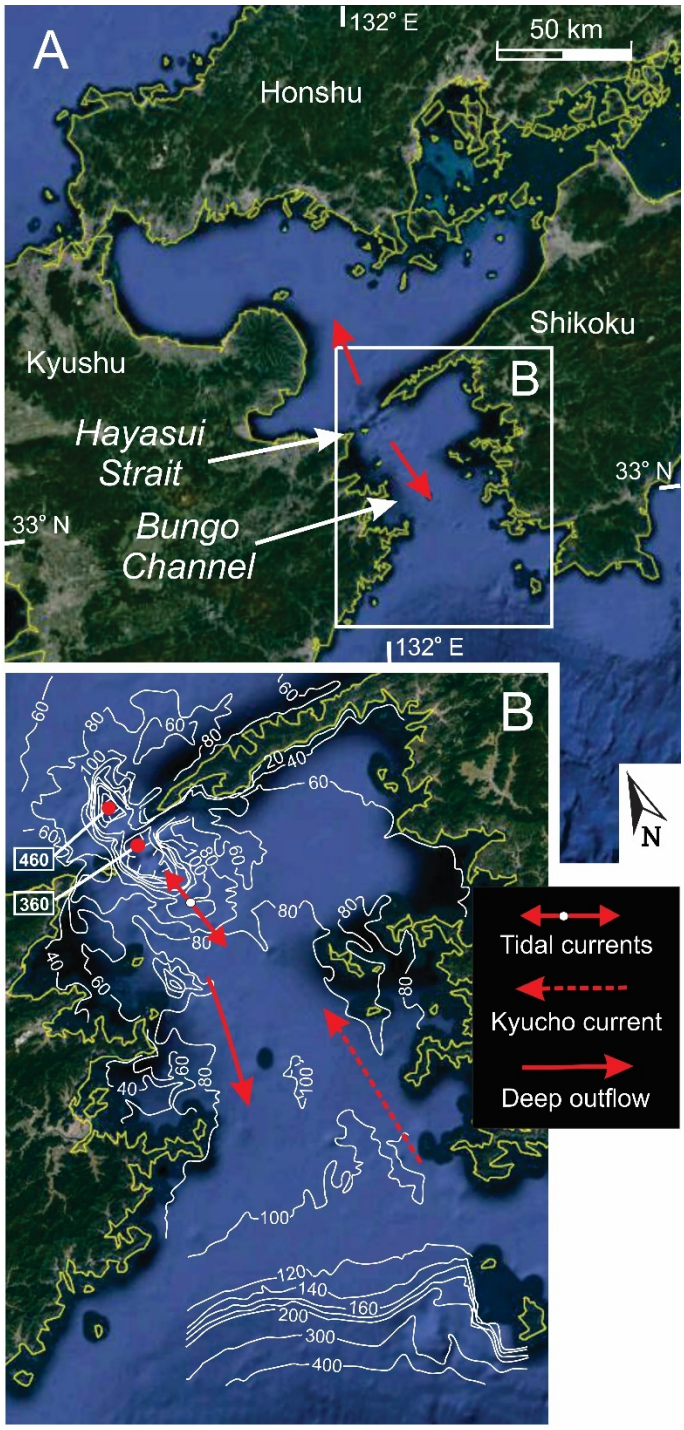

Fig. A33. *Bungo Channel–Hayasui Strait: (A) General location of the Hayasui Strait–Bungo Channel system. (B) Detailed bathymetry of the area, modified after Ikehara (1998, fig. 1a; copyright Elsevier; used with permission). Depths in metres. Satellite images from Google Earth ©. (Data: SIO, NOAA, U.S. Navy, NGA, GEBCO. Image: Landsat/Copernicus). Bungo Channel has very complex shorelines, with*

many islands and convoluted embayments. Hayasui Strait is a breach in a narrow ridge of very resistant bedrock. Note the paired tidal scour depressions on either side of this ridge, which are situated in more easily eroded bedrock. The dominant energy source is the system is tidal currents, that show net divergent transport away from the narrows of Hayasui Strait (Ikehara & Kinoshita 1989). There is a weak inverse-estuarine circulation: the water in the open ocean to the south is warm because it is an extension of the Kuroshio Current, and it is lighter than the colder water in the Seto Sea to the north of Hayasui Strait. Therefore, water flows southward along the seafloor, and inward at the surface (Nakajima 1975; Fujihara & Kawachi 1995; Kaneda et al. *2002). Oceanic currents episodically penetrate into Bungo Channel along its eastern margin as the 'Kyucho' current (Takeoka* et al. *1993).*

Length

~60 km long from just north of Hayasui Strait to the open Pacific Ocean.

Width

Narrowest width is 12 km at Hayasui Strait where the two deep scours exist. Next narrowest part is 24 km. The larger embayments along the margins of Bungo Channel reach up to 45 km wide. The sides are very irregular because of bedrock islands and promontories.

Depth

Very irregular bottom topography, with many islands along both sides and cross-strait bedrock sills. Sills are zero to slightly more than 100 m deep. Deep scours reach 350-450 m below sea level. The average depth of the main part of Bungo Channel is ~80-90 m.

Description

Bungo Channel is located between the islands of Shikoku and Kyushu in southwest Japan, and connects an 'inland sea' (Seto Inland Sea) with the Pacific Ocean. The eastern side of Bungo Channel undergoes intermittent, slow (aseismic) tectonic slip to the southeast relative to the west side, implying that the Channel is an oblique pull-apart basin. The dominant flow is to the south (i.e. ebb dominant). The dominant currents are tidal; they reach 0.7 m s^{-1} and then decrease outward away from the deep scours (mainly toward the south). The water is thermally stratified, with colder water at the bottom. Pacific water is generally warmer than the water in the Channel, but, although salinity increases seaward, from values in the 20 ppt's in the inner part of the Channel, the water of the inner part of the Channel is denser, so that density decreases seaward, implying outward flow at the bottom. This presumably encourages in inward flow of Pacific water (the Kyucho current; Takeoka *et al.* 1993), which mainly occurs on the east side because of the Coriolis effect. Elongate sand banks occur where the current speeds are 0.7-0.5 m s^{-1}. The sea floor is very irregular, with deep scour holes that continue to deepen today. In both directions outward (NW and SE) from the scours, there are sand accumulations covered by dunes (termed a 'transgressive sand sheet'). The banks continue to grow today. Sand is medium sand on the largest banks, and becomes fine sand at the mouth of Bungo Channel. Most dunes in the axis of Bungo Channel are migrating to the south and southwest. Locally at the north side of the mouth, dunes are migrating to the north, perhaps due to influx of Kuroshio Current at times. Alternatively, they

are due to intrusions of cold, bottom water along the floor of the Channel... speeds of these intrusions are, however, only ~15 cm s^{-1}. Modelled residual currents show paired vortices on the inside of Hayasui Strait, with a residual inward jet in the middle... in water < 50 m deep. Modelled near-bed residual currents are complex, but mainly appear to show inward residuals, with gyres associated with headlands. Bottom residuals converge on the narrow Hayasui Strait, which is the opposite of what the sediment distribution suggests. This suggests that tidal currents were stronger at a lower sea level and have become weaker as sea level has risen, although I find the arguments for this weak: it is based on a presumed average depth of the deepest erosion of bedrock, which doesn't apply in the scour holes.

References

Fujihara, M. and Kawachi, T. 1995. An adaptation of diagnostic numerical model of residual current to Bungo Channel, Japan. *Transactions of JSIDRE*, **180**, 75-84.

Ikehara, K. 1998. Sequence stratigraphy of tidal sand bodies in the Bungo Channel, southwest Japan. *Sedimentary Geology*, **122**, 233-244.

Ikehara, K. and Kinoshita, Y. 1989. Bedforms and their migration patterns in southern Bungo Strait, Japan. *In*: *Sedimentary Facies in the Active Plate Margin*, Taira, A. and Masuda, F. (eds), Terra Scientific Publishing Co., Tokyo, 251-260.

Kaneda, A., Takeoka, H., Nagaura, E. and Koizumi, Y. 2002. Periodic instruction of cold water from the Pacific Ocean into the bottom layer of the Bungo Channel in Japan. *Journal of Oceanography*, **58**, 547-556.

Nakajima, H. 1975. Structure of tidal mixing in Hayasui Straits. *Journal of the Oceanographical Society of Japan*, **31**, 227-234.

Ozawa, S., Yarai, H., Imakiire, T. and Tobita, M. 2013. Spatial and temporal evolution of the long-term slow slip in the Bungo Channel, Japan. *Earth Planets Space*, **65**, 67-73.

Takeoka, H., Akiyama, H. and Kikuchi, T. 1993. The Kyucho in the Bungo Channel, Japan—periodic intrusion of oceanic warm water. *Journal of Oceanography*, **49**, 369-382.

Return to List of Straits